Supporting Information

for

Inverse Potential Scaling in Co-Electrocatalytic Activity for CO_2 Reduction Through Redox Mediator Tuning and Catalyst Design

Amelia G. Reid, Juan J. Moreno, Shelby L. Hooe, Kira R. Baugh, Isobel H. Thomas, Diane A. Dickie, Charles W. Machan*

* - machan@virginia.edu; ORCID 0000-0002-5182-1138

AGR ORCID 0000-0002-2868-4091; JJM ORCID 0000-0003-1809-6170; SLH ORCID 0000-0002-6991-2273; DAD ORCID 0000-0003-0939-3309

Department of Chemistry, University of Virginia, PO Box 400319, Charlottesville, VA 22904-4319

Table of Contents

Controlled Potential Electrolysis Experiments (Aprotic Conditions)........ 91

Materials and Methods

General

All chemicals and solvents (ACS or HPLC grade) were commercially available and used as received unless otherwise indicated. For all air-sensitive reactions and electrochemical experiments, HPLC-grade solvents were obtained as anhydrous and air-free from a PPT Glass Contour Solvent Purification System. Gas cylinders were obtained from Praxair (Ar as 5.0; CO_2 as 4.0) and passed through activated molecular sieves prior to use. Gas mixing for variable concentration experiments was accomplished using a gas proportioning rotameter from Omega Engineering. UV-vis absorbance spectra were obtained on a Cary 60 from Agilent. An Anton-Parr Multiwave Pro SOLV, NXF-8 microwave reactor was used for microwave syntheses.

Electrochemistry

All electroanalytical experiments were performed using a Metrohm Autolab PGSTAT302N potentiostat. Glassy carbon working (⌀ = 3 mm) and non-aqueous silver/silver chloride pseudoreference electrodes behind PTFE tips were obtained from CH Instruments. The pseudoreference electrodes were obtained by depositing chloride on bare silver wire in 10% HCl at oxidizing potentials and stored in a 0.1 M tetrabutylammonium hexafluorophosphate/*N,N*-dimethylformamide (*N,N*-DMF) solution in the dark prior to use. The counter electrode was a glassy carbon rod (⌀ = 3 mm). All CV experiments were performed in a modified scintillation vial (20 mL volume) as a single-chamber cell with a cap modified with ports for all electrodes and a sparging needle. Tetrabutylammonium hexafluorophosphate ($TBAPF_6$) was purified by recrystallization from ethanol and dried in a vacuum oven before being stored in a desiccator. All data were referenced to an internal ferrocene standard (ferricenium/ferrocene (Fc^+/Fc) reduction potential under stated conditions) unless otherwise specified. All voltammograms were corrected for internal resistance. Ferrocene was purified by sublimation prior to use.

Controlled Potential Electrolysis (CPE)

CPE experiments were performed in a glass Pine Research Instrumentation H-cell with two compartments separated by a glass frit. A 55 mL stock solution of *N,N*-DMF with 0.1 M $TBAPF_6$ was prepared for each bulk electrolysis experiment. Approximately 26 mL of the stock solution was added to each half of the H-cell. One side of the H-cell contained the catalyst, any additional substrate, such as the mediator and/or PhOH, and a glassy carbon rod working electrode. The other side of the H-cell contained approximately 0.075 M ferrocene as a sacrificial reductant along with a graphite rod counter electrode and a Ag/AgCl pseudoreference electrode. The electrolysis experiment was referenced by taking a CV of the side of the H-cell that contained the ferrocene solution. The H-cell was sealed with two septa that were connected by a piece of PTFE tubing which aided to maintain equal pressure between each half of the cell during the electrolysis. Before starting the electrolysis experiment, both sides of the H-cell were sparged with the desired gas for 20 minutes and the sealed cell was allowed to equilibrate for 1 hour. The resistance between the two halves of the H-cell was measured using the i-interrupt procedure available in the NOVA software provided by Metrohm.

The concentration of catalyst was chosen so that the concentration of product within the H-cell remained in the optimal concentration range for GC product analysis described below. The ratio of catalyst to PhOH remained the same as well as the ratios for RM described for each individual experiment.

Controlled Potential Electrolysis (CPE) Product Analysis

During CPE experiments, either 50 or 250 µL GC injections of the headspace were periodically taken for the detection and quantification of any gaseous products produced. After each CPE experiment, the total volume of solution was measured. The total volume of the sealed H-cell was also measured to account for the total headspace volume for accurate quantification of gaseous products. A calibration curve for CO and H_2 was used to quantify gaseous products produced during electrolysis experiments in the same manner as we previously reported.[1]

Analysis of gas phase products was done by sampling electrolysis headspace through syringe injections into an Agilent 7890B GC equipped with a specialty gas split column 5 Å mol sieve/Porabond Q column (15 m length; 0.320 mm diameter; 25.0 µm film) and thermal conductivity detector with He as a carrier gas. A calibration curve for CO and H_2 was made in the H-cell with an experimental setup containing identical volumes of *N,N*-DMF in 0.1 M $TBAPF_6$ to those used during electrolysis. Known volumes of CO and H_2 were injected into the cell with stirring and 250 µL injections of the headspace were taken for GC injections after equilibration. The limit of detection (LOD) and limit of quantitation (LOQ) for CO and H_2 in the GC were determined from seven consecutive injections at the lowest observable concentrations of each gaseous product respectively. For CO, the LOD was determined to be 5.77×10^{-7} moles and the LOQ was determined to be 1.92×10^{-6} moles. For H_2, the LOD was determined to be 4.55×10^{-6} moles and the LOQ was determined to be 1.52×10^{-5} moles.

Gas Chromatography/Mass Spectrometry (GC/MS) Analysis of CPE Solutions

The samples for GC/MS analysis were prepared by diluting 0.1 mL of the CPE solution with 0.9 mL of dichloromethane (DCM). 1 µL of these solutions were injected by a 7693A ALS into a 7890B GC equipped with an ultra inert column (30 m length; 0.25 mm diameter; 0.25 µm film) and 5977B MSD.

Calculation of Overpotential for CO_2 Reduction with PhOH Present (Adapted)

The calculation of overpotential for all catalysts was performed according to reported methods.[2] The following equation was used for the determination of the reaction standard potential in V with respect to the Fc^+/Fc couple:

$$E_{CO2/CO} = -0.73\,V - 0.059(pK_a) \qquad \textbf{Eq (1)}$$

The pK_a for PhOH in *N,N*-DMF is reported as 18.8:[3]

$$E_{CO2/CO}(PhOH) = -1.84\,V\ vs\ Fc^+/Fc \qquad \textbf{Eq (2)}$$

The $E_{cat/2}$ determined experimentally for $Cr(^{tbu}dhbpy)Cl(H_2O)$ and $Cr(^{tbu}dh^{tbu}bpy)Cl(H_2O)$ is –1.95 V[1] and –2.00 V vs Fc^+/Fc, respectively. For protic CO_2 reduction (1.0 mM catalyst and 0.1 M PhOH under CO_2 saturation); the overpotential is:

$$\eta = \left|E_{cat/2} - E_{CO2/CO}\right| \qquad \textbf{Eq (3)}$$

$Cr(^{tbu}dhbpy)Cl(H_2O)$	η = 110 mV
$Cr(^{tbu}dh^{tbu}bpy)Cl(H_2O)$	η = 160 mV

This assumes no contribution from homoconjugation of the acid. We note that the homoconjugation constant (HA_2^-) for PhOH in *N,N*-DMF has been reported as $\log(K_{HA_2^-}) = 3.8$.[4] Therefore, we emphasize that the described overpotential calculated above for PhOH is the lower-limit approximation, as homoconjugation is expected to alter the effective overpotential. The overpotential equation can be modified to account for homoconjugation:

$$E_{CO2/CO} = -0.73\,V - 0.059(pK_a) - \frac{-2.303RT}{nF}\log\left(mK_{HA_2^-}\right) \qquad \textbf{Eq (4)}$$

Where n = number of electrons (2) and m = number of proton transfers (2). The modified equation provides $E^0_{CO2/CO} = -1.72$ V and the following η values:

Cr(^{tbu}dhbpy)Cl(H_2O)	η = 230 mV
Cr(^{tbu}dh^{tbu}bpy)Cl(H_2O)	η = 280 mV

This value does not account for the possible thermodynamic contributions of the water coordinated to the pre-catalyst, the equimolar quantities of water produced for each equivalent of CO generated, or any adventitious H_2O present in the CO_2, solvent, or electrolyte. Under CO_2 saturation, any water present can form carbonic acid, pK_a(*N,N*-DMF) 7.37,[5] and generate new equilibria involving CO_2 and bicarbonate. The role of carbonic acid (and the general hydration of CO_2 in non-aqueous solvent systems) in altering the overall thermodynamics combined with the effects of homoconjugation has been assessed by Matsubara.[6] Considering the role of water, Matsubara obtained a standard potential for CO_2 reduction to CO of −1.70 V versus Fc^+/Fc for PhOH in *N,N*-DMF with 10 mM water present (see below). Note the same value is obtained considering 10 mM water only.

For 10 mM H_2O in *N,N*-DMF, where AH = PhOH:[6]

$$3CO_{2(g)} + H_2O_{(sol,x)} + 2e^- \rightleftharpoons CO_{(g)} + 2HCO^-_{3\,(sol)} \qquad E^0 = -1.70\,V\,vs.Fc^+/Fc$$

$$CO_{2(g)} + 2AH_{(sol)} + 2e^- \rightleftharpoons CO_{(g)} + 2A^-{}_{(sol)} + H_2O_{(sol,x)} \qquad E^0 = -1.96\,V\,vs.Fc^+/Fc$$

$$CO_{2(g)} + 4AH_{(sol)} + 2e^- \rightleftharpoons CO_{(g)} + 2HA^-_{2\,(sol)} + H_2O_{(sol,x)} \qquad E^0 = -1.70\,V\,vs.Fc^+/Fc$$

Determination of TOF$_{max}$ from Cyclic Voltammetry

The expression for TOF$_{max}$ for a homogeneous electrocatalytic response (considering an application of steady-state conditions to the substrate) has been solved previously.[1, 7]

$$TOF_{max} = 0.1992\frac{n_p^3}{n_{cat}^2}\frac{Fv}{RT}\left(\frac{i_{cat}}{i_p}\right)^2 \qquad \textbf{Eq (6)}$$

Where n_p is the number of electrons transferred under faradaic conditions, n_{cat} is the number of electrons transferred under catalytic conditions, R is the ideal gas constant, F is Faraday's constant, v is the scan rate, T is temperature, i_{cat} is the catalytic current, and i_p is the Faradaic current.

Determination of TOF from Preparative Electrolysis

The integrated expression of current for a homogeneous electrocatalytic response (considering an application of steady-state conditions to the substrate) has been solved previously:[8, 9]

$$\frac{i}{FA} = \frac{n_{cat}^{\sigma}[cat]\sqrt{(k_{obs}D_{cat})}}{1 + \exp\left[\frac{F}{RT}\left(E_{app} - E_{1/2}\right)\right]}$$

$$k_{obs} = k_{cat}[CO_2]$$

where i is the average current (Amps) specific to the reaction product of interest, F is Faraday's constant (96485 C mol^{-1}), A is the area of the electrode (cm^2), n_{cat}^{σ} is the number of electrons in the catalytic process (2) with $\sigma = 1$ under the assumption that all electrons are delivered to the catalyst by the electrode electrode[10] ($\sigma = 0.5$ corresponds to homogeneous electron transfer occuring between catalyst molecules in solution; used here for co-electrocatalytic conditions), $[cat]$ is the concentration of the catalyst (mol cm^{-3}), k_{obs} is the apparent turnover frequency (s^{-1}), $[CO_2]$ is the concentration of CO_2 saturated in *N,N*-DMF (mol cm^{-3}), D_{cat} is the diffusion coefficient of the catalyst (cm^2 s^{-1}), R is the ideal gas constant (Joule mol^{-1} K^{-1}), T is the temperature (K), E_{app} is the applied potential during preparative electrolysis (V), and $E_{1/2}$ is the standard potential of the catalyst (V).

and

$$\frac{i}{A} = J = CO\ specific\ current\ density$$

Substituting and rearranging the first expression to solve for k_{obs}

$$k_{obs} = \frac{J^2\left(1 + \exp\left[\frac{F}{RT}\left(E_{app} - E_{1/2}\right)\right]\right)^2}{F^2(n_{cat}^{\sigma}[cat])^2 D_{cat}}$$

with k_{obs} in hand, the TOF can be expressed for a given potential according to the following relationship

$$TOF = \frac{k_{obs}}{1 + \exp\left[\frac{F}{RT}\left(E_{app} - E_{1/2}\right)\right]}$$

Parameters for CPE experiments reported here not found in **Table 1**.

- $E_{1/2}$ catalyst:
    - −1.95 V vs Fc^+/Fc for Cr(^{tbu}dhbpy)Cl(H_2O) **1**
    - −2.00 V vs Fc^+/Fc for Cr(^{tbu}dh^{tbu}bpy)Cl(H_2O) **2**
- Temperature: 298.15 K
- [CO_2]: 2.3 x 10^{-4} mol cm^{-3}
- Diffusion coefficient:
    - 2.0 x 10^{-6} cm^2 s^{-1} for Cr(^{tbu}dhbpy)Cl(H_2O) **1**
    - 2.3 x 10^{-6} cm^2 s^{-1} for Cr(^{tbu}dh^{tbu}bpy)Cl(H_2O) **2**
- Electrode area: 3.93 cm^2

Calculation of Diffusion Coefficients

The calculation of the diffusion coefficient for each redox mediator was performed by reported methods.[11] Cyclic voltammetry (CV) experiments were done with a solution of 2.5 mM RM in 0.1 M TBAPF$_6$/*N,N*-DMF under Ar saturation conditions. The scan rate of these CVs was varied from 25 mV/s to 5000 mV/s (**Figures S22-S25**). The increase in current observed as the scan rate increases can be represented by the following equation where i_p is the peak current, n is the number of electrons, A is the area of the electrode, D is the diffusion coefficient, C is the concentration of analyte, and v is the scan rate:

$$i_p = (2.69 \times 10^5) n^{3/2} A C D^{1/2} v^{1/2}$$

By plotting the current density as a function of $v^{1/2}$ (**Figures S22-S24**), the slope can be used to find D for each RM.

$$D_{cat} = \frac{(\text{slope})^2}{n^3 C^2 (2.69 \times 10^5)^2}$$

Calculation of i_{cat}/i_p for Co-electrocatalytic Systems

A common technique for evaluating diffusion, electrode surface area, and concentration independent observed rate constants (k_{obs}) for a two-electron catalytic process is to determine i_{cat}/i_p for a catalytic system, where i_{cat} is the catalytic plateau current and i_p is the one-electron peak in the absence of substrate.[12] Due to the complex nature of the co-catalytic systems we present here, we are unable to calculate k_{obs} by this method. However, these ratios still offer an insightful measure into the relative current increase under catalytic conditions between systems that are sensitive to the diffusion coefficient of both co-catalysts.

To calculate the values of i_p and i_{cat} for all systems, the capacitive current must be subtracted from the measured current at either the peak or the plateau. To determine the potential to find the capacitive, peak, catalytic, and co-catalytic plateau currents, the first derivative was taken of the forward trace for CVs obtained with **1** or **2**, RM, and PhOH under Ar (i_p) and under CO$_2$ (i_{cat}). Where the first derivative is equal to zero there is a plateau in the CV trace. The current in the CV at the same potential corresponding to a value of zero in the first derivative was used (**Figure S80A**). However, due to close overlap of features in the co-catalytic trace under CO$_2$, the local minima corresponding to the inflection point of the curve were used to determine an effective current plateau (**Figure S80B**). All CV data used had a scan rate = 100 mV/s.

Computational Methods

Geometry optimizations were performed without geometry constraints at the DFT level with the Gaussian 16 program, Rev B.01,[13] employing the hybrid functional B3LYP[14-17] and the def2-SVP basis set was used for all atoms.[18, 19] Dispersion and bulk solvent effects (*N,N*-dimethylformamide = *N,N*-DMF; $\varepsilon = 37.219$) were accounted for at the optimization stage, by using Grimme's D3 parameter set with Becke-Johnson (BJ) damping[20, 21] and the CPCM continuum model,[22] respectively. The stationary points and their nature as minima (no imaginary frequencies) were characterized by vibrational analysis using the IGRRHO approach as implemented by default in the software package, which also produced enthalpy (H), entropy (S) and Gibbs energy (G) data at 298.15 K. The minima connected by a given transition state were determined by perturbing the transition states along the TS coordinate and optimizing to the nearest minimum. Free energies were corrected (ΔG_{qh}) to account for concentration effects and for errors associated with the harmonic oscillator approximation. Thus, according to Truhlars's quasi-harmonic approximation for vibrational entropy and enthalpy, all vibrational frequencies below 100 cm^{-1} were set to this value.[23] These anharmonic and concentration corrections were calculated with the Goodvibes code.[24] Concentrations were set at 0.001 M for metal complexes, 0.005 for RM and RM^{-}, and 12.92 M for *N,N*-DMF. Energies were refined by means of single point calculations with the larger def2-TZVP basis set. The stability of the wavefunction and spin contamination were studied at the double- and triple-zeta levels of theory. Nucleus-Independent Chemical Shift (NICS)[25] values were computed for the mediators by computing magnetic shielding tensors of ghost atoms placed at the centroid of each ring using the Gauge Independent Atomic Orbital (GIAO)[26-29] method at the B3LYP-D3BJ/def2-TZVP level of theory with the ORCA 5.0 program.[30]

Kohn-Sham orbital projections and spin densities were plotted in ChemCraft with contour values of 0.030 and 0.0025, respectively. The color scheme used for atoms is C = black, O = red, N = blue, H = grey, S = yellow and Cr = maroon. For added clarity, select figures were generated with truncated structures and omitted H atoms as indicated in the respective captions; all calculations were performed using the complete structural model. The labelling scheme for minima is ${}^{\text{multiplicity}}_{\text{\# bound DMF}}\mathbf{Cr}(\boldsymbol{axial\ ligands})^{\text{charge}}$ and ${}^{\text{multiplicity}}\mathbf{RM}^{\text{charge}}$ for RM species; the $[{}^{\mathrm{tbu}}\mathrm{dhbpy}]^{2-}$ or $[{}^{\mathrm{tbu}}\mathrm{dh}{}^{\mathrm{tbu}}\mathrm{bpy}]^{2-}$ ligand framework is a common feature of all Cr species and does not change its coordination mode during the reaction, so it is omitted in the notation where possible for clarity. The spin doublets considered for all co-electrocatalytic assemblies showed significant spin contamination; these are included in the .xyz file for completeness.

Single crystal X-ray diffraction

A single crystal of each sample was coated with Paratone oil and mounted on a MiTeGen MicroLoop. The X-ray intensity data were measured on a Bruker Kappa APEXII Duo system equipped with an Incoatec Microfocus IμS (Cu K_{α}, λ = 1.54178 Å) and a multi-layer mirror monochromator, and a fine-focus sealed tube (Mo K_{α}, λ = 0.71073 Å) and a graphite monochromator or Bruker D8 Venture Kappa four-circle diffractometer system equipped with an Incoatec IμS 3.0 micro-focus sealed X-ray tube (Mo Kα, λ = 0.71073 Å) and a HELIOS double bounce multilayer mirror monochromator.

The frames were integrated with the bruker SAINT software package[31] using a narrow-frame algorithm. Data were corrected for absorption effects using the Multi-Scan method (SADABS or TWINABS).[32] Each structure was solved and refined using the Bruker SHELXTL Software Package[32] within APEX3[31] and OLEX2.[33] Non-hydrogen atoms were refined anisotropically. The O-H hydrogen atoms were located in the electron density map and refined isotropically. All other hydrogen atoms were placed in geometrically calculated positions with $U_{iso} = 1.2U_{equiv}$ of the parent atom ($U_{iso} = 1.5U_{equiv}$ for methyl).

Both polymorphs of ${}^{\mathrm{tbu}}\mathrm{dhbpy(H)}_2$ were twinned. For polymorph 1, a two-domain twin was identified using CELL_NOW.[34] Starting with 767 reflections, 620 reflections were fit to the first domain, and 539 to the second domain (132 exclusively), with 15 unindexed reflection remaining.

The twin domain was oriented at a 179.8° rotation about the reciprocal axis 0.000 0.001 1.000. The twin law was -0.998 -0.004 0.001 / 0.004 -1.002 0.001 / -0.642 -0.366 1.000. It was refined on on HKLF5 data, with the BASF for the twin domain refining to 0.33031. For polymorph 2, a three-domain twin was identified using CELL_NOW.[34] Starting with 1469 reflections, 1084 reflections were fit to the first domain, 1073 to the second domain (246 exclusively), and 189 to the third domain (43 exclusively) with 96 unindexed reflection remaining. The second domain was oriented at a 179.9° rotation about the reciprocal axis 0.000 0.000 1.000. The twin law was -0.999 0.002 0.004 / 0.000 -1.001 -0.002 / 0.539 0.999 1.000. The third domain was oriented at a 179.7° rotation about the real axis 1.000 -0.411 -0.412 and its twin law was -0.039 -0.398 -0.398 / -0.553 -0.768 0.234 / -1.956 0.796 -0.193. It was refined on HKLF5 data, with the BASF for the twin domains refining to 0.47711 and 0.02195. For **2**, one *tert*-butyl group was found to be disordered across two positions. The relative occupancy of the positions was freely refined, with constraints on the anisotropic displacement parameters of the disordered atoms. Chloroform and hexane solvent located in the crystal lattice was severely disordered and could not be adequately modeled with or without restraints. Thus, the structure factors were modified using the PLATON SQUEEZE[35] technique, in order to produce a “solvate-free” structure factor set. PLATON reported a total electron density of 326 e^- and total solvent accessible volume of 1276 Å^3.

Table S1. Crystallographic data for ^{tbu}dhbpy(H)$_2$, ^{tbu}dh^{tbu}bpy(H)$_2$, and Cr(^{tbu}dh^{tbu}bpy)Cl(H$_2$O) **2**.

	^{tbu}dhbpy(H)$_2$ polymorph 1	^{tbu}dhbpy(H)$_2$ polymorph 2	^{tbu}dh^{tbu}bpy(H)$_2$	Cr(^{tbu}dh^{tbu}bpy)Cl(H$_2$O) **2**
CCDC number	1984949	1984950	2150929	2150930
Formula	$C_{38}H_{48}N_2O_2$	$C_{38}H_{48}N_2O_2$	$C_{46}H_{64}N_2O_2$	$C_{99}H_{139}Cl_5Cr_2N_6O_6$
FW (g/mol)	564.78	564.78	676.99	1790.40
Temp (K)	100(2)	100(2)	100(2)	100(2)
λ (Å)	1.54178	0.71073	0.71073	1.54178
Size (mm)	0.051 x 0.067 x 0.157	0.077 x 0.091 x 0.589	0.164 x 0.222 x 0.362	0.048 x 0.048 x 0.059
Crystal habit	yellow plate	yellow plate	yellow block	orange plate
Crystal system	triclinic	triclinic	monoclinic	triclinic
Space group	P -1	P -1	I 2/m	P -1
a (Å)	10.0611(10)	6.142(2)	13.809(3)	15.1726(10)
b(Å)	11.5414(11)	9.094(3)	8.7376(17)	19.0611(13)
c (Å)	15.8166(15)	15.431(5)	17.190(5)	20.9243(15)
α (°)	77.316(7)	106.415(5)	90	84.198(5)
β (°)	74.707(7)	93.806(5)	99.585(5)	81.186(5)
γ (°)	65.801(7)	97.936(6)	90	73.704(5)
Volume (Å^3)	1602.9(3)	813.8(5)	2045.1(8)	5729.0(7)
Z	2	1	2	2
Density (g/cm^3)	1.170	1.152	1.099	1.038
μ (mm^{-1})	0.549	0.070	0.066	2.990
F(000)	612	306	740	1912
θ range (°)	2.92 to 68.33	2.36 to 25.26	1.76 to 29.63	2.14 to 50.63
Index ranges	$-11 \leq h \leq 12$ $-13 \leq k \leq 13$ $0 \leq l \leq 19$	$-7 \leq h \leq 7$ $-10 \leq k \leq 10$ $0 \leq l \leq 18$	$-19 \leq h \leq 19$ $-12 \leq k \leq 12$ $-23 \leq l \leq 23$	$-15 \leq h <= 15$ $-19 \leq k \leq 19$ $-20 \leq l \leq 20$

Data / restraints /parameters	5760 / 0 / 400	3031 / 0 / 202	3058 / 0 / 149	11907 / 0 / 1104
GOF on F^2	1.068	1.047	1.023	0.996
R_1 ($I>2\sigma(I)$)	0.0738	0.0815	0.0450	0.0996
wR_2 (all data)	0.2099	0.2350	0.1281	0.3073

Table S2. Crystallographic data for TPTD, Mes$_2$DBTD, and Ph$_2$DBTD.

	TPTD	Mes$_2$DBTD	Ph$_2$DBTD
CCDC number	2154597	2154599	2154598
Formula	$C_{18}H_{10}O_2S$	$C_{30}H_{28}O_2S$	$C_{31}H_{24}O_2S$
FW (g/mol)	290.32	452.58	460.56
Temp (K)	100.00	100.00	100.00
λ (Å)	0.71073	0.71073	0.71073
Size (mm)	0.438 × 0.164 × 0.068	0.375 × 0.095 × 0.043	0.233 × 0.064 × 0.039
Crystal habit	colorless plate	colorless rod	colorless needle
Crystal system	monoclinic	orthorhombic	orthorhombic
Space group	$P2_1/c$	$Pca2_1$	Pbcn
a (Å)	7.0219(4)	19.7648(12)	15.4383(16)
b(Å)	20.7503(10)	7.4276(4)	20.371(2)
c (Å)	17.2210(10)	16.1962(9)	7.3501(7)
α (°)	90	90	90
β (°)	91.096(2)	90	90
γ (°)	90	90	90
Volume (Å^3)	2508.8(2)	2377.7(2)	2311.6(4)
Z	8	4	4
Density (g/cm^3)	1.537	1.264	1.323
μ (mm^{-1})	0.258	0.161	0.168
F(000)	1200.0	960.0	968.0
θ range (°)	2.562 to 28.294	2.061 to 26.377	1.999 to 28.296
Index ranges	$9 \le h \le 9$ $-22 \le k \le 27$ $-22 \le l \le 22$	$-24 \le h \le 24$ $-9 \le k \le 7$ $-20 \le l \le 20$	$-20 \le h \le 20$ $-27 \le k \le 27$ $-9 \le l \le 7$
Data / restraints /parameters	6229/0/379	4845/1/305	2870/0/157
GOF on F^2	1.208	1.104	1.095
R_1 ($I>2\sigma(I)$)	0.0773	0.0754	0.0530
wR_2 (all data)	0.1738	0.1936	0.1153

Synthesis and Characterization

Synthesis of 6,6′-Di(3,5-di-*tert*-butyl-2-hydroxybenzene)-2,2′-bipyridine, ^{tbu}dhbpy(H)$_2$

The synthesis of ^{tbu}dhbpy(H)$_2$ was carried out as previously reported.[1]

Synthesis of Cr(^{tbu}dhbpy)Cl(H_2O) (1)

The metalation of ^{tbu}dhbpy(H)$_2$ to generate Cr(^{tbu}dhbpy)Cl(H_2O) (**1**) was carried out as previously reported[1] with one modification: the resulting product was further purified by dissolving in dichloromethane (DCM) and passing through a PTFE syringe filter to remove excess starting metal salt.

Synthesis of 6,6′-Di(3,5-di-*tert*-butyl-2-hydroxybenzene)-4,4’-di-*tert*-butyl-2,2′-bipyridine, ^{tbu}dh^{tbu}bpy(H)$_2$

The starting materials for this reaction, dichloro-4,4′-di-*tert*-butyl-2,2′-bipyridine[36, 37] and (3,5-di-*tert*-butyl-2-hydroxy-phenyl)boronic acid[1], were all prepared by previously reported methods.

Two microwave tubes were each charged with 6,6′-dichloro-4,4′-di-*tert*-butyl-2,2′-bipyridine (0.755 g, 2.24 mmol), unpurified (3,5-di-*tert*-butyl-2-hydroxy-phenyl)boronic acid (1.96 g, 38.2 mmol), sodium carbonate (1.76 g, 16.6 mmol), $Pd(PPh_3)_4$ (0.04 g, 0.03 mmol), and degassed toluene (30 mL), water (12 mL), and methanol (8 mL). The microwave conditions were set to heat the reaction mixture to 170 °C as fast as possible and then held at that temperature for 140 minutes. After cooling, the two tubes were combined, and aqueous and organic fractions were separated and extracted. The organic layer was washed with brine (3 x 50 mL) and the aqueous layer was extracted with dichloromethane (4 x 75 mL). All organic fractions were combined and dried over $MgSO_4$ before removing the solvent via reduced pressure leaving a bright yellow oil. Methanol was added to the flask to dissolve excess boronic acid still present and a yellow solid crashed out of solution. Finally, the solution was filtered and the solid collected on the frit was washed with additional methanol leaving a bright yellow solid with an isolated yield of 30.5% (0.922 g). ^{1}H NMR (CD_2Cl_2, 600 MHz): δ 14.60 (s, 2H, O*H*), 8.22 (d, 2H, Ar*H*), 7.98 (d, 2H, Ar*H*), 7.74 (d, 2H, Ar*H*), 7.44 (d, 2H, Ar*H*), 1.51 (s, 18H, $-C(CH_3)_3$), 1.50 (s, 18H, $-C(CH_3)_3$), 1.40 (s, 18H, $-C(CH_3)_3$). ^{13}C{^{1}H} NMR (CD_2Cl_2, 150 MHz): δ 163.7 (Ar*C*), 159.0 (Ar*C*), 157.0 (Ar*C*), 152.2 (Ar*C*), 140.5 (Ar*C*), 126.56 (Ar*C*), 121.5 (Ar*C*), 119.0 (Ar*C*), 117.7 (Ar*C*), 116.8 (Ar*C*), 110.5 (Ar*C*), 35.9 (tbu*C*), 35.7 (tbu*C*), 34.7 (tbu*C*), 31.8 (tbu*C*), 30.7 (tbu*C*), 29.8 (tbu*C*). Elemental Analysis for $C_{46}H_{64}N_2O_2$ calc’d: C 81.61, H 9.53, N 4.14; found: C 81.10, H 9.79, N 4.15.

Synthesis of Cr(^{tbu}dh^{tbu}bpy)Cl(H_2O) (2)

Metalation of ^{tbu}dh^{tbu}bpy(H)$_2$ with Cr(III) to generate Cr(^{tbu}dh^{tbu}bpy)Cl(H_2O) (**3**) was achieved by stirring ^{tbu}dh^{tbu}bpy(H)$_2$ (0.295 g, 0.436 mmol) and 1.05 equivalents of chromium(II) dichloride (0.0562 g, 0.458 mmol) in tetrahydrofuran (60 mL) at room temperature under an inert atmosphere for seven days. After exposing the reaction to air, the THF was removed under reduced pressure. The solid was then dissolved in DCM and washed with brine (3 x 50 mL) and saturated ammonium chloride (6 x 50 mL). The organic layer was then dried over $MgSO_4$ and condensed under reduced pressure. The resulting solid was dissolved in minimal DCM and passed through a PTFE syringe filter. Finally, the DCM was removed, and the resulting solid was collected in a frit using pentanes to give a bright red solid. 54.5% isolated yield (0.185 g). Elemental analysis for $C_{46}H_{64}ClCrN_2O_3\cdot CH_2Cl_2$ calc’d: C 65.23, H 7.69, N 3.24; found: C 65.36, H 7.64, N 3.69. ESI-MS (m/z): [Cr(^{tbu}dh^{tbu}bpy)]–Cl–H_2O+CH_3OH calc’d: 458.4479 found: 758.4084.

Synthesis of Triphenylothiophene 4,4-dioxide, TPTD

The synthesis of triphenylothiophene 4,4-dioxide (TPTD) was carried out following a previously reported method.[38, 39]

Synthesis of 2,8-Dimesityldibenzothiophene 5,5-dioxide, Mes$_2$DBTD

2,8-dibromodibenzothiophene 5,5-dioxide was prepared by a previously reported method.[40, 41] Three microwave tubes were each filled with 2,8-dibromodibenzothiophene 5,5-dioxide (0.503 g, 1.35 mmol), (2,4,6-trimethylphenyl)boronic acid (0.553 g, 3.37 mmol), sodium carbonate (3.77 g, 35.7 mmol), Pd(PPh$_3$)$_4$ (0.124 g, 0.108 mmol), and degassed toluene (30 mL), water (12 mL), and methanol (8 mL). The microwave conditions were set to heat the reaction mixture to 170 °C as fast as possible and then held at that temperature for 200 minutes. After cooling, the three tubes were combined, and the toluene layer was set aside. The aqueous layer was extracted with dichloromethane (6 x 100 mL). All organic fractions were combined and dried over MgSO$_4$ before removing the solvent via reduced pressure leaving a white solid. The solid was first recrystallized by methanol and then a second recrystallization was done using minimal hot ethyl acetate and methanol to give a fluffy white solid. 51.9% isolated yield (0.949 g). ^{1}H NMR (CD$_2$Cl$_2$, 600 MHz): δ 7.88 (dd, 2H, Ar*H*), 7.57 (dd, 2H, Ar*H*), 7.34 (dd, 2H, Ar*H*), 6.96 (s, 4H, Ar*H*), 2.31 (s, 6H, −CH$_3$), 2.02 (s, 6H, −CH$_3$). ^{13}C{^{1}H} NMR (CD$_2$Cl$_2$, 150 MHz): δ 148.4 (Ar*C*), 138.2 (Ar*C*), 137.5 (Ar*C*), 137.0 (Ar*C*), 135.9 (Ar*C*), 132.7 (Ar*C*), 132.3 (Ar*C*), 128.9 (Ar*C*), 123.5 (Ar*C*), 122.6 (Ar*C*), 21.3 (Me*C*), 21.0 (Me*C*). Elemental Analysis for $C_{30}H_{28}O_2S\cdot[C_4H_8O_2]_{1/3}$ calc'd: C 78.08, H 6.41, N 0.00; found: C 78.14, H 6.29, N 0.02. ESI-MS (m/z): calc'd: 452.1010; found 452.1803.

Synthesis of 2,8-Diphenyldibenzothiophene 5,5-dioxide, Ph$_2$DBTD

2,8-Dibromodibenzothiophene 5,5-dioxide (1.00 g, 2.67 mmol), phenylboronic acid (0.750 g, 6.15 mmol), K$_3$PO$_4$ (0.57 g, 2.7 mmol), Pd(PPh$_3$)$_4$ (0.15 g, 0.13 mmol), and 1,4-dioxane (100 mL) were added to a 250 mL pressure flask with a stir bar in an inert atmosphere glovebox. The reaction was stirred at 130 °C under inert atmosphere for 3 days. After cooling to room temperature, the reaction was exposed to air. The reaction was then diluted with brine (75 mL) and the dioxane layer was separated. The aqueous layer was then extracted with DCM (5 x 75 mL) and all organic layers were dried over MgSO$_4$. Silica was added to the flask (15 g) and the solvent was removed to dryness under reduced pressure. The dry loaded sample was then separated by column chromatography with hexanes and DCM as eluent. Solvent mixture was initially 50% hexanes and 50% DCM and gradually adjusted to 100% DCM. The third fraction was collected and solvent was removed to yield an off-white solid with an isolated yield of 0.288 g, 29.2% yield. ^{1}H NMR (CD$_2$Cl$_2$, 600 MHz): δ 8.74 (s, 1H, Ar*H*), 8.06 (d, 1H, Ar*H*), 7.97 (dd, 1H, Ar*H*), 7.91 (d, 2H, Ar*H*), 7.57 (t, 2H, Ar*H*) 7.50 (t, 1H, Ar*H*). ^{13}C{^{1}H} NMR (CD$_2$Cl$_2$, 150 MHz): δ 147.8 (Ar*C*), 139.8 (Ar*C*), 137.4 (Ar*C*), 132.8 (Ar*C*), 130.0 (Ar*C*), 129.7 (Ar*C*), 129.4 (Ar*C*), 127.9 (Ar*C*), 122.8 (Ar*C*), 121.0 (Ar*C*). Elemental Analysis for $C_{24}H_{16}O_2S$ calcd: C 78.27, H 4.38, N 0.00; found: C 77.67, H 4.38, N 0.01. ESI-MS (m/z): calcd: 368.0871; found 368.0872.

Evans' Method Characterization of 2

The spin state of the Cr(^{tbu}dh^{tbu}bpy)Cl(H$_2$O) (**2**) catalyst was characterized as a Cr(III) species via Evans' Method.[42, 43] Three capillary inserts were made with a 50% v/v mixture of *N,N*-DMF and *N,N*-DMF-d_7. Each insert was flame sealed, and then placed in an NMR tube. Then 8.3 mg of **2** was dissolved in 3 mL of *N,N*-DMF. Approximately 0.6 mL of the solution of **2** was added to each of the three NMR tubes containing a flame sealed insert. ^{1}H NMR spectra with 64 scans were then taken using a 600 MHz Varian NMR Spectrometer. The results of this experiment, which was run in triplicate, can be seen in **Table S3**. The average μ_{eff} of **2** was 3.86±0.10.

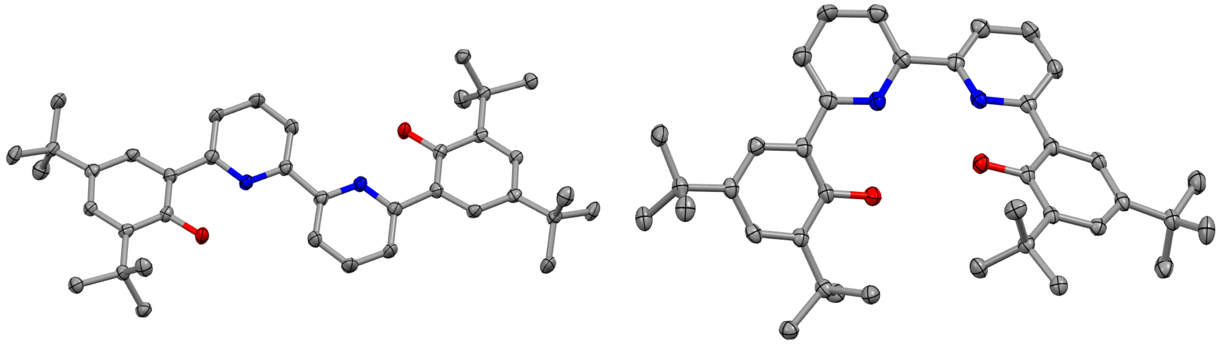

Figure S1. The two polymorphs of single crystal structures of ^{tbu}dhbpy(H)$_2$ ligand obtained from X-ray diffraction studies. Blue = N, red = O, gray = C; thermal ellipsoids at 50%; H atoms omitted for clarity. CCDC 1984950 (left) and 1984949 (right).

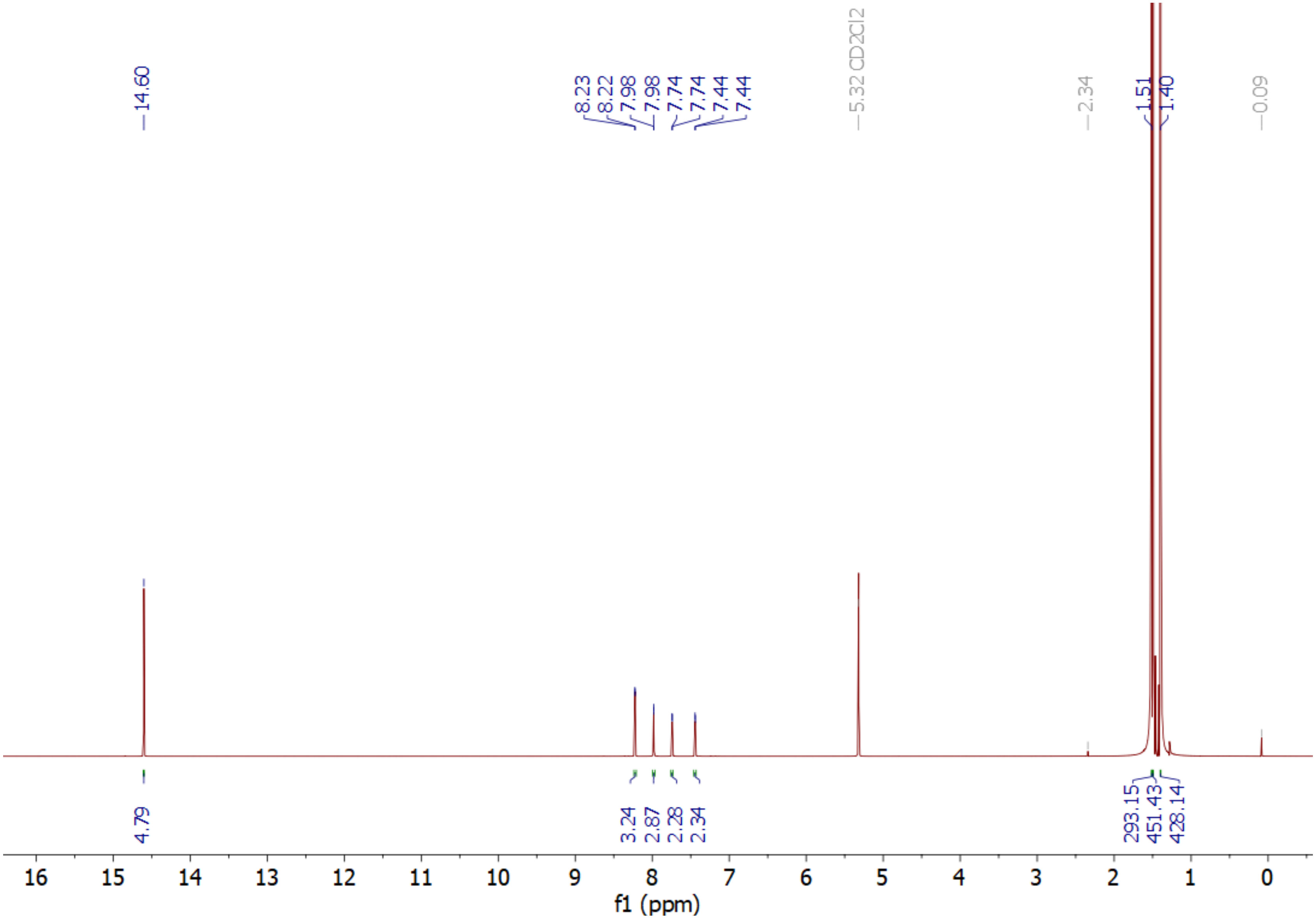

Figure S2. ^{1}H NMR of ^{tbu}dh^{tbu}bpy(H)$_2$ ligand; CD_2Cl_2; 600 MHz.

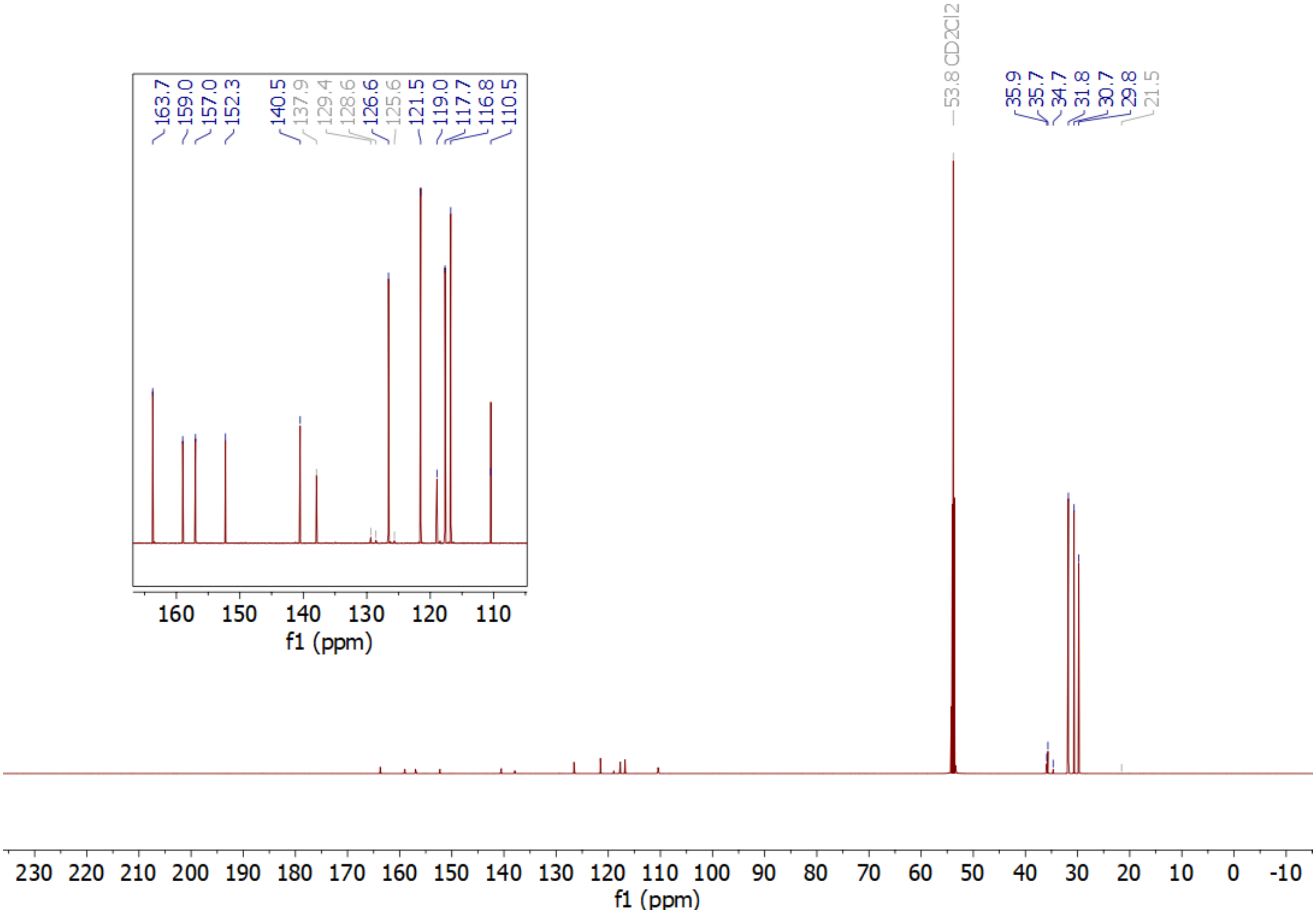

Figure S3. ^{13}C{^{1}H} NMR of ^{tbu}dh^{tbu}bpy(H)$_2$ ligand; CD$_2$Cl$_2$; 150 MHz.

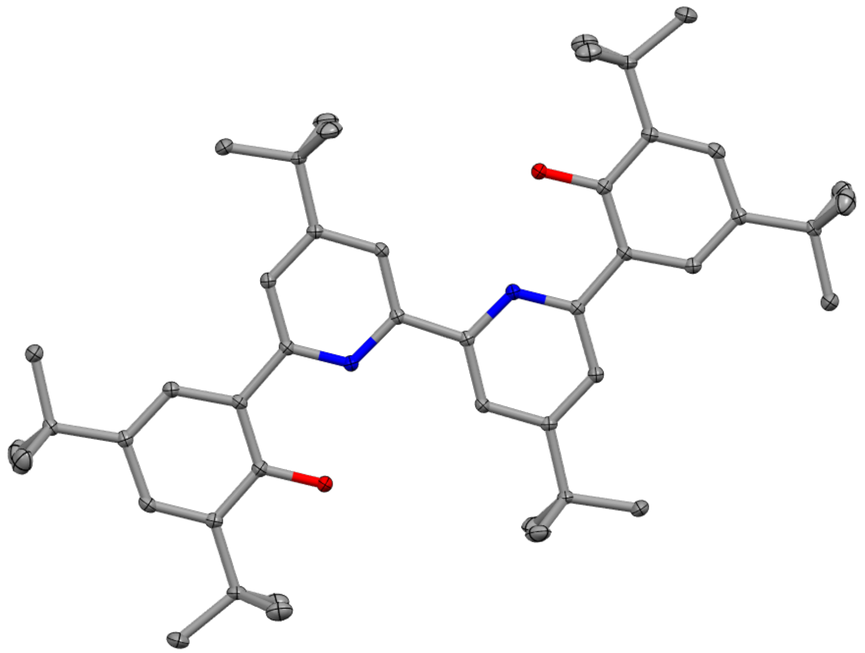

Figure S4. Single crystal structures of $^{tbu}dh^{tbu}bpy(H)_2$ ligand obtained from single-crystal X-ray diffraction studies. Blue = N, red = O, gray = C; thermal ellipsoids at 50%; H atoms omitted for clarity. CCDC 2150929.

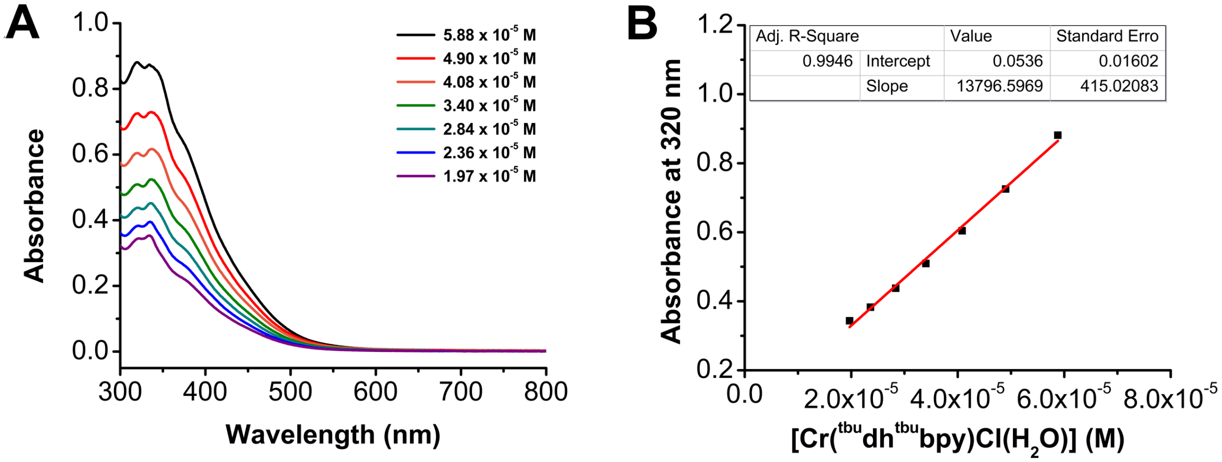

Figure S5. (**A**) UV-vis serial dilution absorbance data obtained from Cr($^{tbu}dh^{tbu}bpy$)Cl(H_2O) **2** in a *N,N*-DMF solution. Conditions: varying concentration; quartz cell with 1 cm pathlength. (**B**) Plot of absorbance versus concentration (M) for Cr($^{tbu}dh^{tbu}bpy$)Cl(H_2O) **2** in *N,N*-DMF at 320 nm (13800 M^{-1} cm^{-1}); $R^2 = 0.995$. All: λ_{max} = 333 nm (13300 M^{-1} cm^{-1}) and 383 nm (9780 M^{-1} cm^{-1}).

Table S3. Evans' method results for Cr(^{tbu}dh^{tbu}bpy)Cl(H_2O) (**2**) in *N,N*-DMF.[42, 43]

Trial	Chemical Shift (ppm)	Chemical Shift (Hz)	Total Magnetic Moment (emu mol^{-1})	Paramagnetic Moment (emu mol^{-1})	μ_{eff} (Bohr Magnetons)
1	0.0805	48.3	0.00542	5.96×10^{-3}	3.77
2	0.0896	53.8	0.00603	6.57×10^{-3}	3.96
3	0.0803	48.2	0.00541	5.94×10^{-3}	3.76

Electrochemistry of 2

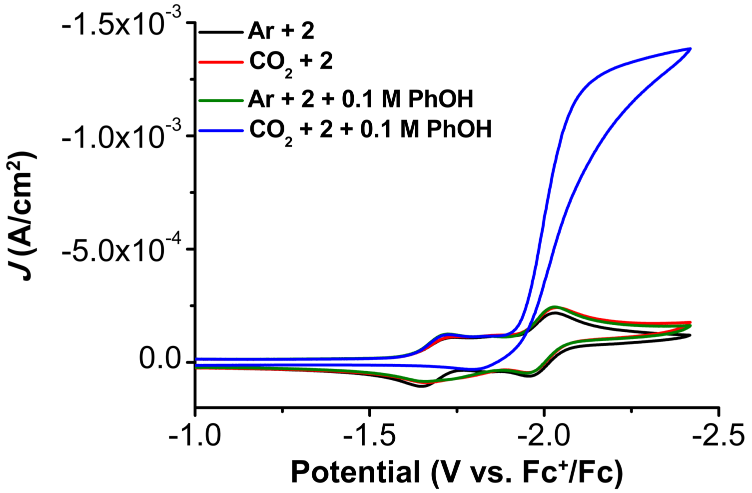

Figure S6. Comparison of CVs of 1.0 mM Cr(^{tbu}dh^{tbu}bpy)Cl(H_2O) **2** under Ar and CO_2 saturation conditions with and without 0.1 M PhOH. Conditions: 0.1 M $TBAPF_6$/DMF; glassy carbon working electrode, glassy carbon rod counter electrode, Ag/AgCl pseudoreference electrode; referenced to Fc$^+$/Fc internal standard; 100 mV/s scan rate.

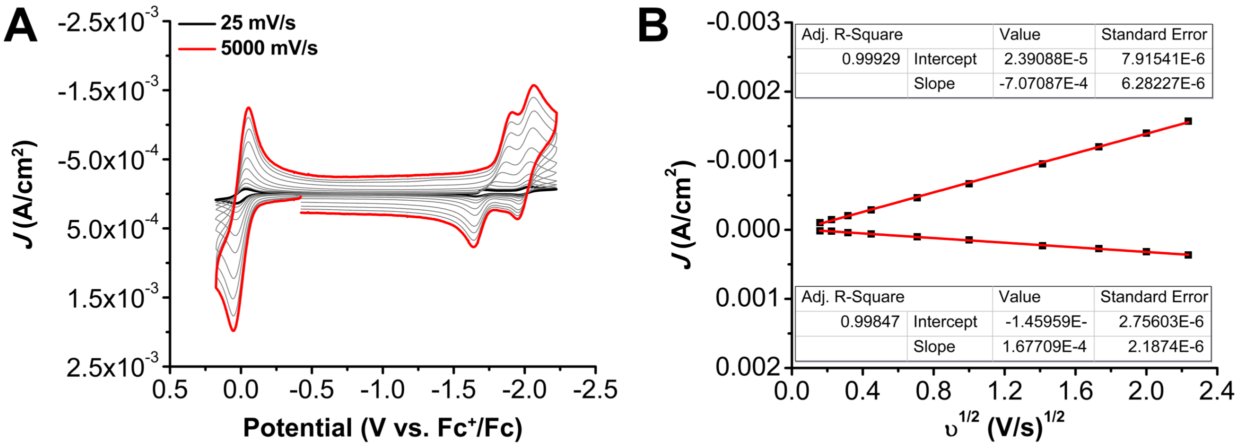

Adj. R-Square		Value	Standard Error
0.99929	Intercept	2.39088E-5	7.91541E-6
	Slope	-7.07087E-4	6.28227E-6

Adj. R-Square		Value	Standard Error
0.99847	Intercept	-1.45959E-	2.75603E-6
	Slope	1.67709E-4	2.1874E-6

Figure S7. (**A**) CVs of Cr(^{tbu}dh^{tbu}bpy)Cl(H_2O) **2** at variable scan rates ranging from 25 (black) to 5000 (red) mV/s, obtained under Ar saturation conditions. (**B**) Linear Fit of variable scan rate data from (**A**) demonstrating that Cr(^{tbu}dh^{tbu}bpy)Cl(H_2O) **2** shows a diffusion-limited current response. The data in (**B**) was obtained from the reversible redox feature at −2.00 V vs Fc^+/Fc. Conditions: 1.0 mM **2**, 0.1 M $TBAPF_6$/DMF; glassy carbon working electrode, glassy carbon counter electrode, Ag/AgCl pseudoreference electrode; varied scan rate; referenced to internal ferrocene standard.

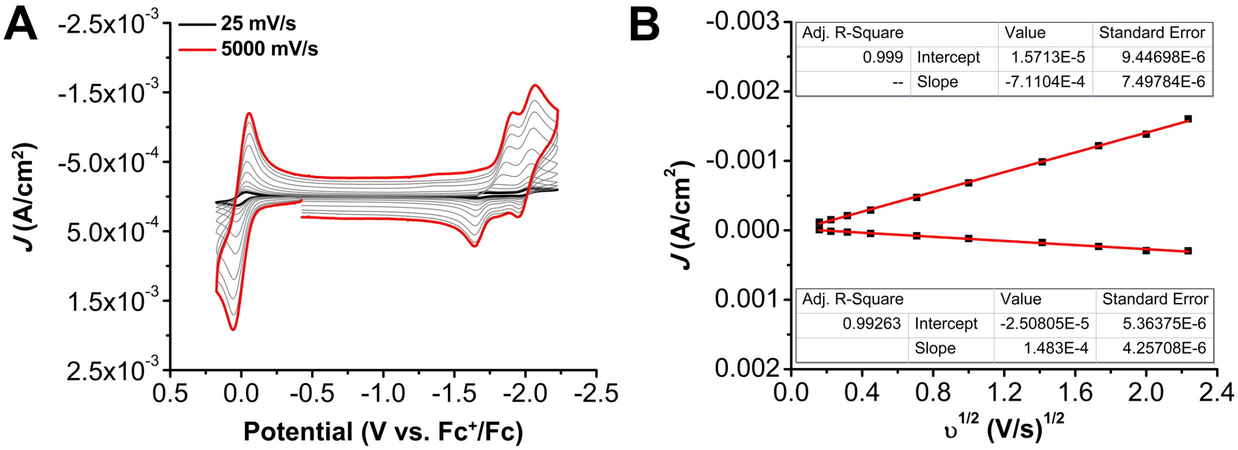

Adj. R-Square		Value	Standard Error
0.999	Intercept	1.5713E-5	9.44698E-6
--	Slope	-7.1104E-4	7.49784E-6

Adj. R-Square		Value	Standard Error
0.99263	Intercept	-2.50805E-5	5.36375E-6
	Slope	1.483E-4	4.25708E-6

Figure S8. (**A**) CVs of Cr(^{tbu}dh^{tbu}bpy)Cl(H_2O) **2** at variable scan rates ranging from 25 (black) to 5000 (red) mV/s, obtained under CO_2 saturation conditions. (**B**) Linear Fit of variable scan rate data from (**A**) demonstrating that Cr(^{tbu}dh^{tbu}bpy)Cl(H_2O) **2** shows a diffusion-limited current response. The data in (**B**) was obtained from the reversible redox feature at −2.00 V vs Fc^+/Fc. Conditions: 1.0 mM **2**, 0.1 M $TBAPF_6$/DMF; glassy carbon working electrode, glassy carbon counter electrode, Ag/AgCl pseudoreference electrode; varied scan rate; referenced to internal ferrocene standard.

For all variable concentration studies without the presence of RMs (Figures S9-S11) analysis was adapted from Sathrum and Kubiak J. Phys. Chem. Lett. 2011, *2*, 2372.[44] F is Faraday's constant, A is the electrode area, [Q] is the substrate concentration, k_{cat} is the catalytic rate, D is the diffusion constant of the catalyst, [cat] is the concentration of the catalyst, and n_{cat} is the number of electrons involved in the catalytic process.

$$\boldsymbol{i_{cat} = n_{cat}FA[cat](Dk_{cat}[Q]^{y})^{1/2}}$$

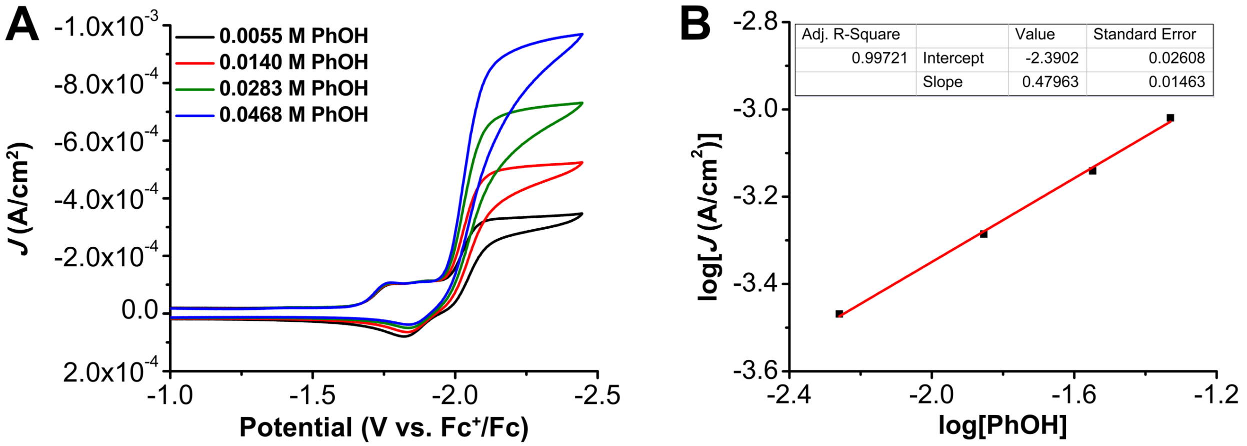

Figure S9. (**A**) CVs of 1.0 mM Cr(^{tbu}dh^{tbu}bpy)Cl(H_2O) **2**, obtained under CO_2 saturation conditions with variable PhOH concentration. Conditions: 1.0 mM **2**, 0.1 M $TBAPF_6$/DMF; glassy carbon working electrode, glassy carbon counter electrode, Ag/AgCl pseudoreference electrode; 100 mV/s scan rate; referenced to internal ferrocene standard. (**B**) Log-log plot from data obtained from CVs in **A** at −2.36 V vs. Fc^+/Fc.

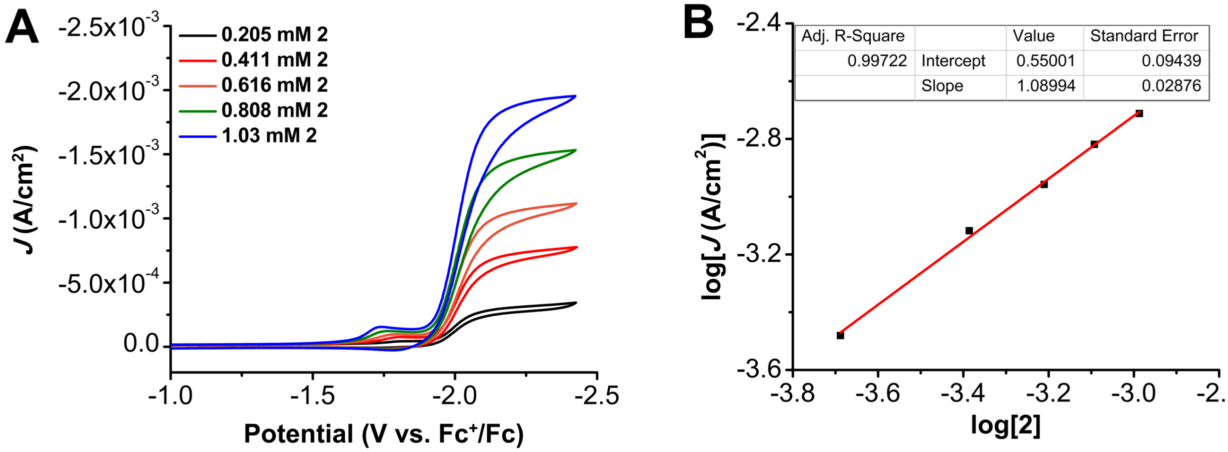

Figure S10. (**A**) CVs of Cr(^{tbu}dh^{tbu}bpy)Cl(H_2O) **2** at variable concentrations, obtained under CO_2 saturation with 0.325 M PhOH. Conditions: 0.1 M $TBAPF_6$/DMF; glassy carbon working electrode, glassy carbon counter electrode, Ag/AgCl pseudoreference electrode; 100 mV/s scan rate; referenced to internal ferrocene standard. (**B**) Log-log plot from data obtained from CVs in **A** at −2.36 V vs. Fc$^+$/Fc.

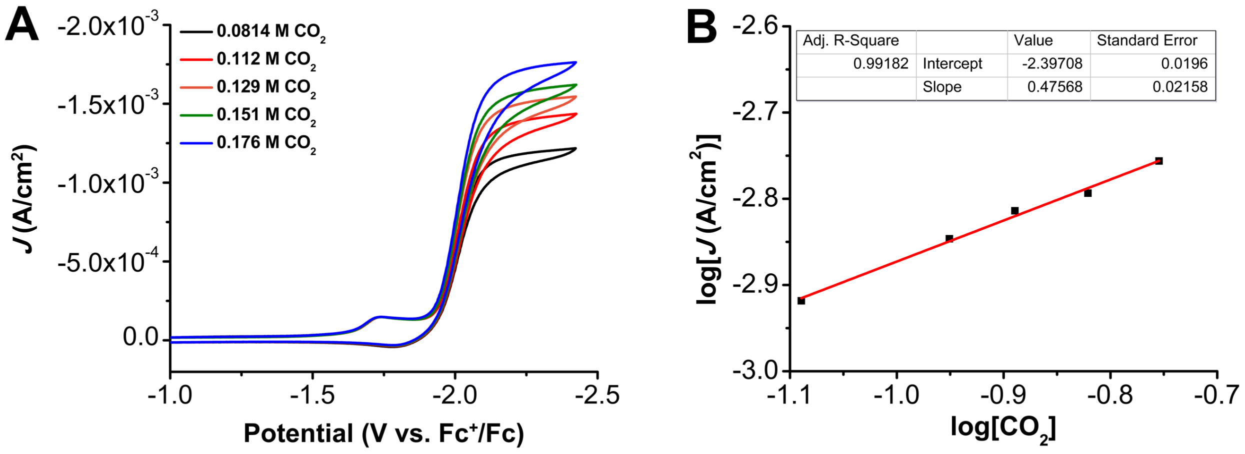

Figure S11. (**A**) CVs of 1.0 mM Cr(^{tbu}dh^{tbu}bpy)Cl(H_2O) **2** obtained under variable CO_2 concentration with 0.325 M PhOH. Conditions: 0.1 M $TBAPF_6$/DMF; glassy carbon working electrode, glassy carbon counter electrode, Ag/AgCl pseudoreference electrode; 100 mV/s scan rate; referenced to internal ferrocene standard. (**B**) Log–log plot from data obtained from CVs in **A** at −2.36 V vs. Fc$^+$/Fc.

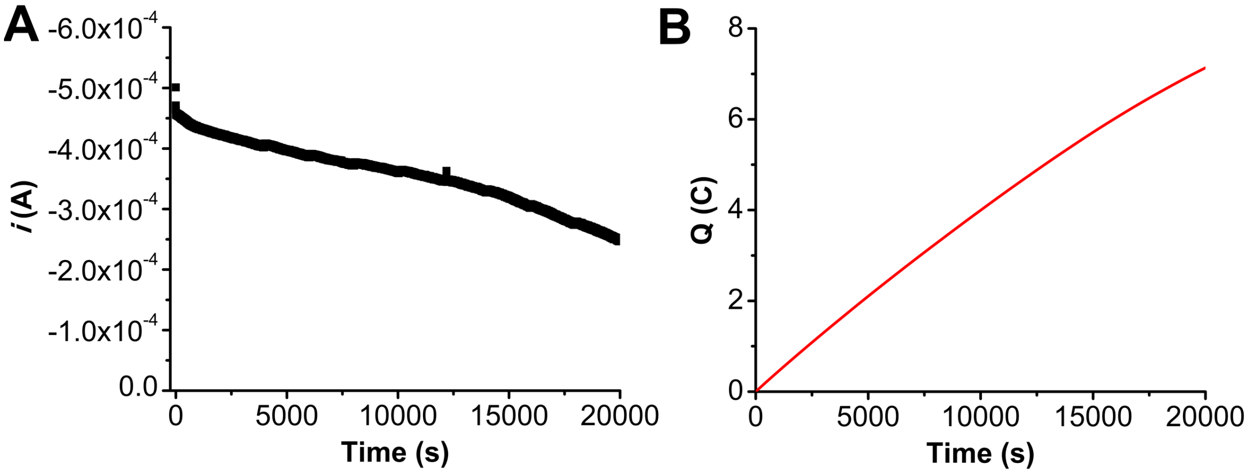

Figure S12. (**A**) Current versus time trace from CPE experiment for **2**+PhOH. (**B**) Charge passed versus time for the CPE experiment shown in **A**. Conditions were 0.1 mM Cr(^{tbu}dh^{tbu}bpy)Cl(H_2O) **2** and 0.12 M PhOH under a CO_2 atmosphere at −2.30 V vs Fc^+/Fc in 0.1 M $TBAPF_6$/*N,N*-DMF; working electrode was a glassy carbon rod, counter electrode was a graphite rod, and the reference was a nonaqueous Ag/AgCl pseudoreference electrode; 0.075 M Fc was used as sacrificial oxidant.

Table S4. Results from CPE experiment in Figure S12, **2** + PhOH.

Time (s)	**Charge (coulombs)**	**moles (e^-)**	**Moles of CO**	**FE_{CO}**
17914	6.58	6.82×10^{-5}	3.64×10^{-5}	106.8
20000*	7.14	7.40×10^{-5}	3.53×10^{-5}	95.34
20000*	7.14	7.40×10^{-5}	3.16×10^{-5}	85.34
20000*	7.14	7.40×10^{-5}	3.39×10^{-5}	91.68

* indicates a triplicate series of injections carried out upon completion of electrolysis.

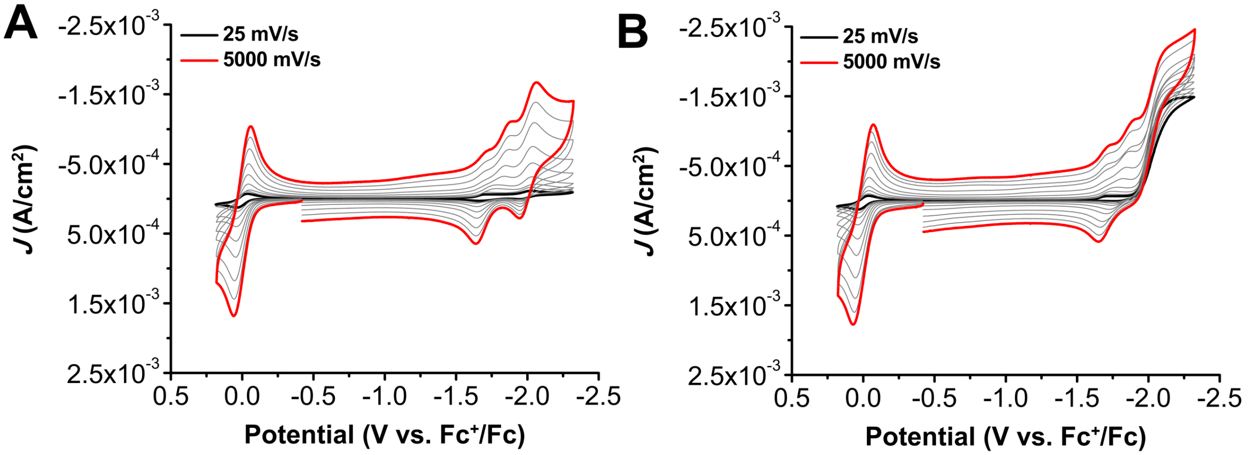

Figure S13. CVs of Cr(^{tbu}dh^{tbu}bpy)Cl(H_2O) **2** with 0.1 M PhOH at variable scan rates ranging from 25 (black) to 5000 (red) mV/s, obtained under Ar (**A**) and CO_2 (**B**) saturation conditions. Conditions: 1.0 mM **2**, 0.1 M $TBAPF_6$/DMF; glassy carbon working electrode, glassy carbon counter electrode, Ag/AgCl pseudoreference electrode; varied scan rate; referenced to internal ferrocene standard.

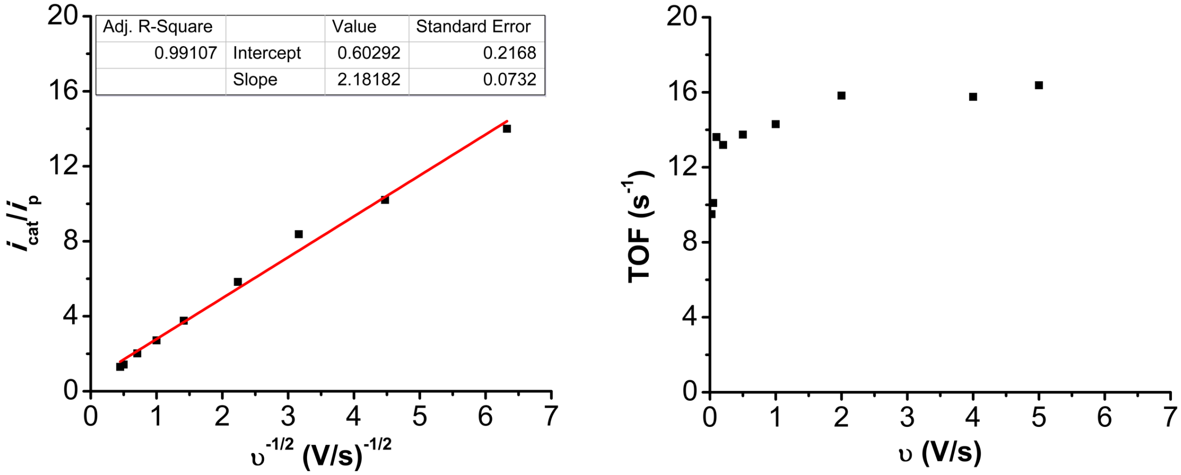

Adj. R-Square		Value	Standard Error
0.99107	Intercept	0.60292	0.2168
	Slope	2.18182	0.0732

Figure S14. Plots of (**A**) i_{cat}/i_p versus the inverse of the square root of the scan rate and (**B**) TOF Fversus scan rate for Cr(^{tbu}dh^{tbu}bpy)Cl(H_2O) **2**, with 0.1 M PhOH from data in Figure S13.

Table S5. TOF values determined from the i_{cat}/i_p method with variable scan rates in Figure S13 and S14.

Scan Rate (V/s)	TOF (s^{-1})
0.025	9.50
0.05	10.1
0.1	13.6
0.2	13.2
0.5	13.7
1	14.3
2	15.8
4	15.8
5	16.4

Characterization of RMs

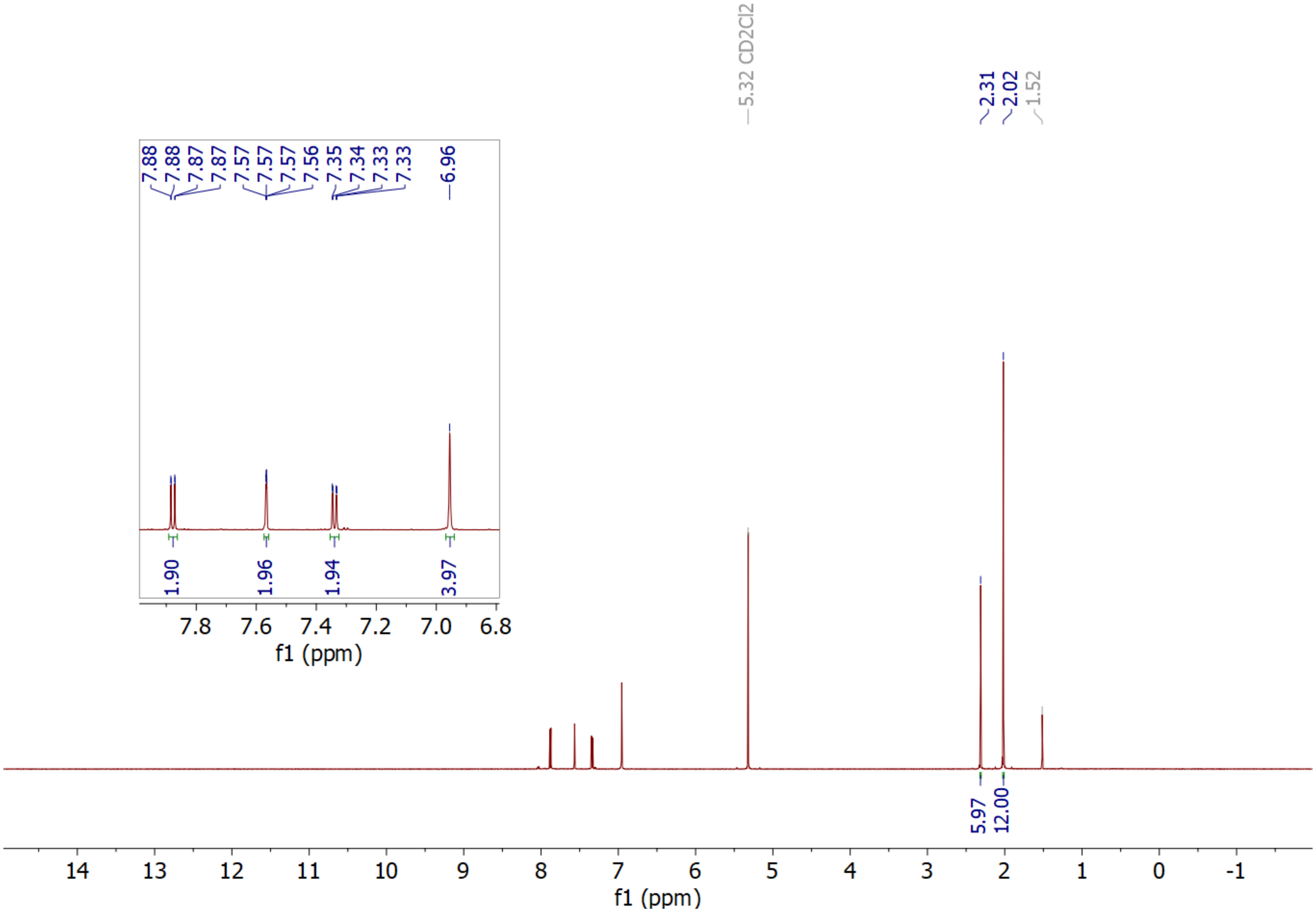

Figure S15. ^{1}H NMR of Mes$_2$DBTD; CD$_2$Cl$_2$; 600 MHz.

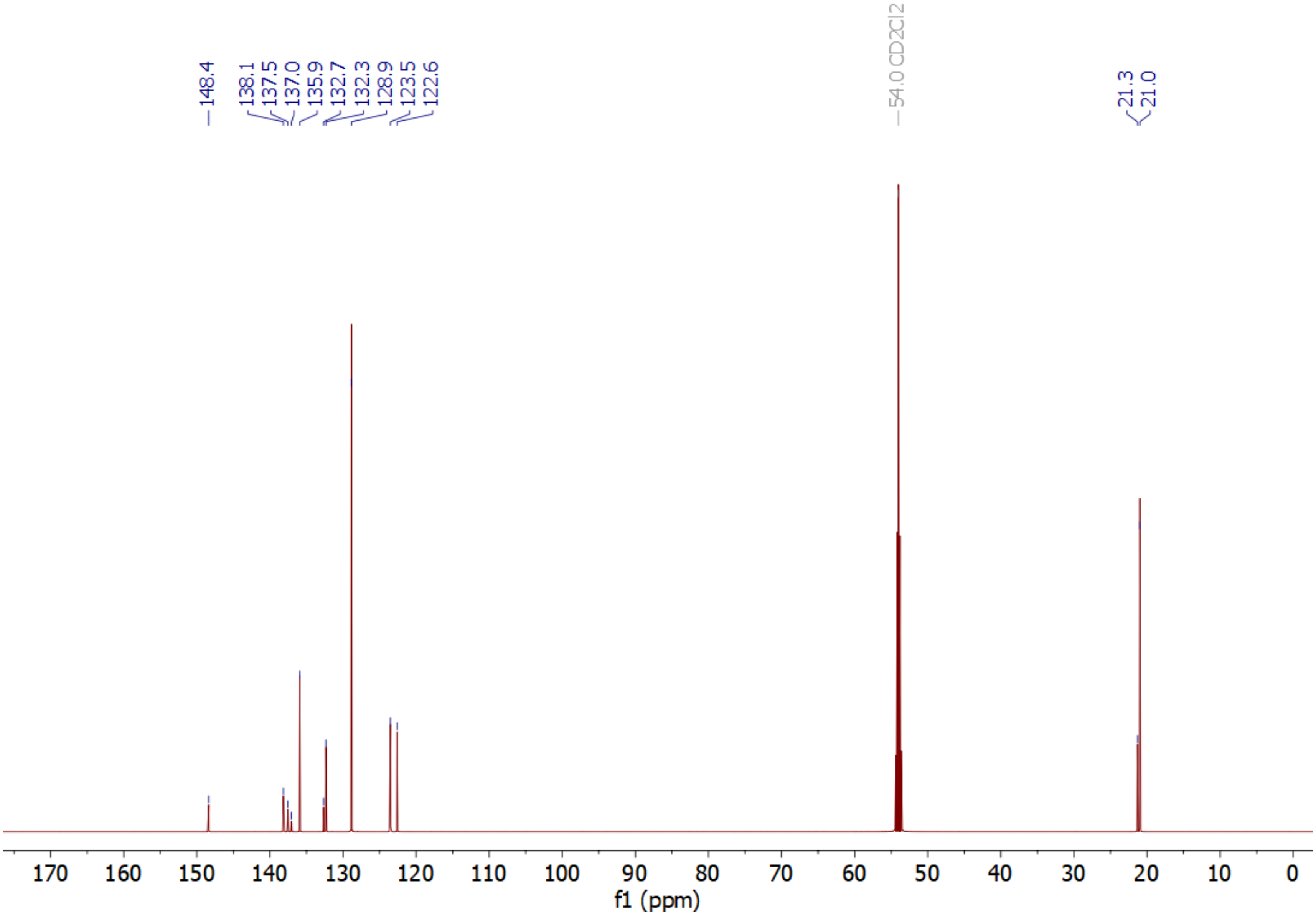

Figure S16. $^{13}C\{^{1}H\}$ NMR of Mes_2DBTD; CD_2Cl_2; 150 MHz.

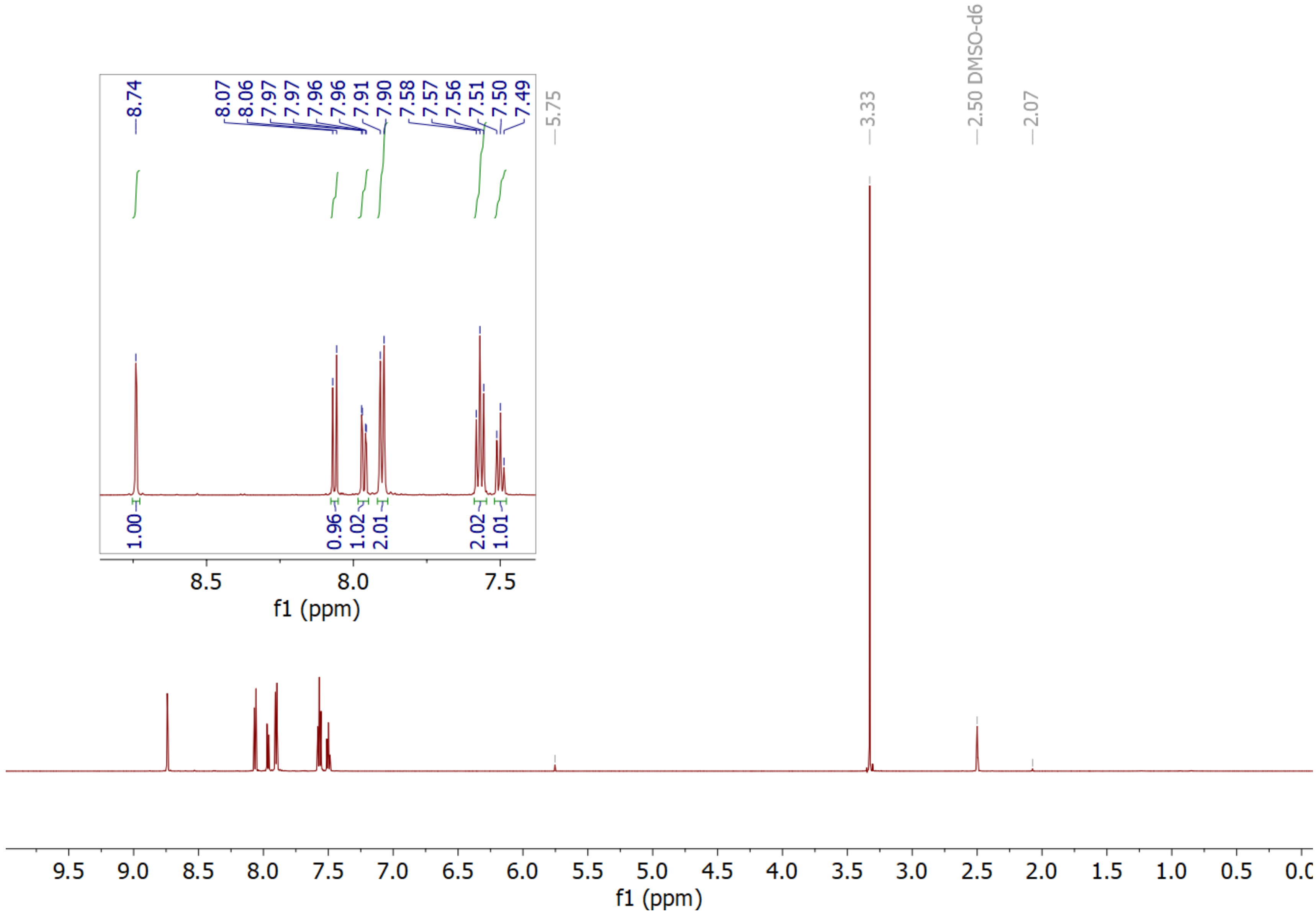

Figure S17. ^{1}H NMR of Ph_2DBTD; CD_2Cl_2; 600 MHz.

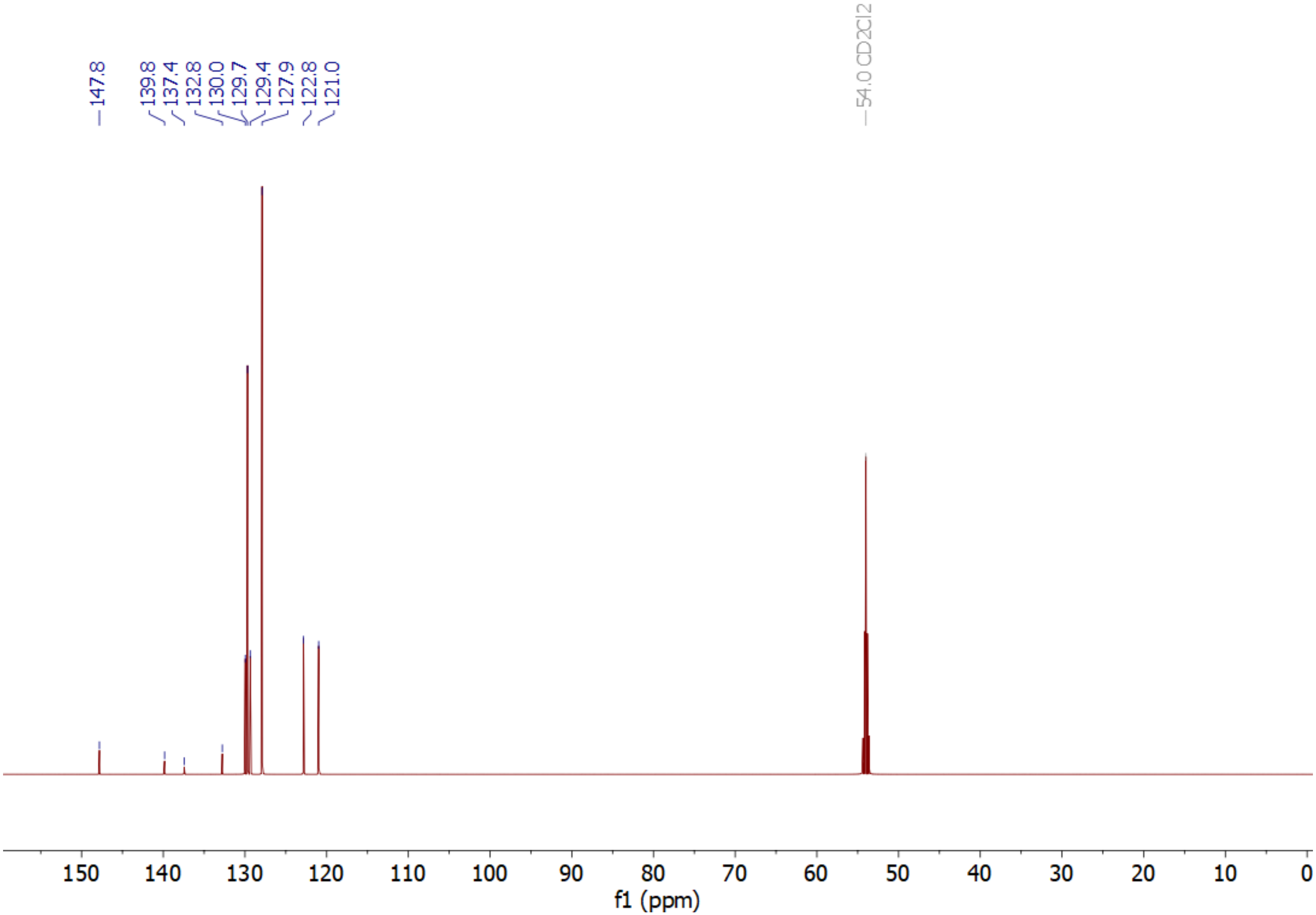

Figure S18. $^{13}C\{^{1}H\}$ NMR of Ph_2DBTD; CD_2Cl_2; 150 MHz.

Electrochemistry of RMs

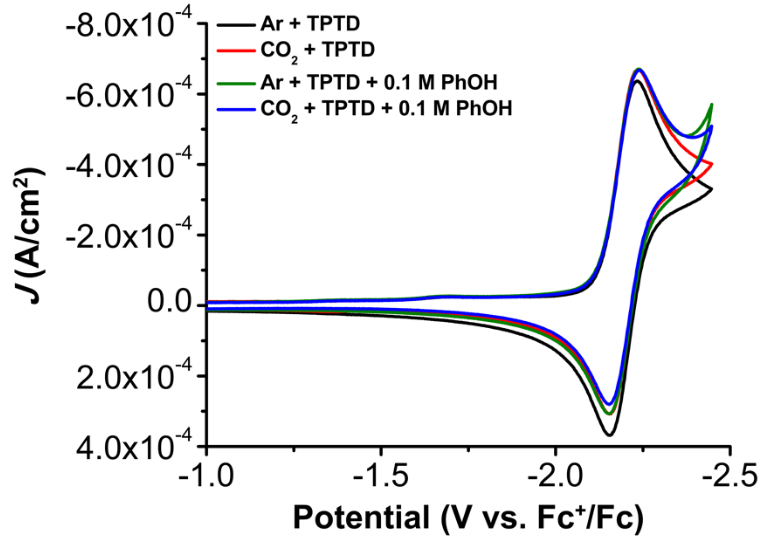

Figure S19. CVs of 2.5 mM TPTD both with and without 0.1 M PhOH obtained under Ar and CO_2 saturation conditions. Conditions: 0.1 M $TBAPF_6$/DMF; glassy carbon working electrode, glassy carbon rod counter electrode, Ag/AgCl pseudoreference electrode; referenced to Fc^+/Fc internal standard; 100 mV/s scan rate.

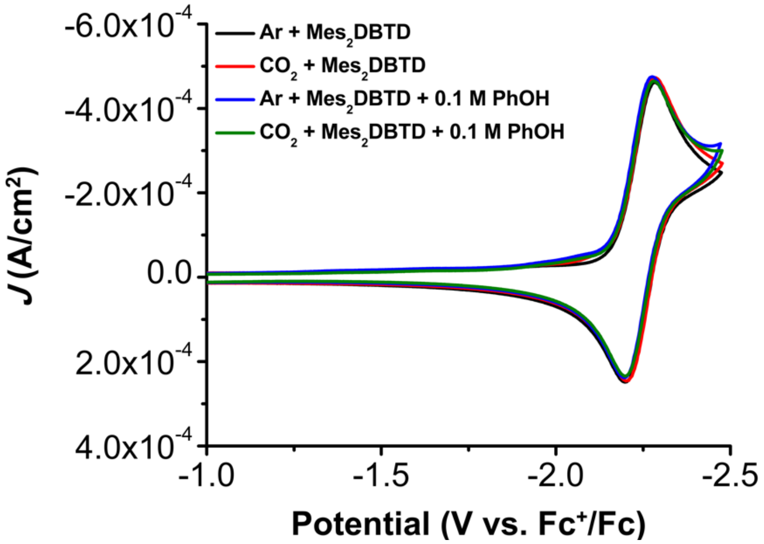

Figure S20. CVs of 2.5 mM Mes_2DBTD both with and without 0.1 M PhOH obtained under Ar and CO_2 saturation conditions. Conditions: 0.1 M $TBAPF_6$/DMF; glassy carbon working electrode, glassy carbon rod counter electrode, Ag/AgCl pseudoreference electrode; referenced to Fc^+/Fc internal standard; 100 mV/s scan rate.

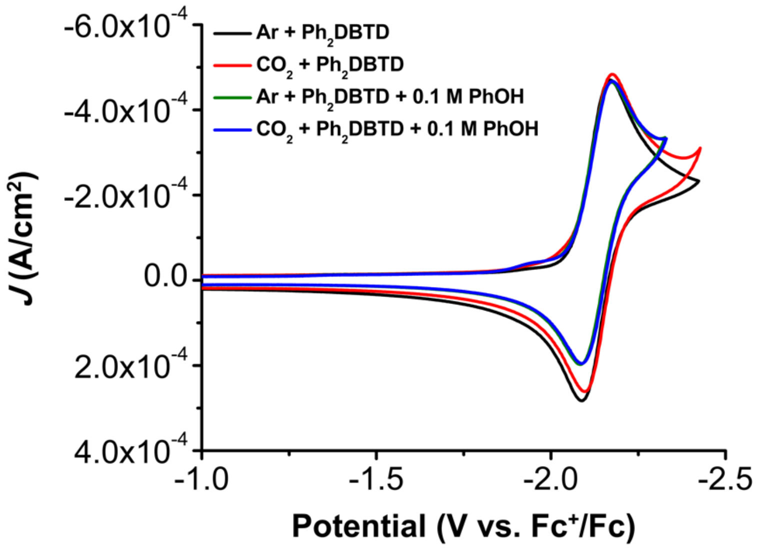

Figure S21. CVs of 2.5 mM Ph$_2$DBTD both with and without 0.1 M PhOH obtained under Ar and CO$_2$ saturation conditions. Conditions: 0.1 M TBAPF$_6$/DMF; glassy carbon working electrode, glassy carbon rod counter electrode, Ag/AgCl pseudoreference electrode; referenced to Fc$^+$/Fc internal standard; 100 mV/s scan rate.

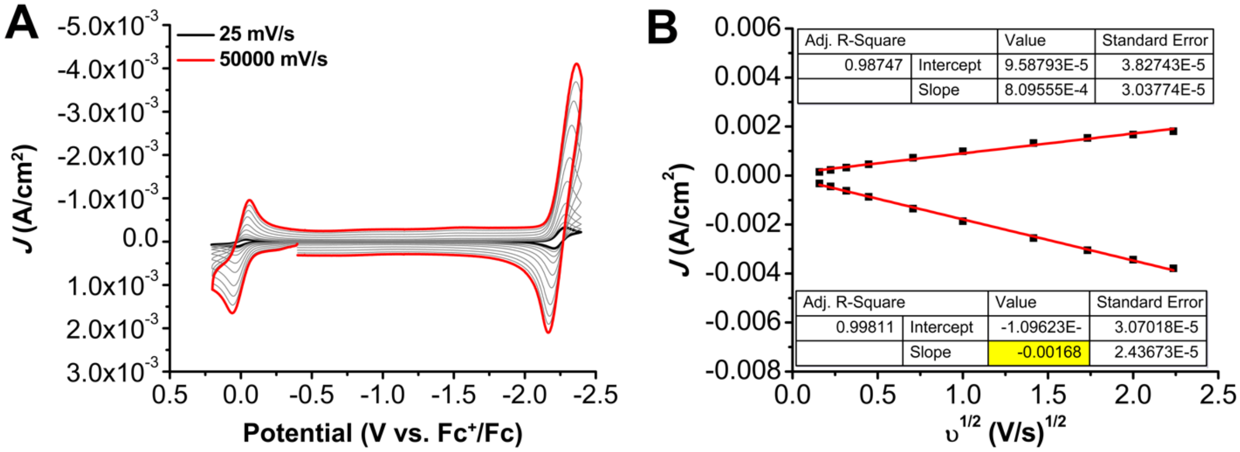

Adj. R-Square		Value	Standard Error
0.98747	Intercept	9.58793E-5	3.82743E-5
	Slope	8.09555E-4	3.03774E-5

Adj. R-Square		Value	Standard Error
0.99811	Intercept	-1.09623E-	3.07018E-5
	Slope	-0.00168	2.43673E-5

Figure S22. (**A**) CVs of 2.5 mM DBTD at variable scan rates ranging from 25 (black) to 5000 (red) mV/s, obtained under Ar saturation conditions. (**B**) Linear Fit of variable scan rate data from **A** demonstrating that DBTD shows a diffusion-limited current response. The slope highlighted in yellow was used to calculate the diffusion coefficient in Table S6. The data in **B** was obtained from the reversible redox feature at −2.25 V vs Fc$^+$/Fc. Conditions: 0.1 M TBAPF$_6$/DMF; glassy carbon working electrode, glassy carbon counter electrode, Ag/AgCl pseudoreference electrode; varied scan rate; referenced to internal ferrocene standard.

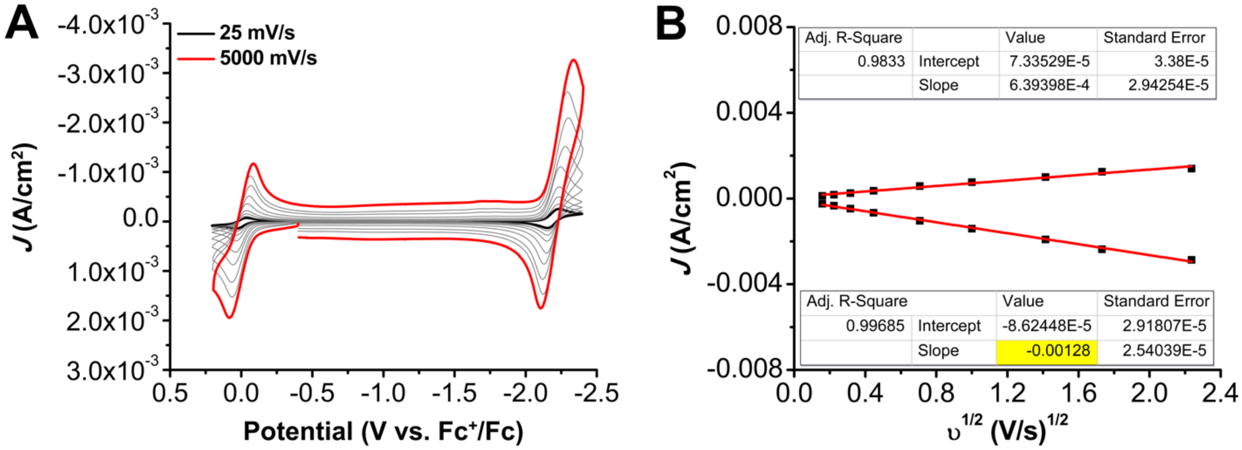

Figure S23. (**A**) CVs of 2.4 mM TPTD at variable scan rates ranging from 25 (black) to 5000 (red) mV/s, obtained under Ar saturation conditions. (**B**) Linear Fit of variable scan rate data from **A** demonstrating that DBTD shows a diffusion-limited current response. The slope highlighted in yellow was used to calculate the diffusion coefficient in Table S6. The data in **B** was obtained from the reversible redox feature at −2.19 V vs Fc^+/Fc. Conditions: 0.1 M $TBAPF_6$/DMF; glassy carbon working electrode, glassy carbon counter electrode, Ag/AgCl pseudoreference electrode; varied scan rate; referenced to internal ferrocene standard.

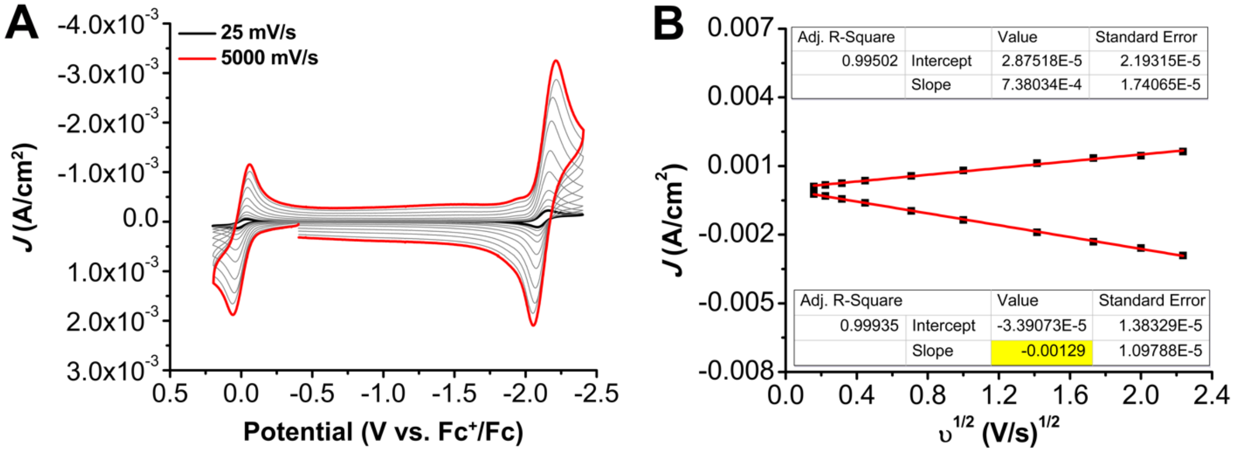

Figure S24. (**A**) CVs of 2.5 mM Ph_2DBTD at variable scan rates ranging from 25 (black) to 5000 (red) mV/s, obtained under Ar saturation conditions. (**B**) Linear Fit of variable scan rate data from **A** demonstrating that DBTD shows a diffusion-limited current response. The slope highlighted in yellow was used to calculate the diffusion coefficient in Table S6. The data in **B** was obtained from the reversible redox feature at −2.12 V vs Fc^+/Fc. Conditions: 0.1 M $TBAPF_6$/DMF; glassy carbon working electrode, glassy carbon counter electrode, Ag/AgCl pseudoreference electrode; varied scan rate; referenced to internal ferrocene standard.

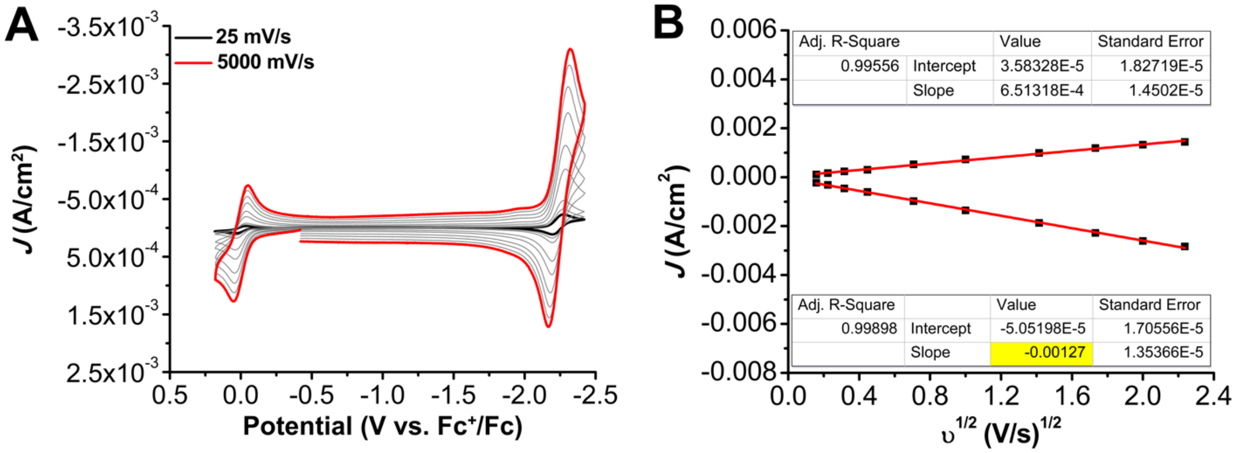

Figure 25. (**A**) CVs of 2.5 mM Mes_2DBTD at variable scan rates ranging from 25 (black) to 5000 (red) mV/s, obtained under Ar saturation conditions. (**B**) Linear Fit of variable scan rate data from **A** demonstrating that DBTD shows a diffusion-limited current response. The slope highlighted in yellow was used to calculate the diffusion coefficient in Table S6. The data in **B** was obtained from the reversible redox feature at −2.24 V vs Fc^+/Fc. Conditions: 0.1 M $TBAPF_6$/DMF; glassy carbon working electrode, glassy carbon counter electrode, Ag/AgCl pseudoreference electrode; varied scan rate; referenced to internal ferrocene standard.

Table S6. Results of Diffusion Coefficient Calculations

	Number of electrons	**Concentration (mM)**	**Slope**	**Diffusion Coefficient (cm^2/s)**
DBTD	1	2.50	−0.00168	6.22×10^{-6}
TPTD	1	2.40	−0.00128	3.93×10^{-6}
Ph_2DBTD	1	2.50	−0.00129	3.68×10^{-6}
Mes_2DBTD	1	2.50	-0.00127	3.57×10^{-6}

Cyclic Voltammetry Under Protic Conditions

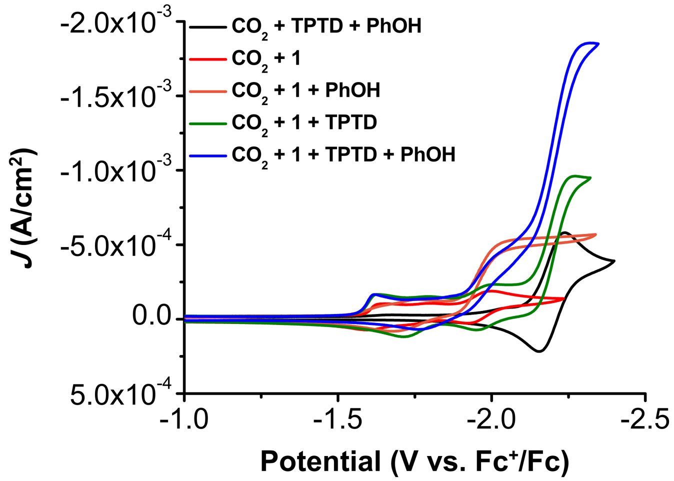

Figure S26. Comparison of CVs of 1.0 mM Cr(^{tbu}dhbpy)Cl(H_2O) **1** with and without 2.5 mM TPTD and 0.1 M PhOH under CO_2 saturation conditions. Conditions: 0.1 M $TBAPF_6$/DMF; glassy carbon working electrode, glassy carbon rod counter electrode, Ag/AgCl pseudoreference electrode; referenced to Fc^+/Fc internal standard; 100 mV/s scan rate.

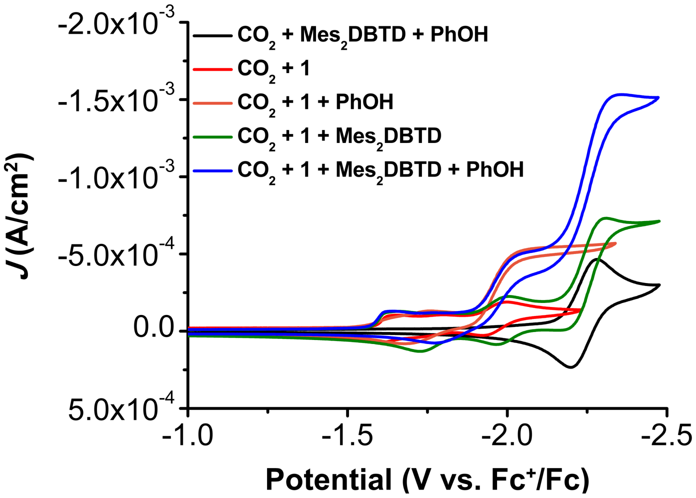

Figure S27. Comparison of CVs of 1.0 mM Cr(^{tbu}dhbpy)Cl(H_2O) **1** with and without 2.5 mM Mes_2DBTD and 0.1 M PhOH under CO_2 saturation conditions. Conditions: 0.1 M $TBAPF_6$/DMF; glassy carbon working electrode, glassy carbon rod counter electrode, Ag/AgCl pseudoreference electrode; referenced to Fc^+/Fc internal standard; 100 mV/s scan rate.

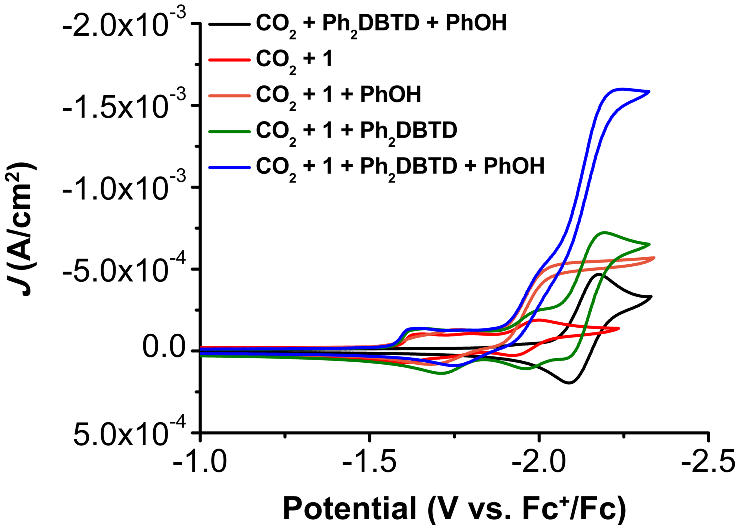

Figure S28. Comparison of CVs of 1.0 mM Cr(^{tbu}dhbpy)Cl(H_2O) **1** with and without 2.5 mM Ph_2DBTD and 0.1 M PhOH under CO_2 saturation conditions. Conditions: 0.1 M $TBAPF_6$/DMF; glassy carbon working electrode, glassy carbon rod counter electrode, Ag/AgCl pseudoreference electrode; referenced to Fc^+/Fc internal standard; 100 mV/s scan rate.

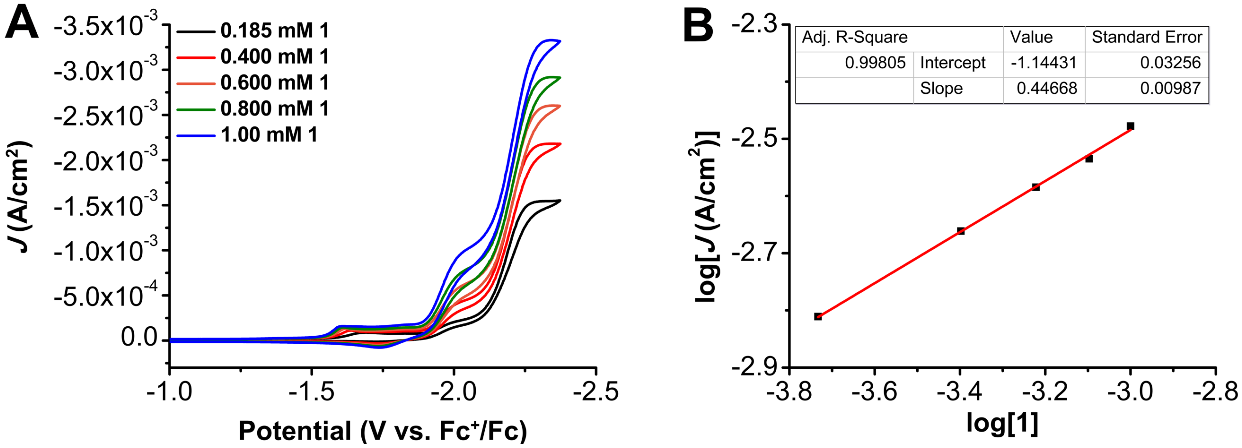

Figure S29. (**A**) CVs of Cr(^{tbu}dhbpy)Cl(H_2O) **1** at variable concentrations, obtained under CO_2 saturation with 2.5 mM TPTD and 0.325 M PhOH. Conditions: 0.1 M $TBAPF_6$/*N,N*-DMF; glassy carbon working electrode, glassy carbon counter electrode, Ag/AgCl pseudoreference electrode; 100 mV/s scan rate; referenced to internal ferrocene standard. (**B**) Log-log plot from data obtained from CVs in **A** at −2.34 V vs. Fc^+/Fc.

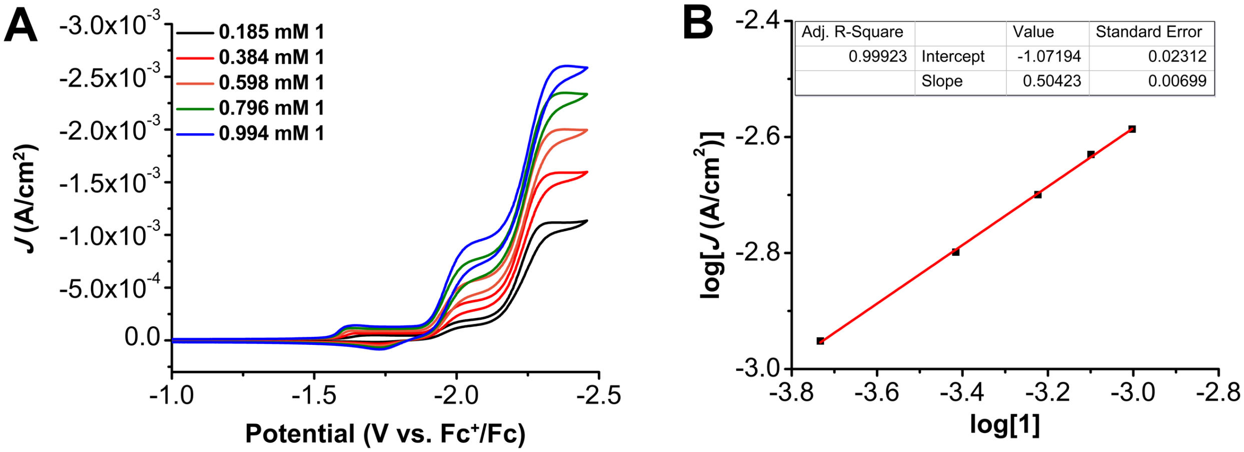

Figure S30. (**A**) CVs of Cr(^{tbu}dhbpy)Cl(H_2O) **1** at variable concentrations, obtained under CO_2 saturation with 2.5 mM Mes_2DBTD and 0.325 M PhOH. Conditions: 0.1 M $TBAPF_6$/*N,N*-DMF; glassy carbon working electrode, glassy carbon counter electrode, Ag/AgCl pseudoreference electrode; 100 mV/s scan rate; referenced to internal ferrocene standard. (**B**) Log-log plot from data obtained from CVs in **A** at −2.36 V vs. Fc^+/Fc.

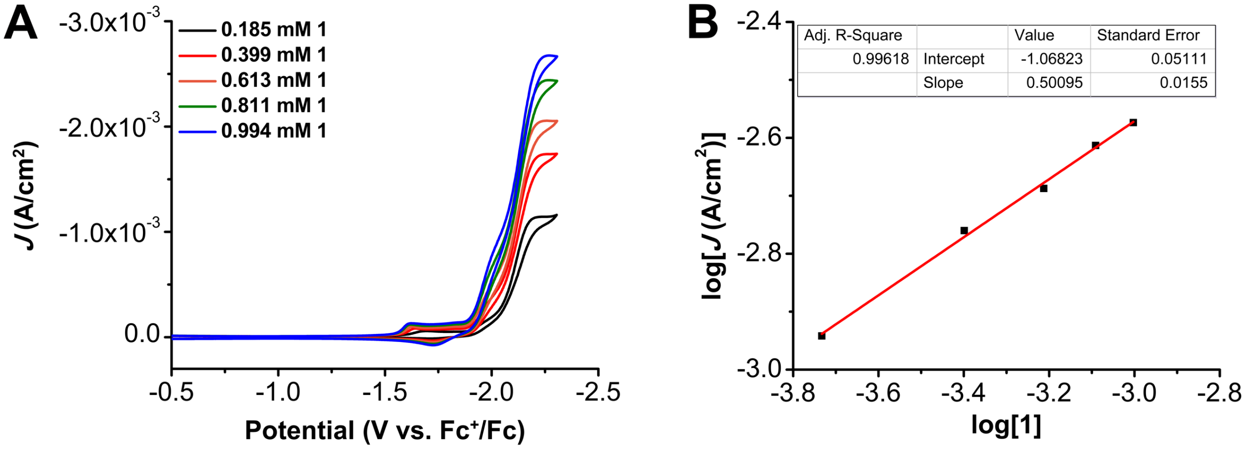

Figure S31. (**A**) CVs of Cr(^{tbu}dhbpy)Cl(H_2O) **1** at variable concentrations, obtained under CO_2 saturation with 2.5 mM Ph_2DBTD and 0.325 M PhOH. Conditions: 0.1 M $TBAPF_6$/*N,N*-DMF; glassy carbon working electrode, glassy carbon counter electrode, Ag/AgCl pseudoreference electrode; 100 mV/s scan rate; referenced to internal ferrocene standard. (**B**) Log-log plot from data obtained from CVs in **A** at −2.25 V vs. Fc^+/Fc.

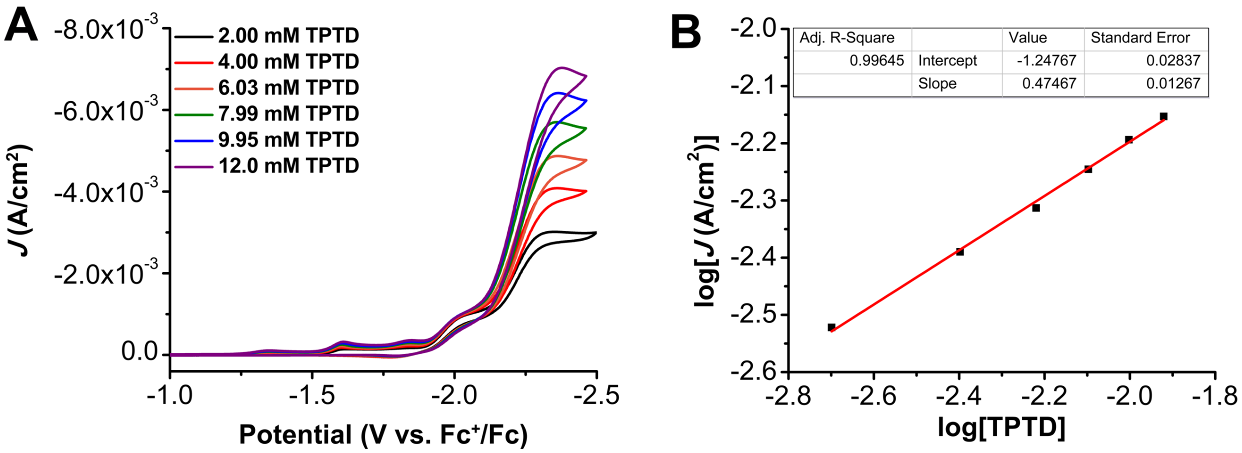

Adj. R-Square		Value	Standard Error
0.99645	Intercept	-1.24767	0.02837
	Slope	0.47467	0.01267

Figure S32. (**A**) CVs of 1.0 mM Cr($^{\text{tbu}}$dhbpy)Cl(H_2O) **1** with 0.325 M PhOH at variable TPTD concentrations, obtained under CO_2 saturation. Conditions: 0.1 M $TBAPF_6$/*N,N*-DMF; glassy carbon working electrode, glassy carbon counter electrode, Ag/AgCl pseudoreference electrode; 100 mV/s scan rate; referenced to internal ferrocene standard. (**B**) Log-log plot from data obtained from CVs in **A** at −2.38 V vs. Fc$^+$/Fc.

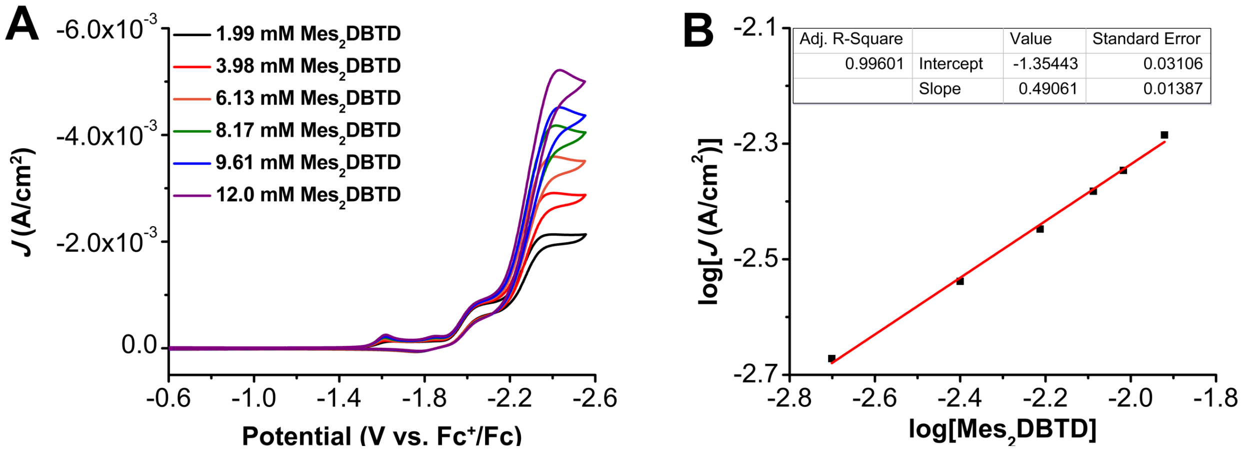

Adj. R-Square		Value	Standard Error
0.99601	Intercept	-1.35443	0.03106
	Slope	0.49061	0.01387

Figure S33. (**A**) CVs of 1.0 mM Cr($^{\text{tbu}}$dhbpy)Cl(H_2O) **1** with 0.325 M PhOH at variable Mes_2DBTD concentrations, obtained under CO_2 saturation. Conditions: 0.1 M $TBAPF_6$/*N,N*-DMF; glassy carbon working electrode, glassy carbon counter electrode, Ag/AgCl pseudoreference electrode; 100 mV/s scan rate; referenced to internal ferrocene standard. (**B**) Log-log plot from data obtained from CVs in **A** at −2.43 V vs. Fc$^+$/Fc.

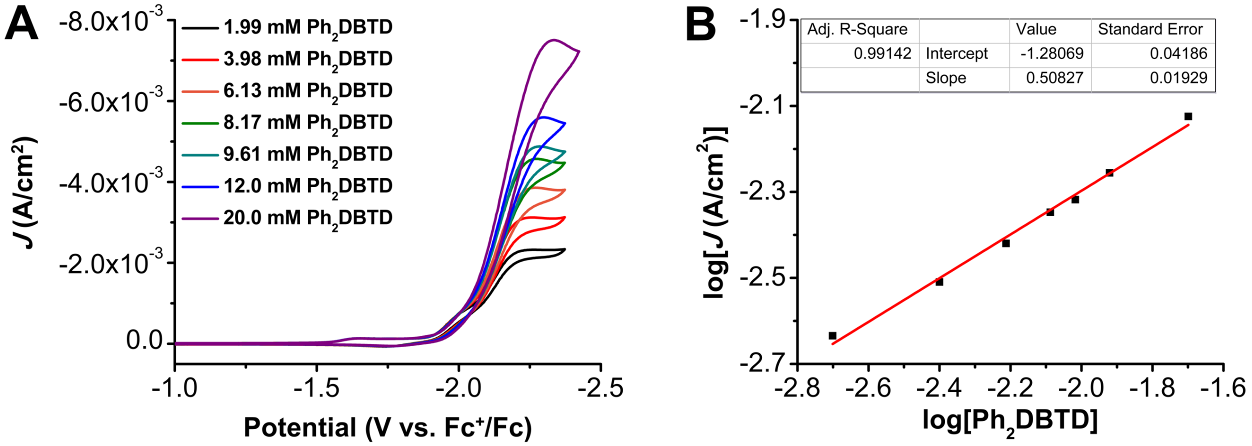

Figure S34. (**A**) CVs of 1.0 mM Cr(^{tbu}dhbpy)Cl(H_2O) **1** with 0.325 M PhOH at variable Ph_2DBTD concentrations, obtained under CO_2 saturation. Conditions: 0.1 M $TBAPF_6$/*N,N*-DMF; glassy carbon working electrode, glassy carbon counter electrode, Ag/AgCl pseudoreference electrode; 100 mV/s scan rate; referenced to internal ferrocene standard. (**B**) Log-log plot from data obtained from CVs in **A** at −2.33 V vs. Fc^+/Fc.

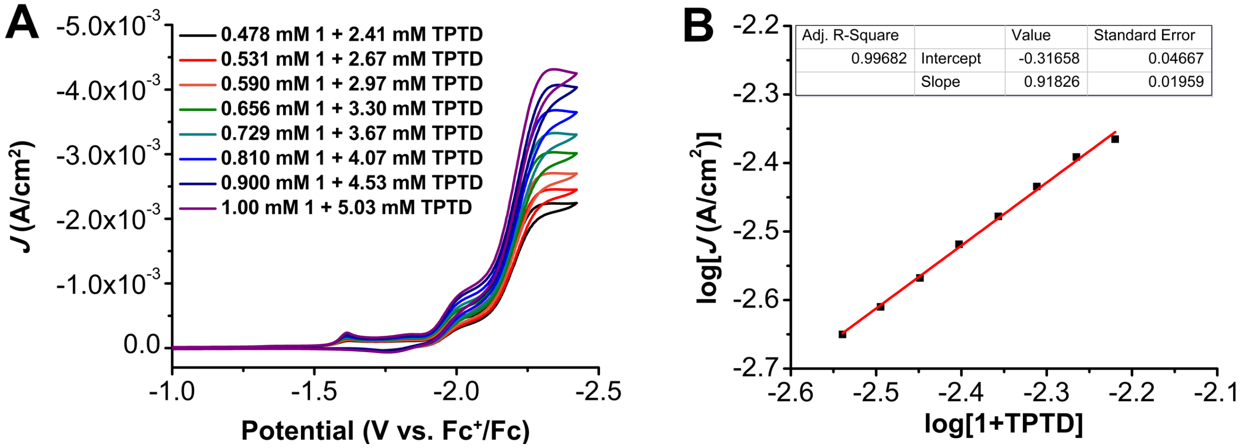

Figure S35. (**A**) CVs where the concentrations of Cr(^{tbu}dhbpy)Cl(H_2O) **1** and TPTD were varied at a fixed 1:5 ratio of **1**:TPTD with 0.325 M PhOH under CO_2 saturation conditions. Conditions: 0.1 M $TBAPF_6$/*N,N*-DMF; glassy carbon working electrode, glassy carbon counter electrode, Ag/AgCl pseudoreference electrode; 100 mV/s scan rate; referenced to internal ferrocene standard. (**B**) Log-log plot from data obtained from CVs in **A** at −2.34 V vs. Fc^+/Fc.

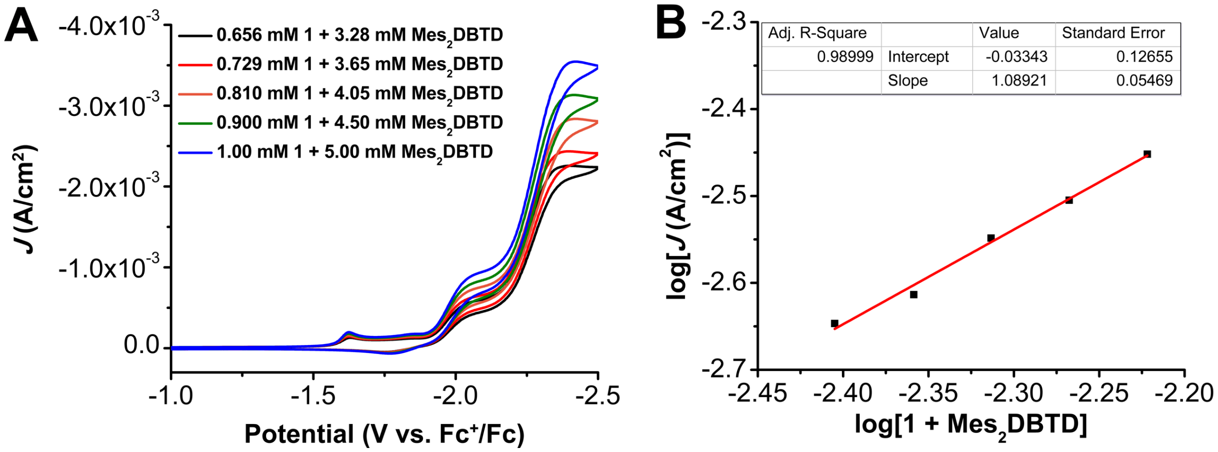

Figure S36. (**A**) CVs where the concentrations of Cr(^{tbu}dhbpy)Cl(H_2O) **1** and Mes_2DBTD were varied at a fixed 1:5 ratio of **1**:Mes_2DBTD with 0.325 M PhOH under CO_2 saturation conditions. Conditions: 0.1 M $TBAPF_6$/*N,N*-DMF; glassy carbon working electrode, glassy carbon counter electrode, Ag/AgCl pseudoreference electrode; 100 mV/s scan rate; referenced to internal ferrocene standard. (**B**) Log-log plot from data obtained from CVs in **A** at −2.40 V vs. Fc^+/Fc.

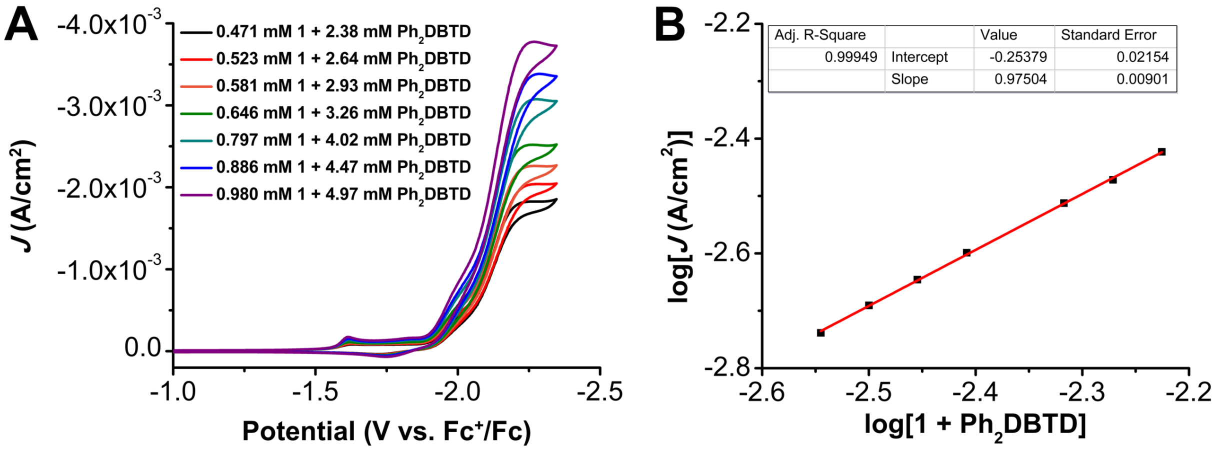

Figure S37. (**A**) CVs where the concentrations of Cr(^{tbu}dhbpy)Cl(H_2O) **1** and Ph_2DBTD were varied at a fixed 1:5 ratio of **1**:Ph_2DBTD with 0.325 M PhOH under CO_2 saturation conditions. Conditions: 0.1 M $TBAPF_6$/*N,N*-DMF; glassy carbon working electrode, glassy carbon counter electrode, Ag/AgCl pseudoreference electrode; 100 mV/s scan rate; referenced to internal ferrocene standard. (**B**) Log-log plot from data obtained from CVs in **A** at −2.27 V vs. Fc^+/Fc.

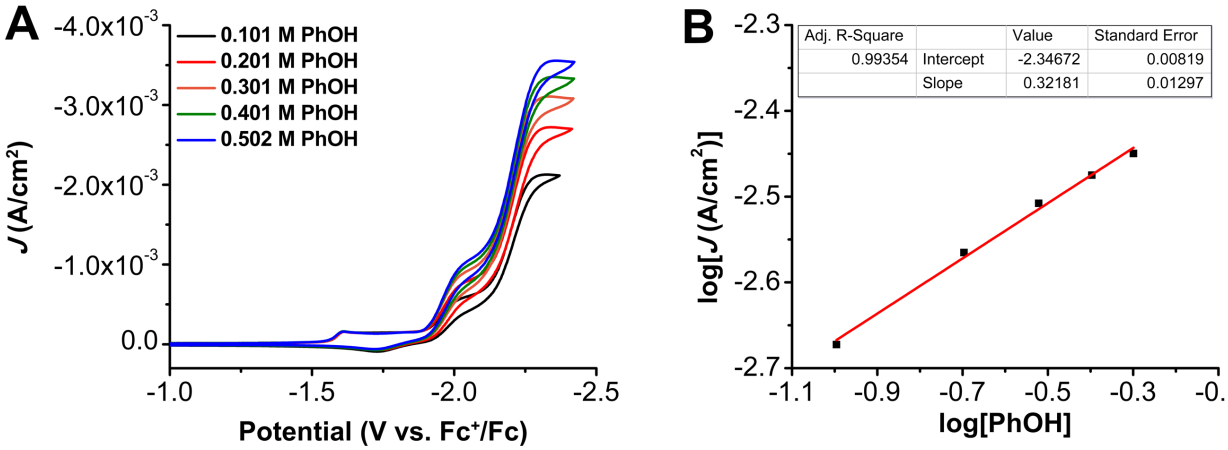

Figure S38. (**A**) CVs of PhOH at variable concentrations, obtained under CO_2 saturation with 1.0 mM Cr(^{tbu}dhbpy)Cl(H_2O) **1** and 2.5 mM TPTD. Conditions: 0.1 M $TBAPF_6$/*N,N*-DMF; glassy carbon working electrode, glassy carbon counter electrode, Ag/AgCl pseudoreference electrode; 100 mV/s scan rate; referenced to internal ferrocene standard. (**B**) Log-log plot from data obtained from CVs in **A** at −2.34 V vs. Fc^+/Fc.

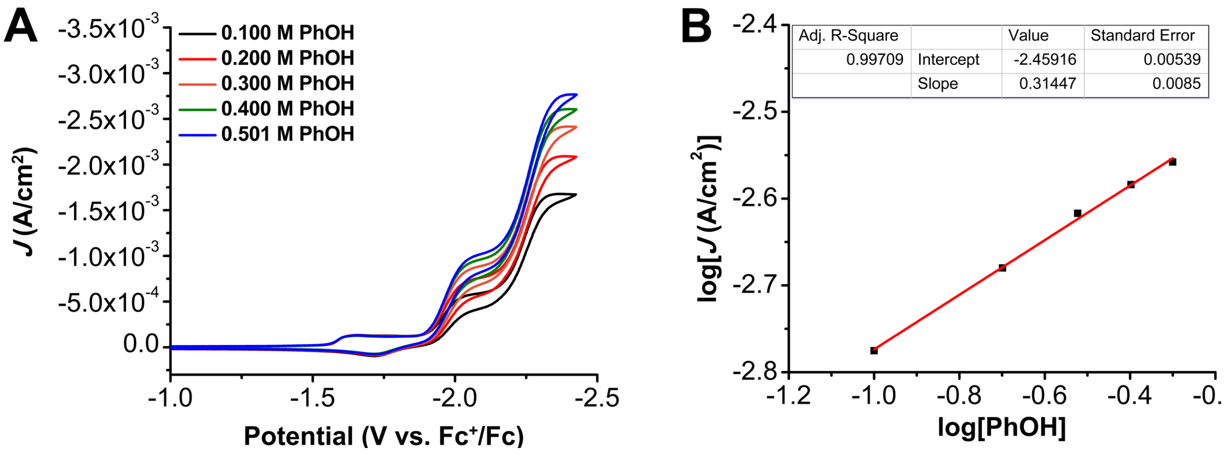

Figure S39. (**A**) CVs of PhOH at variable concentrations, obtained under CO_2 saturation with 1.0 mM Cr(^{tbu}dhbpy)Cl(H_2O) **1** and 2.5 mM Mes_2DBTD. Conditions: 0.1 M $TBAPF_6$/*N,N*-DMF; glassy carbon working electrode, glassy carbon counter electrode, Ag/AgCl pseudoreference electrode; 100 mV/s scan rate; referenced to internal ferrocene standard. (**B**) Log-log plot from data obtained from CVs in **A** at −2.40 V vs. Fc^+/Fc.

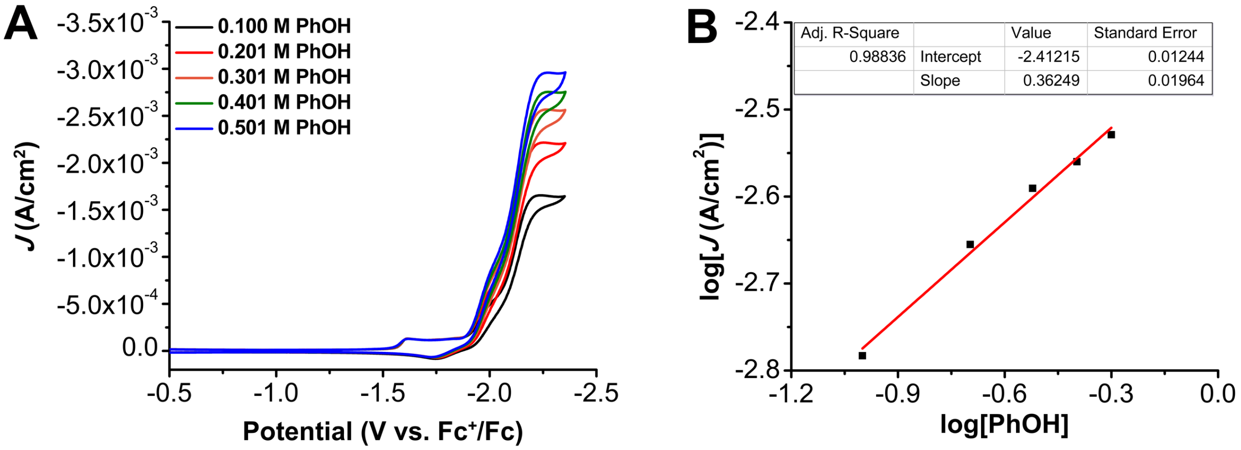

Figure S40. (**A**) CVs of PhOH at variable concentrations, obtained under CO_2 saturation with 1.0 mM Cr(^{tbu}dhbpy)Cl(H_2O) **1** and 2.5 mM Ph_2DBTD. Conditions: 0.1 M $TBAPF_6$/*N,N*-DMF; glassy carbon working electrode, glassy carbon counter electrode, Ag/AgCl pseudoreference electrode; 100 mV/s scan rate; referenced to internal ferrocene standard. (**B**) Log-log plot from data obtained from CVs in **A** at −2.27 V vs. Fc^+/Fc.

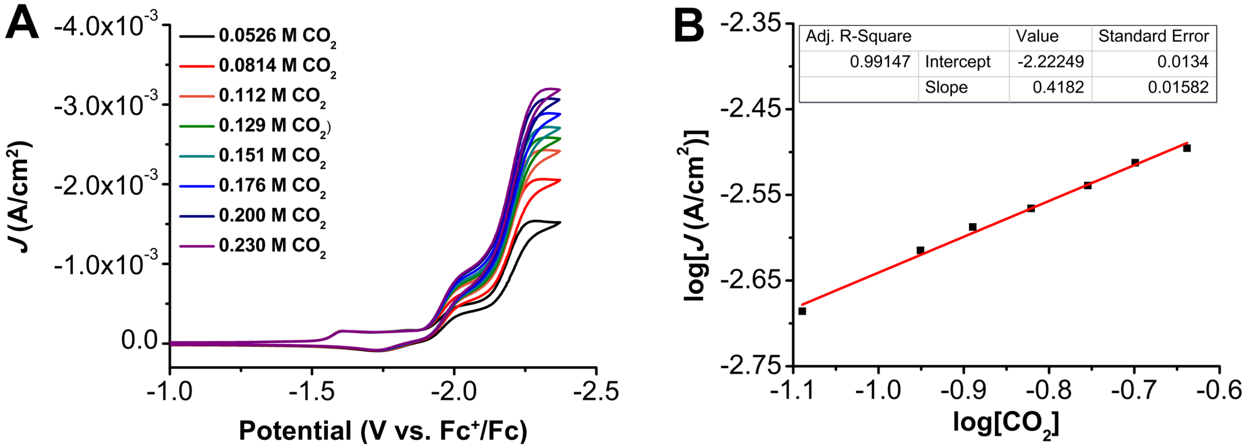

Figure S41. (**A**) CVs of 1.0 mM Cr(^{tbu}dhbpy)Cl(H_2O) **1**, 2.5 mM TPTD, 0.325 M PhOH at varied CO_2 concentrations. Conditions: 0.1 M $TBAPF_6$/*N,N*-DMF; glassy carbon working electrode, glassy carbon counter electrode, Ag/AgCl pseudoreference electrode; 100 mV/s scan rate; referenced to internal ferrocene standard. (**B**) Log-log plot from data obtained from CVs in **A** at −2.29 V vs. Fc^+/Fc.

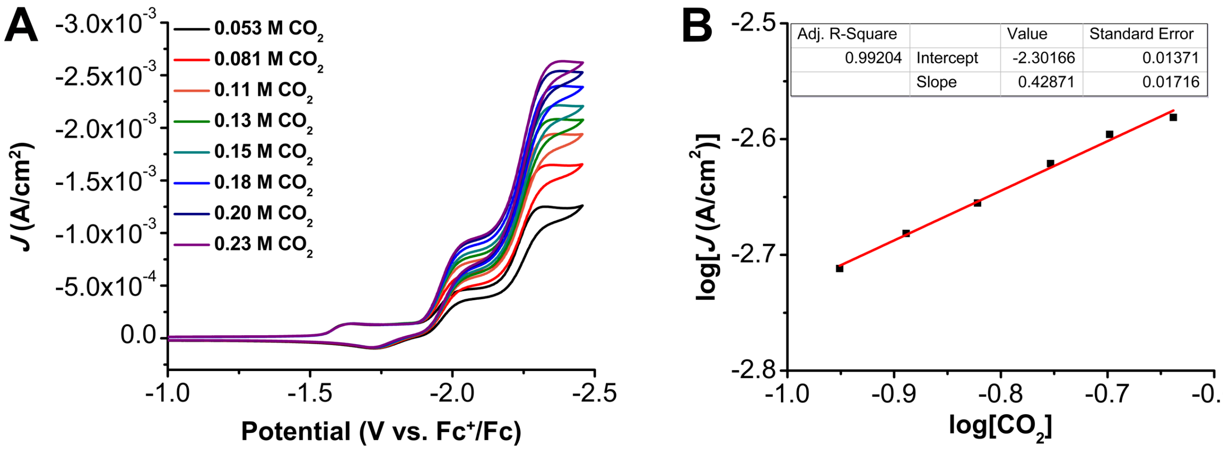

Figure S42. (**A**) CVs of 1.0 mM Cr(^{tbu}dhbpy)Cl(H_2O) **1**, 2.5 mM Mes_2DBTD, 0.325 M PhOH at varied CO_2 concentrations. Conditions: 0.1 M $TBAPF_6$/*N,N*-DMF; glassy carbon working electrode, glassy carbon counter electrode, Ag/AgCl pseudoreference electrode; 100 mV/s scan rate; referenced to internal ferrocene standard. (**B**) Log-log plot from data obtained from CVs in **A** at −2.36 V vs. Fc^+/Fc.

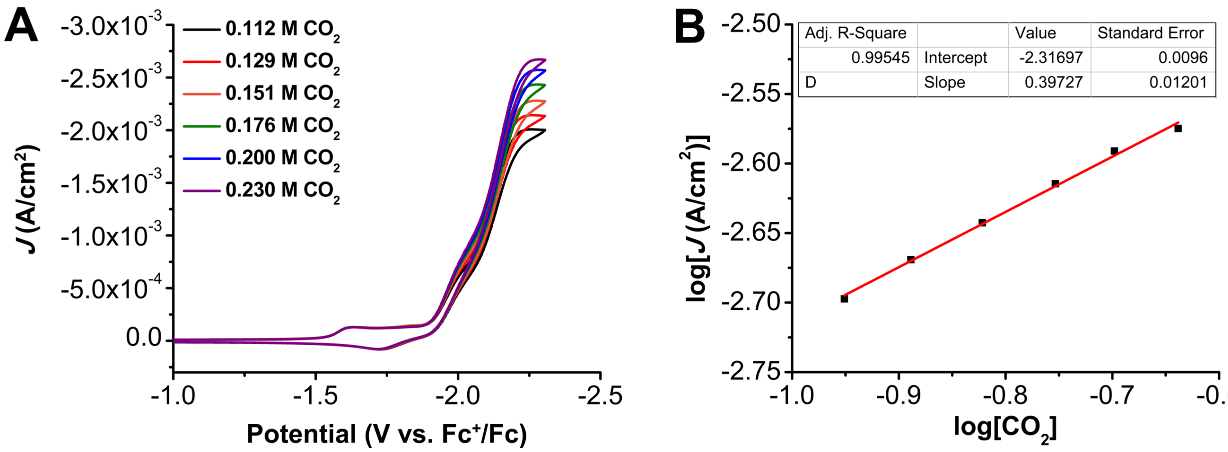

Figure S43. (**A**) CVs of 1.0 mM Cr(^{tbu}dhbpy)Cl(H_2O) **1**, 2.5 mM Ph_2DBTD, 0.325 M PhOH at varied CO_2 concentrations. Conditions: 0.1 M $TBAPF_6$/*N,N*-DMF; glassy carbon working electrode, glassy carbon counter electrode, Ag/AgCl pseudoreference electrode; 100 mV/s scan rate; referenced to internal ferrocene standard. (**B**) Log-log plot from data obtained from CVs in **A** at −2.26 V vs. Fc^+/Fc.

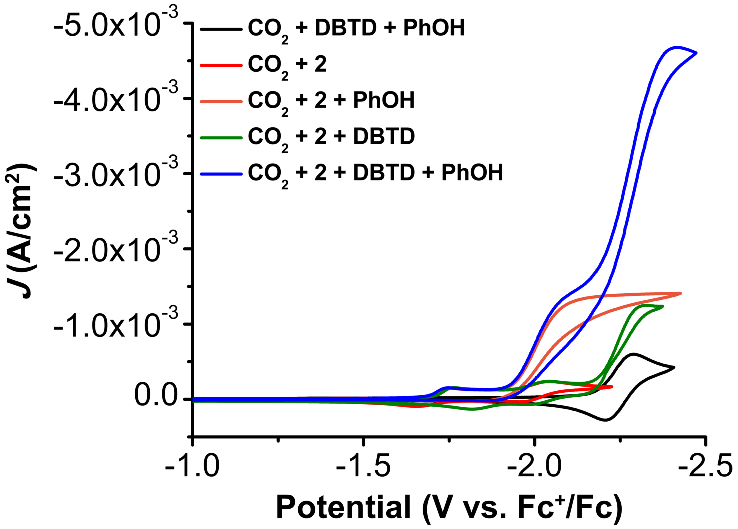

Figure S44. Comparison of CVs of 1.0 mM Cr(^{tbu}dh^{tbu}bpy)Cl(H_2O) **2** with and without 2.5 mM DBTD and 0.1 M PhOH under CO_2 saturation conditions. Conditions: 0.1 M $TBAPF_6$/DMF; glassy carbon working electrode, glassy carbon rod counter electrode, Ag/AgCl pseudoreference electrode; referenced to Fc$^+$/Fc internal standard; 100 mV/s scan rate.

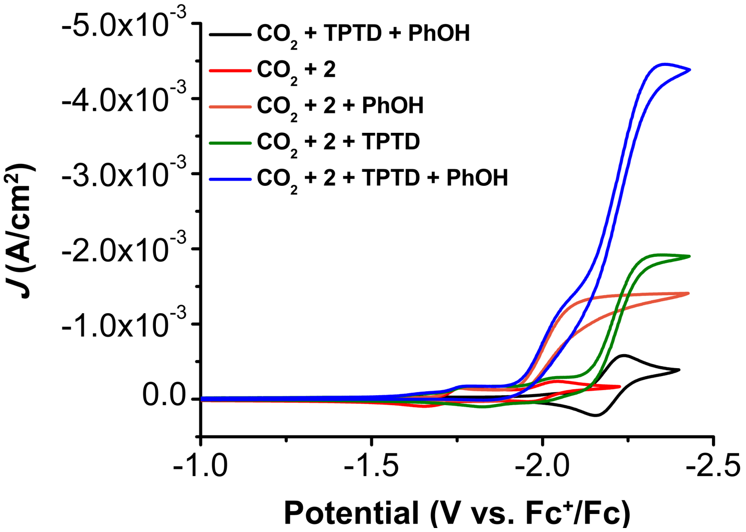

Figure S45. Comparison of CVs of 1.0 mM Cr(^{tbu}dh^{tbu}bpy)Cl(H_2O) **2** with and without 2.5 mM TPTD and 0.1 M PhOH under CO_2 saturation conditions. Conditions: 0.1 M $TBAPF_6$/DMF; glassy carbon working electrode, glassy carbon rod counter electrode, Ag/AgCl pseudoreference electrode; referenced to Fc$^+$/Fc internal standard; 100 mV/s scan rate.

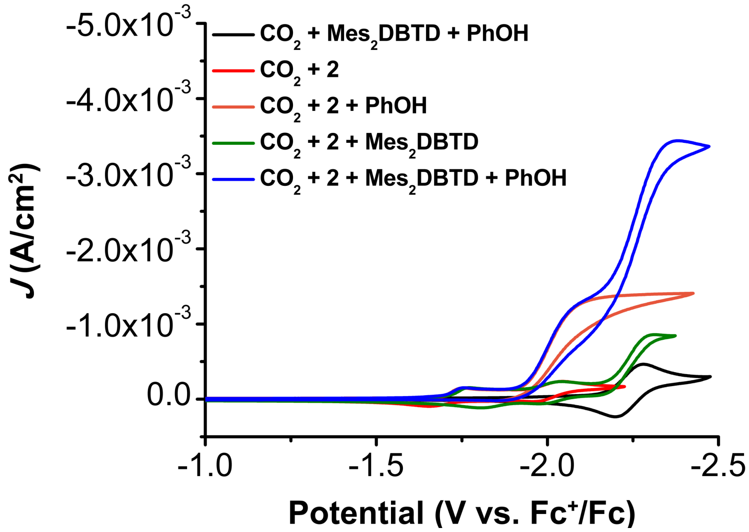

Figure S46. Comparison of CVs of 1.0 mM Cr(^{tbu}dh^{tbu}bpy)Cl(H_2O) **2** with and without 2.5 mM Mes_2DBTD and 0.1 M PhOH under CO_2 saturation conditions. Conditions: 0.1 M TBAPF$_6$/DMF; glassy carbon working electrode, glassy carbon rod counter electrode, Ag/AgCl pseudoreference electrode; referenced to Fc$^+$/Fc internal standard; 100 mV/s scan rate.

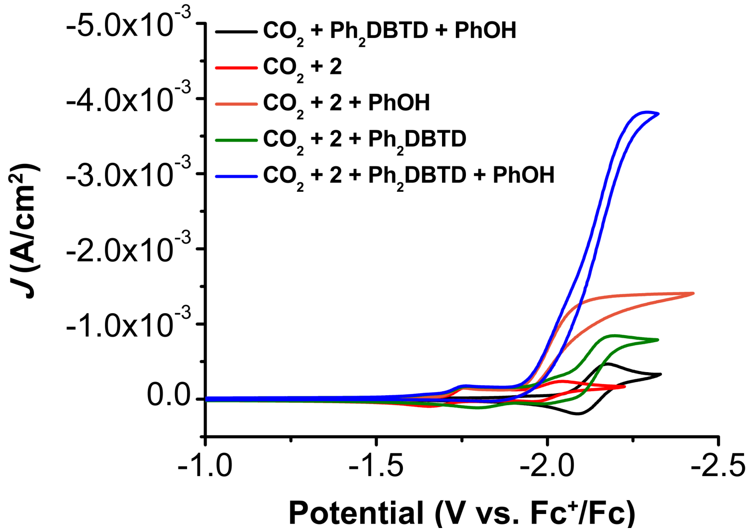

Figure S47. Comparison of CVs of 1.0 mM Cr(^{tbu}dh^{tbu}bpy)Cl(H_2O) **2** with and without 2.5 mM Ph_2DBTD and 0.1 M PhOH under CO_2 saturation conditions. Conditions: 0.1 M TBAPF$_6$/DMF; glassy carbon working electrode, glassy carbon rod counter electrode, Ag/AgCl pseudoreference electrode; referenced to Fc$^+$/Fc internal standard; 100 mV/s scan rate.

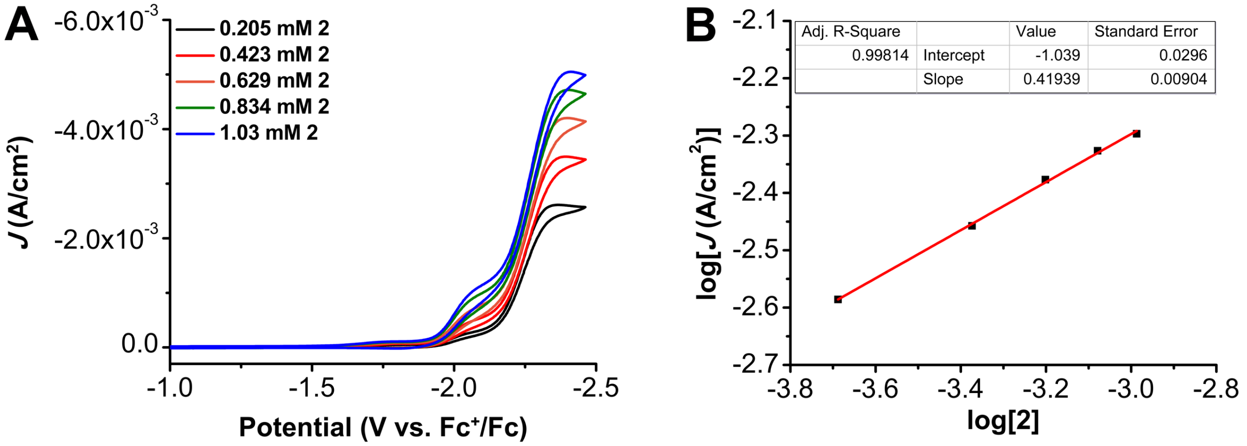

Figure S48. (**A**) CVs of Cr(^{tbu}dh^{tbu}bpy)Cl(H_2O) **2** at variable concentrations, obtained under CO_2 saturation with 2.5 mM DBTD and 0.325 M PhOH. Conditions: 0.1 M $TBAPF_6$/*N,N*-DMF; glassy carbon working electrode, glassy carbon counter electrode, Ag/AgCl pseudoreference electrode; 100 mV/s scan rate; referenced to internal ferrocene standard. (**B**) Log-log plot from data obtained from CVs in **A** at −2.41 V vs. Fc$^+$/Fc.

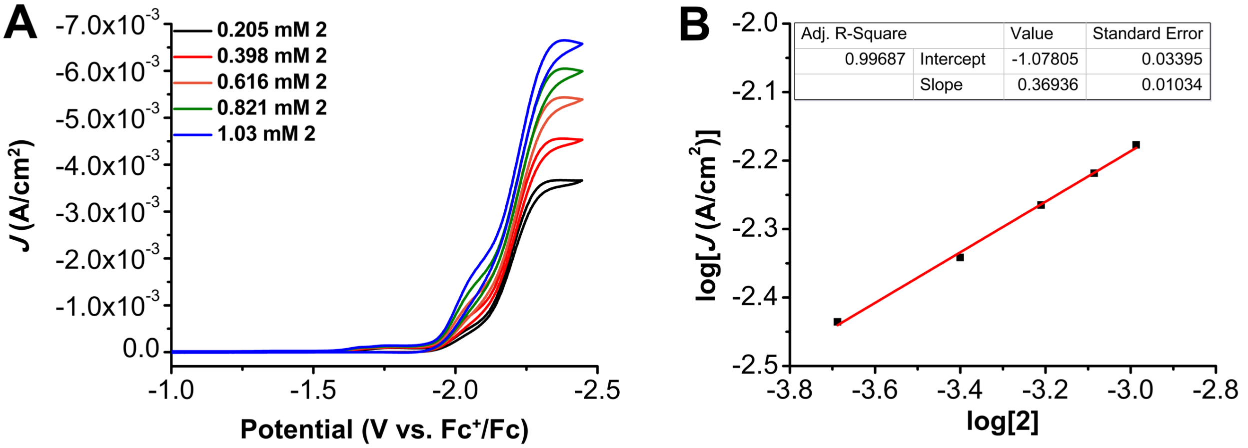

Figure S49. (**A**) CVs of Cr(^{tbu}dh^{tbu}bpy)Cl(H_2O) **2** at variable concentrations, obtained under CO_2 saturation with 2.5 mM TPTD and 0.325 M PhOH. Conditions: 0.1 M $TBAPF_6$/*N,N*-DMF; glassy carbon working electrode, glassy carbon counter electrode, Ag/AgCl pseudoreference electrode; 100 mV/s scan rate; referenced to internal ferrocene standard. (**B**) Log-log plot from data obtained from CVs in **A** at −2.38 V vs. Fc$^+$/Fc.

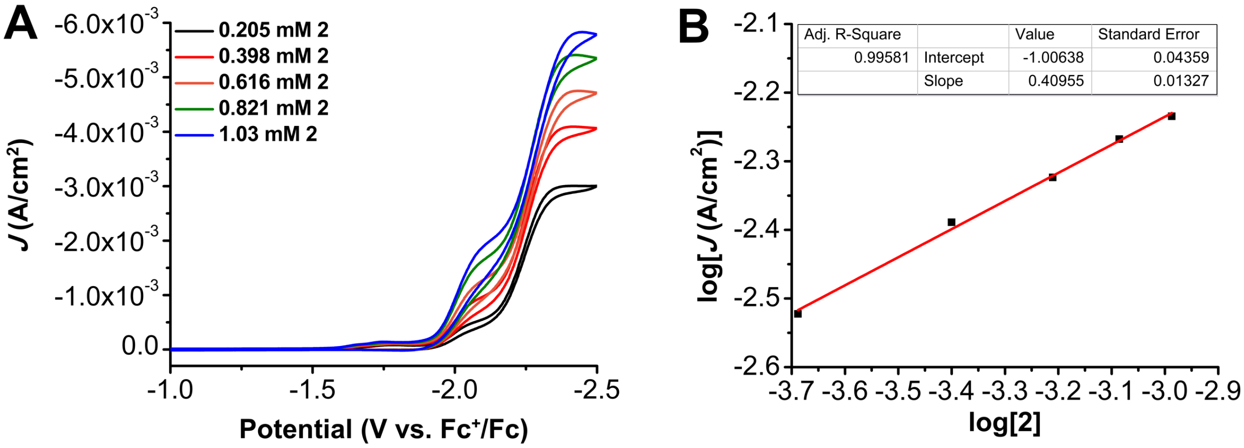

Figure S50. (**A**) CVs of Cr(^{tbu}dh^{tbu}bpy)Cl(H_2O) **2** at variable concentrations, obtained under CO_2 saturation with 2.5 mM Mes_2DBTD and 0.325 M PhOH. Conditions: 0.1 M $TBAPF_6$/*N,N*-DMF; glassy carbon working electrode, glassy carbon counter electrode, Ag/AgCl pseudoreference electrode; 100 mV/s scan rate; referenced to internal ferrocene standard. (**B**) Log-log plot from data obtained from CVs in **A** at −2.45 V vs. Fc^+/Fc.

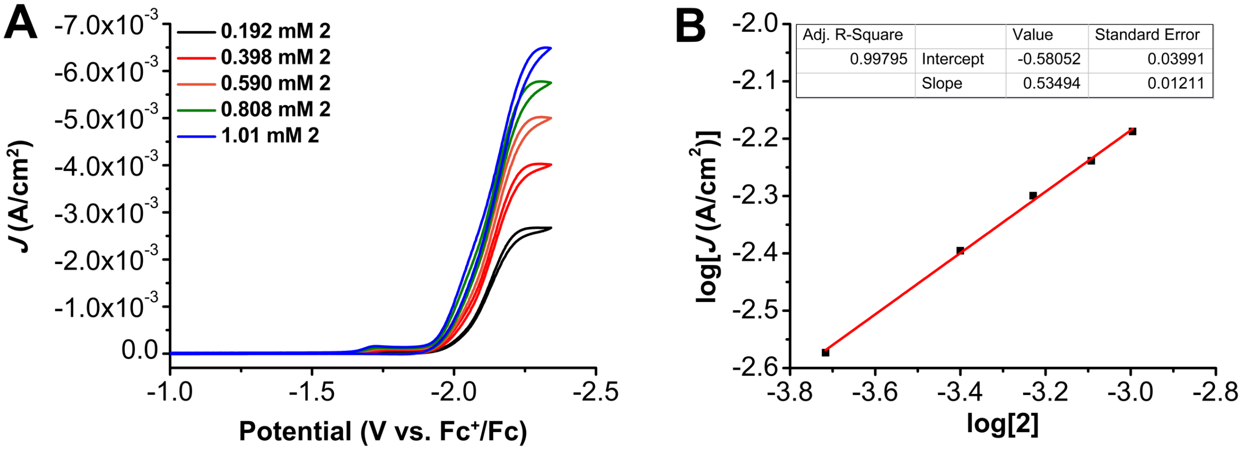

Figure S51. (**A**) CVs of Cr(^{tbu}dh^{tbu}bpy)Cl(H_2O) **2** at variable concentrations, obtained under CO_2 saturation with 2.5 mM Ph_2DBTD and 0.325 M PhOH. Conditions: 0.1 M $TBAPF_6$/*N,N*-DMF; glassy carbon working electrode, glassy carbon counter electrode, Ag/AgCl pseudoreference electrode; 100 mV/s scan rate; referenced to internal ferrocene standard. (**B**) Log-log plot from data obtained from CVs in **A** at −2.32 V vs. Fc^+/Fc.

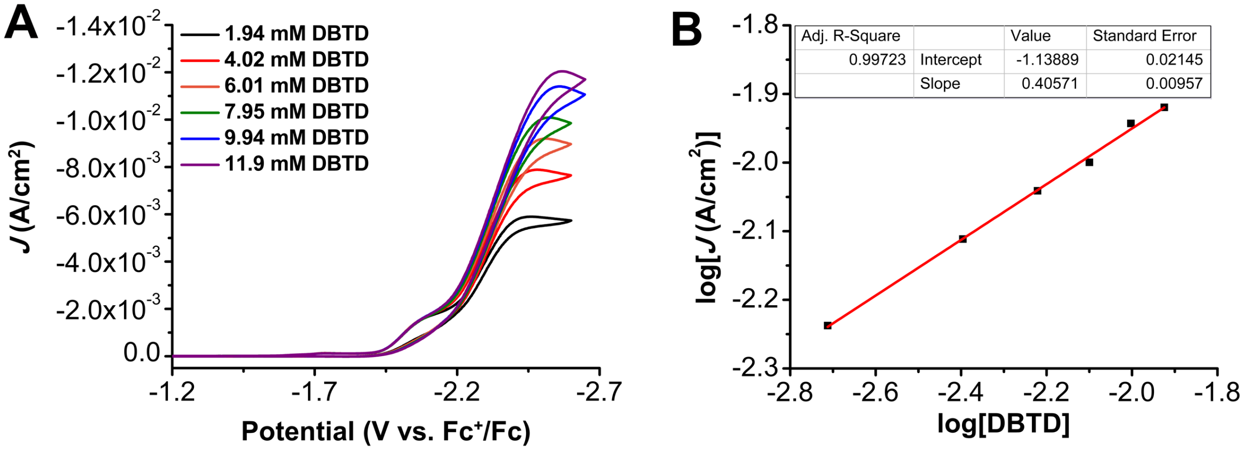

Adj. R-Square		Value	Standard Error
0.99723	Intercept	-1.13889	0.02145
	Slope	0.40571	0.00957

Figure S52. (**A**) CVs of 1.0 mM Cr(^{tbu}dh^{tbu}bpy)Cl(H$_2$O) **2** with 0.325 M PhOH at variable DBTD concentrations, obtained under CO$_2$ saturation. Conditions: 0.1 M TBAPF$_6$/*N,N*-DMF; glassy carbon working electrode, glassy carbon counter electrode, Ag/AgCl pseudoreference electrode; 100 mV/s scan rate; referenced to internal ferrocene standard. (**B**) Log-log plot from data obtained from CVs in **A** at −2.56 V vs. Fc$^+$/Fc.

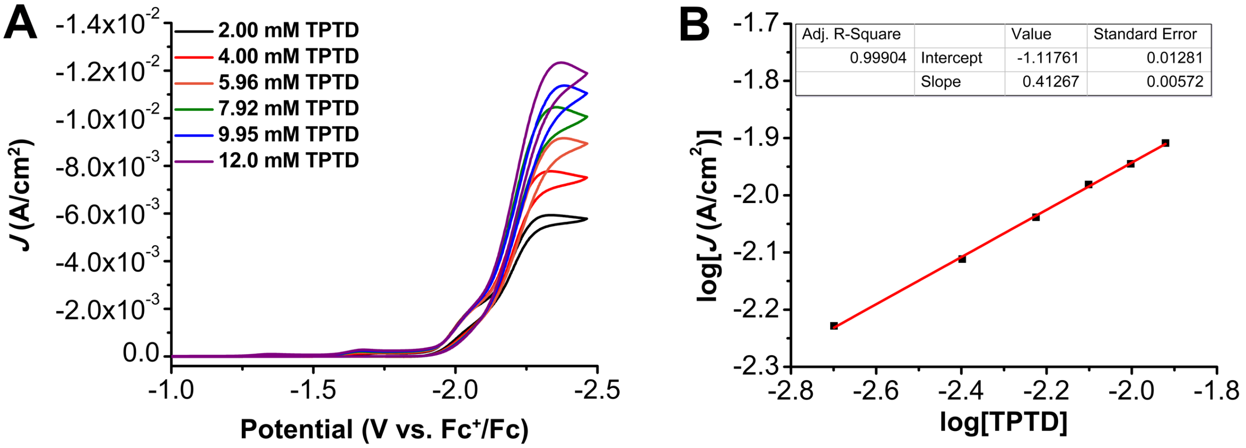

Adj. R-Square		Value	Standard Error
0.99904	Intercept	-1.11761	0.01281
	Slope	0.41267	0.00572

Figure S53. (**A**) CVs of 1.0 mM Cr(^{tbu}dh^{tbu}bpy)Cl(H$_2$O) **2** with 0.325 M PhOH at variable TPTD concentrations, obtained under CO$_2$ saturation. Conditions: 0.1 M TBAPF$_6$/*N,N*-DMF; glassy carbon working electrode, glassy carbon counter electrode, Ag/AgCl pseudoreference electrode; 100 mV/s scan rate; referenced to internal ferrocene standard. (**B**) Log-log plot from data obtained from CVs in **A** at −2.37 V vs. Fc$^+$/Fc.

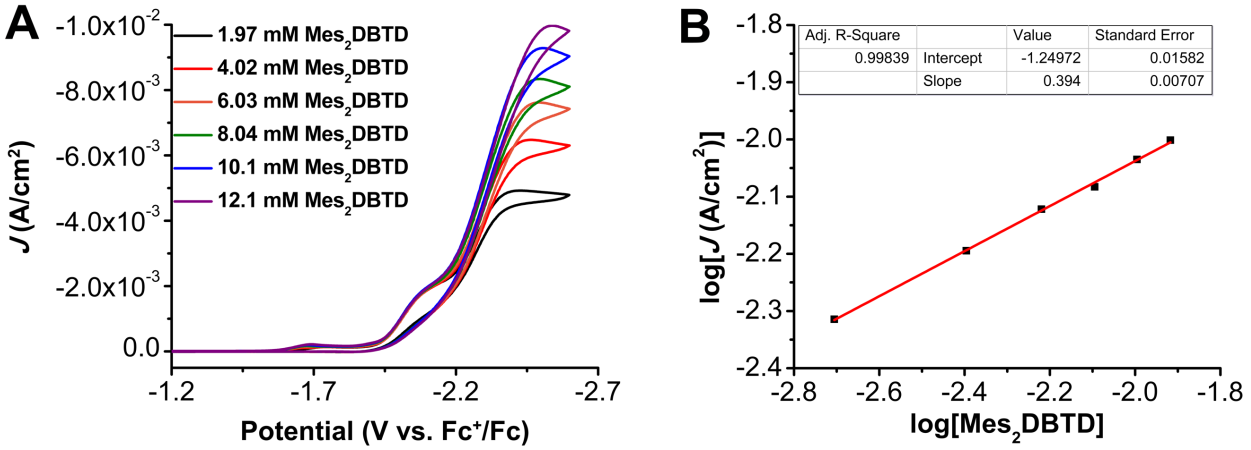

Figure S54. (**A**) CVs of 1.0 mM Cr(^{tbu}dh^{tbu}bpy)Cl(H_2O) **2** with 0.325 M PhOH at variable Mes_2DBTD concentrations, obtained under CO_2 saturation. Conditions: 0.1 M $TBAPF_6$/*N,N*-DMF; glassy carbon working electrode, glassy carbon counter electrode, Ag/AgCl pseudoreference electrode; 100 mV/s scan rate; referenced to internal ferrocene standard. (**B**) Log-log plot from data obtained from CVs in **A** at −2.54 V vs. Fc^+/Fc.

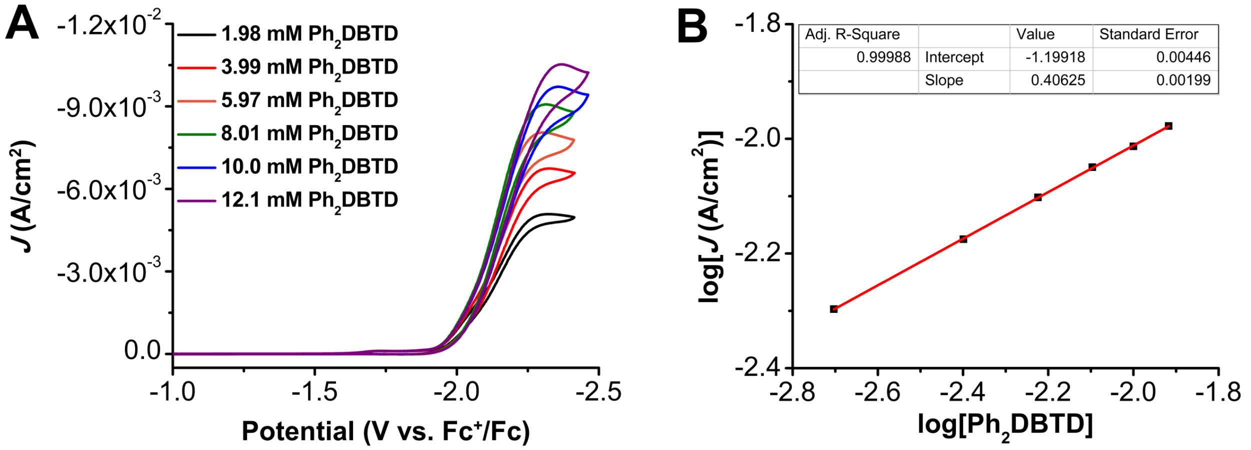

Figure S55. (**A**) CVs of 1.0 mM Cr(^{tbu}dh^{tbu}bpy)Cl(H_2O) **2** with 0.325 M PhOH at variable Ph_2DBTD concentrations, obtained under CO_2 saturation. Conditions: 0.1 M $TBAPF_6$/*N,N*-DMF; glassy carbon working electrode, glassy carbon counter electrode, Ag/AgCl pseudoreference electrode; 100 mV/s scan rate; referenced to internal ferrocene standard. (**B**) Log-log plot from data obtained from CVs in **A** at −2.37 V vs. Fc^+/Fc.

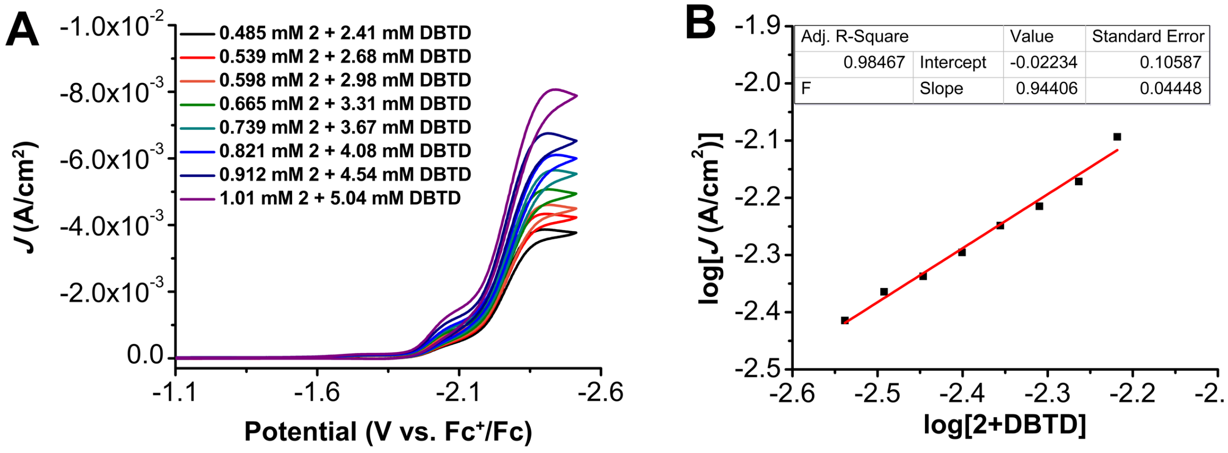

Figure S56. (**A**) CVs where the concentrations of Cr(^{tbu}dh^{tbu}bpy)Cl(H$_2$O) **2** and DBTD were varied at a fixed 1:5 ratio of **1**:DBTD with 0.325 M PhOH under CO$_2$ saturation conditions. Conditions: 0.1 M TBAPF$_6$/*N,N*-DMF; glassy carbon working electrode, glassy carbon counter electrode, Ag/AgCl pseudoreference electrode; 100 mV/s scan rate; referenced to internal ferrocene standard. (**B**) Log-log plot from data obtained from CVs in **A** at −2.43 V vs. Fc$^+$/Fc.

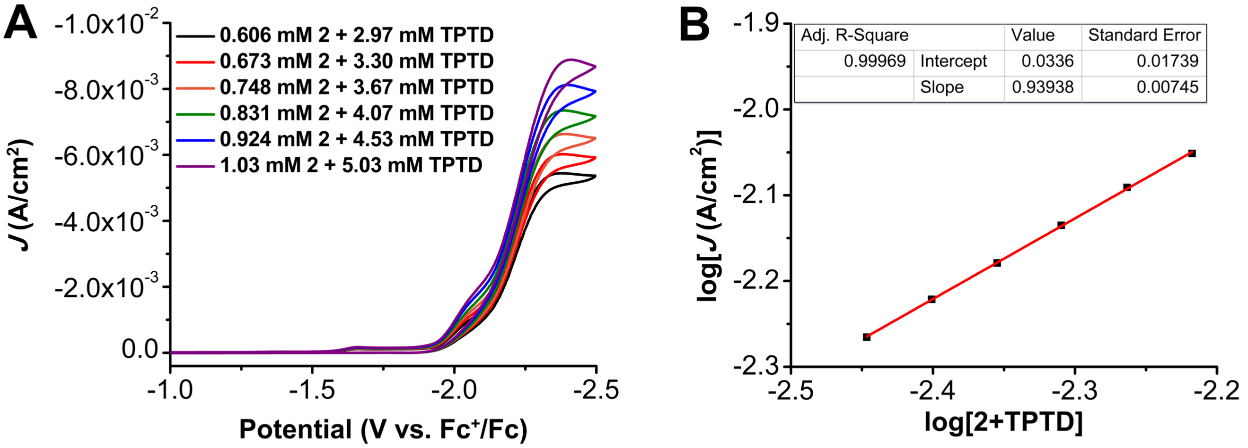

Figure S57. (**A**) CVs where the concentrations of Cr(^{tbu}dh^{tbu}bpy)Cl(H$_2$O) **2** and TPTD were varied at a fixed 1:5 ratio of **1**:TPTD with 0.325 M PhOH under CO$_2$ saturation conditions. Conditions: 0.1 M TBAPF$_6$/*N,N*-DMF; glassy carbon working electrode, glassy carbon counter electrode, Ag/AgCl pseudoreference electrode; 100 mV/s scan rate; referenced to internal ferrocene standard. (**B**) Log-log plot from data obtained from CVs in **A** at −2.41 V vs. Fc$^+$/Fc.

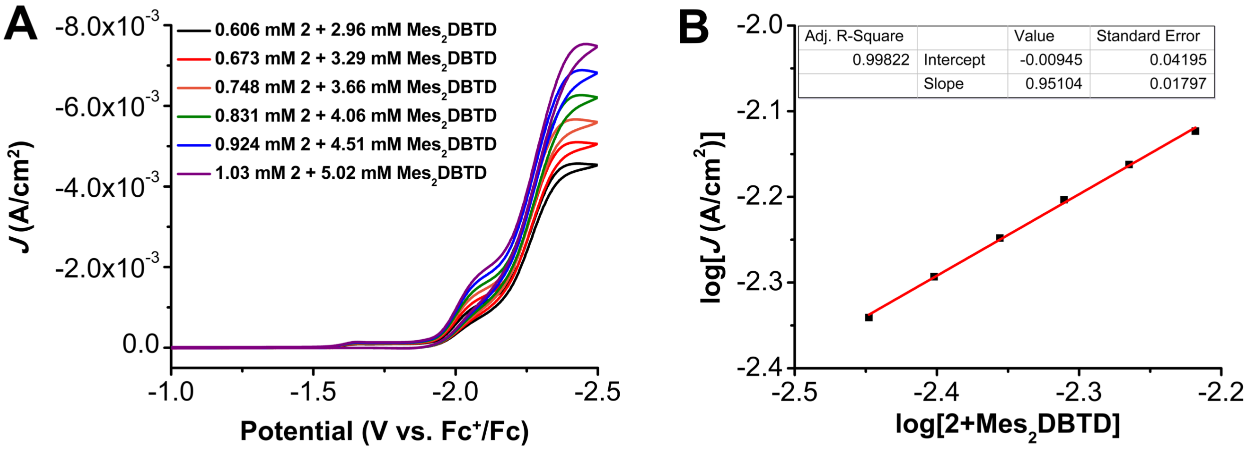

Figure S58. (**A**) CVs where the concentrations of Cr(^{tbu}dh^{tbu}bpy)Cl(H_2O) **2** and Mes_2DBTD were varied at a fixed 1:5 ratio of **1**:Mes_2DBTD with 0.325 M PhOH under CO_2 saturation conditions. Conditions: 0.1 M $TBAPF_6$/*N,N*-DMF; glassy carbon working electrode, glassy carbon counter electrode, Ag/AgCl pseudoreference electrode; 100 mV/s scan rate; referenced to internal ferrocene standard. (**B**) Log-log plot from data obtained from CVs in **A** at −2.45 V vs. Fc^+/Fc.

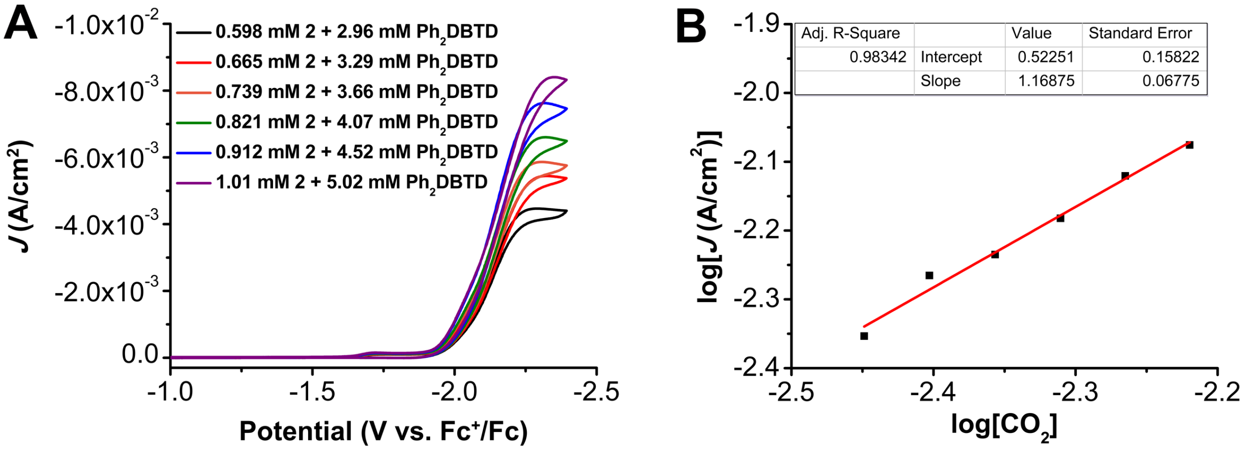

Figure S59. (**A**) CVs where the concentrations of Cr(^{tbu}dh^{tbu}bpy)Cl(H_2O) **2** and Ph_2DBTD were varied at a fixed 1:5 ratio of **1**:Ph_2DBTD with 0.325 M PhOH under CO_2 saturation conditions. Conditions: 0.1 M $TBAPF_6$/*N,N*-DMF; glassy carbon working electrode, glassy carbon counter electrode, Ag/AgCl pseudoreference electrode; 100 mV/s scan rate; referenced to internal ferrocene standard. (**B**) Log-log plot from data obtained from CVs in **A** at −2.35 V vs. Fc^+/Fc.

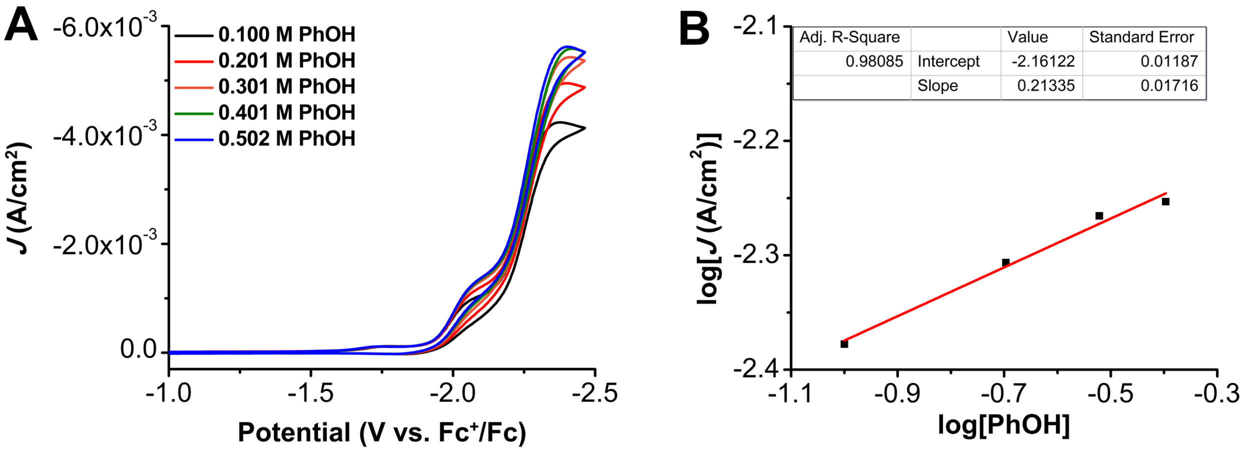

Figure S60. (**A**) CVs of PhOH at variable concentrations, obtained under CO_2 saturation with 1.0 mM Cr(^{tbu}dh^{tbu}bpy)Cl(H_2O) **2** and 2.5 mM DBTD. Conditions: 0.1 M $TBAPF_6$/*N,N*-DMF; glassy carbon working electrode, glassy carbon counter electrode, Ag/AgCl pseudoreference electrode; 100 mV/s scan rate; referenced to internal ferrocene standard. (**B**) Log-log plot from data obtained from CVs in **A** at −2.42 V vs. Fc^+/Fc.

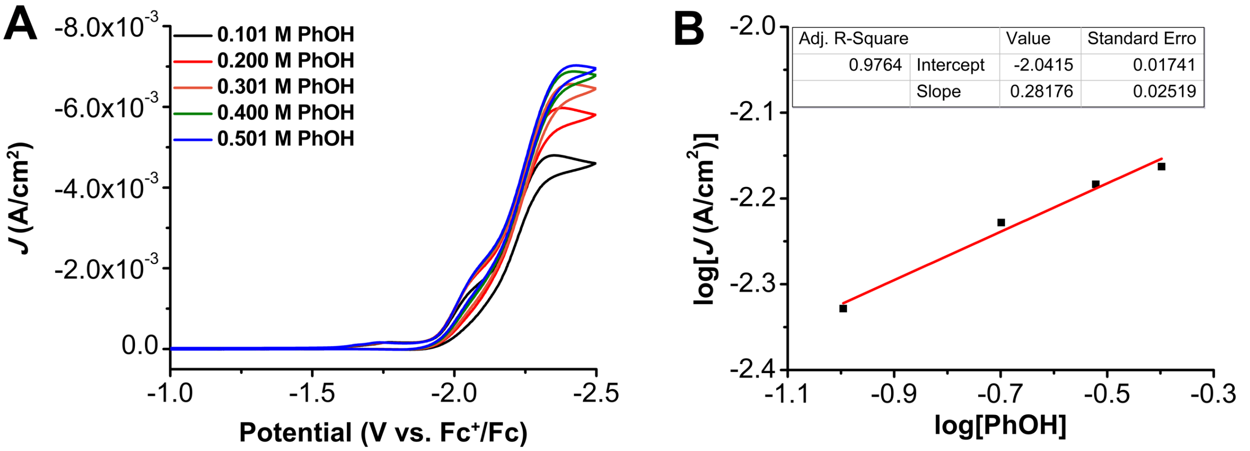

Figure S61. (**A**) CVs of PhOH at variable concentrations, obtained under CO_2 saturation with 1.0 mM Cr(^{tbu}dh^{tbu}bpy)Cl(H_2O) **2** and 2.5 mM TPTD. Conditions: 0.1 M $TBAPF_6$/*N,N*-DMF; glassy carbon working electrode, glassy carbon counter electrode, Ag/AgCl pseudoreference electrode; 100 mV/s scan rate; referenced to internal ferrocene standard. (**B**) Log-log plot from data obtained from CVs in **A** at −2.43 V vs. Fc^+/Fc.

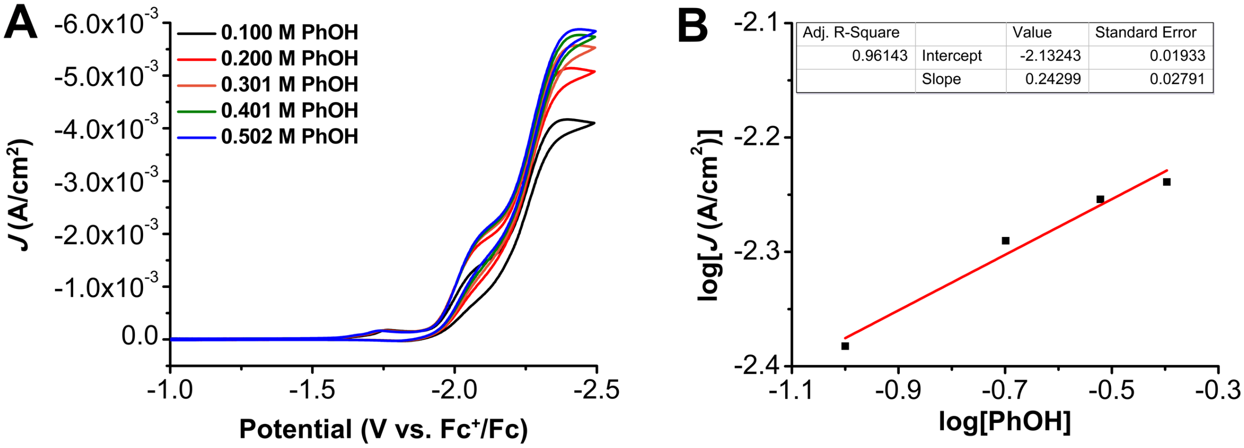

Adj. R-Square		Value	Standard Error
0.96143	Intercept	-2.13243	0.01933
	Slope	0.24299	0.02791

Figure S62. (**A**) CVs of PhOH at variable concentrations, obtained under CO_2 saturation with 1.0 mM Cr(^{tbu}dh^{tbu}bpy)Cl(H_2O) **2** and 2.5 mM Mes_2DBTD. Conditions: 0.1 M $TBAPF_6$/*N,N*-DMF; glassy carbon working electrode, glassy carbon counter electrode, Ag/AgCl pseudoreference electrode; 100 mV/s scan rate; referenced to internal ferrocene standard. (**B**) Log-log plot from data obtained from CVs in **A** at −2.44 V vs. Fc$^+$/Fc.

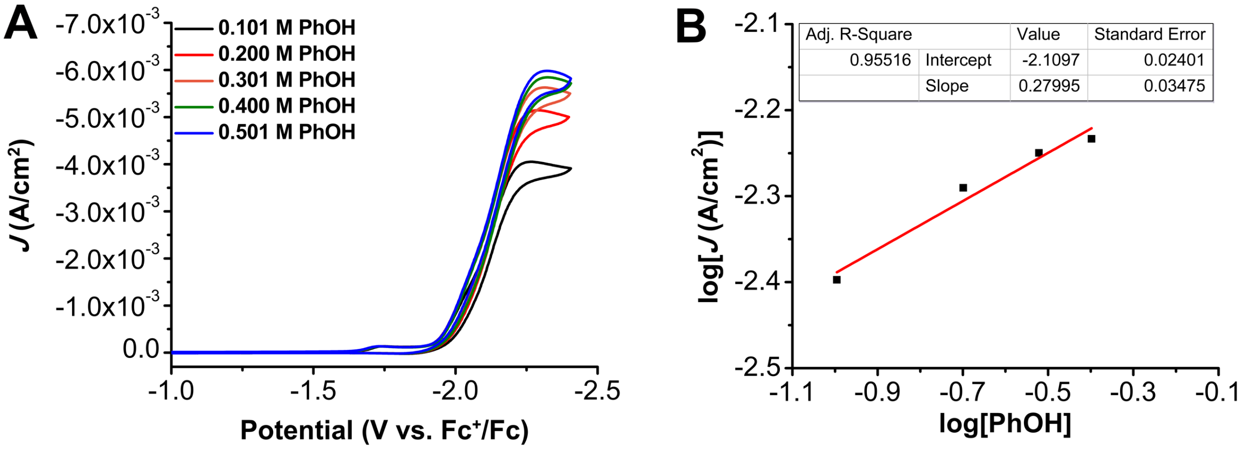

Adj. R-Square		Value	Standard Error
0.95516	Intercept	-2.1097	0.02401
	Slope	0.27995	0.03475

Figure S63. (**A**) CVs of PhOH at variable concentrations, obtained under CO_2 saturation with 1.0 mM Cr(^{tbu}dh^{tbu}bpy)Cl(H_2O) **2** and 2.5 mM Ph_2DBTD. Conditions: 0.1 M $TBAPF_6$/*N,N*-DMF; glassy carbon working electrode, glassy carbon counter electrode, Ag/AgCl pseudoreference electrode; 100 mV/s scan rate; referenced to internal ferrocene standard. (**B**) Log-log plot from data obtained from CVs in **A** at −2.32 V vs. Fc$^+$/Fc.

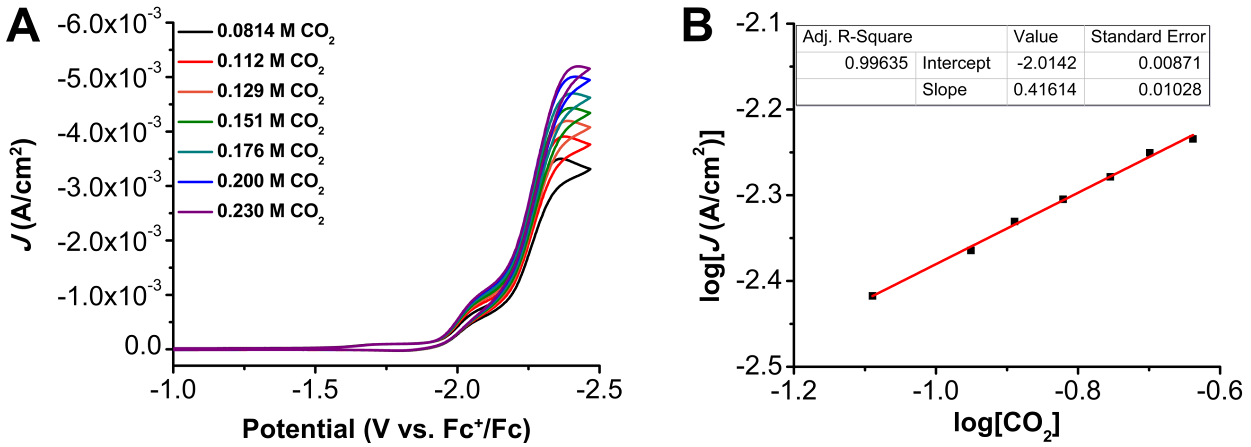

Figure S64. (**A**) CVs of 1.0 mM Cr(^{tbu}dh^{tbu}bpy)Cl(H_2O) **2**, 2.5 mM DBTD, 0.325 M PhOH at varied CO_2 concentrations. Conditions: 0.1 M $TBAPF_6$/*N,N*-DMF; glassy carbon working electrode, glassy carbon counter electrode, Ag/AgCl pseudoreference electrode; 100 mV/s scan rate; referenced to internal ferrocene standard. (**B**) Log-log plot from data obtained from CVs in **A** at −2.42 V vs. Fc^+/Fc.

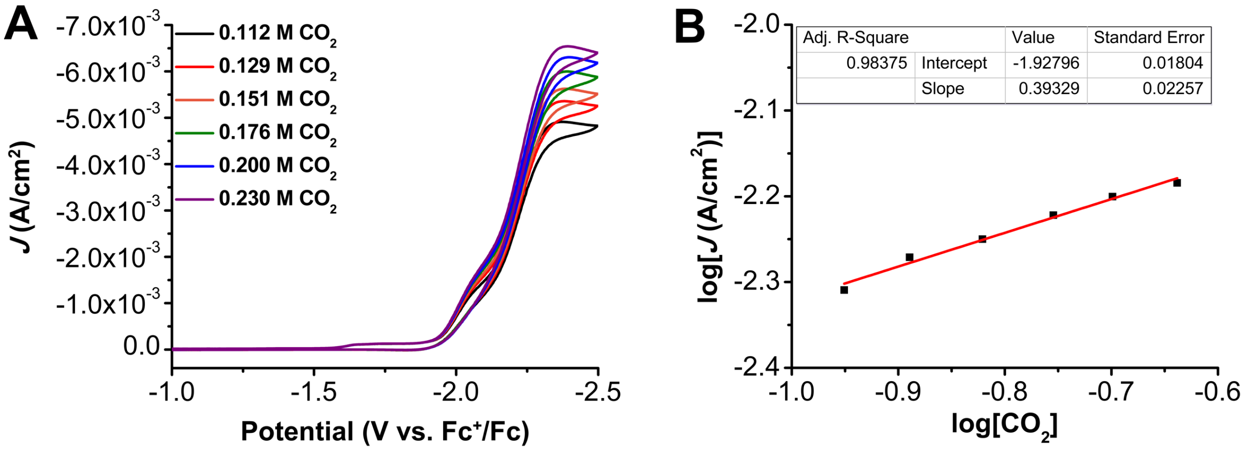

Figure S65. (**A**) CVs of 1.0 mM Cr(^{tbu}dh^{tbu}bpy)Cl(H_2O) **2**, 2.5 mM TPTD, 0.325 M PhOH at varied CO_2 concentrations. Conditions: 0.1 M $TBAPF_6$/*N,N*-DMF; glassy carbon working electrode, glassy carbon counter electrode, Ag/AgCl pseudoreference electrode; 100 mV/s scan rate; referenced to internal ferrocene standard. (**B**) Log-log plot from data obtained from CVs in **A** at −2.39 V vs. Fc^+/Fc.

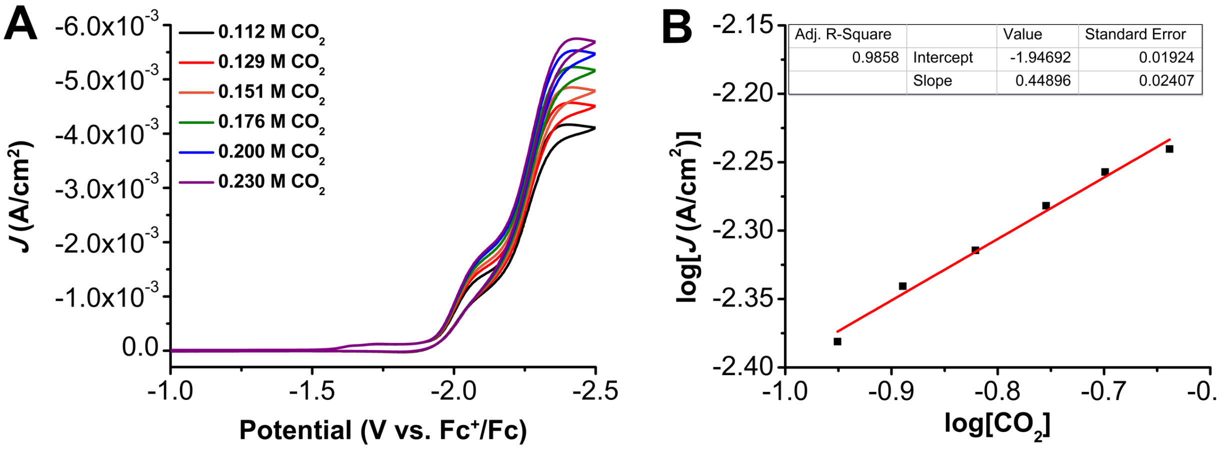

Figure S66. (**A**) CVs of 1.0 mM Cr(^{tbu}dh^{tbu}bpy)Cl(H_2O) **2**, 2.5 mM Mes_2DBTD, 0.325 M PhOH at varied CO_2 concentrations. Conditions: 0.1 M $TBAPF_6$/*N,N*-DMF; glassy carbon working electrode, glassy carbon counter electrode, Ag/AgCl pseudoreference electrode; 100 mV/s scan rate; referenced to internal ferrocene standard. (**B**) Log-log plot from data obtained from CVs in **A** at −2.43 V vs. Fc^+/Fc.

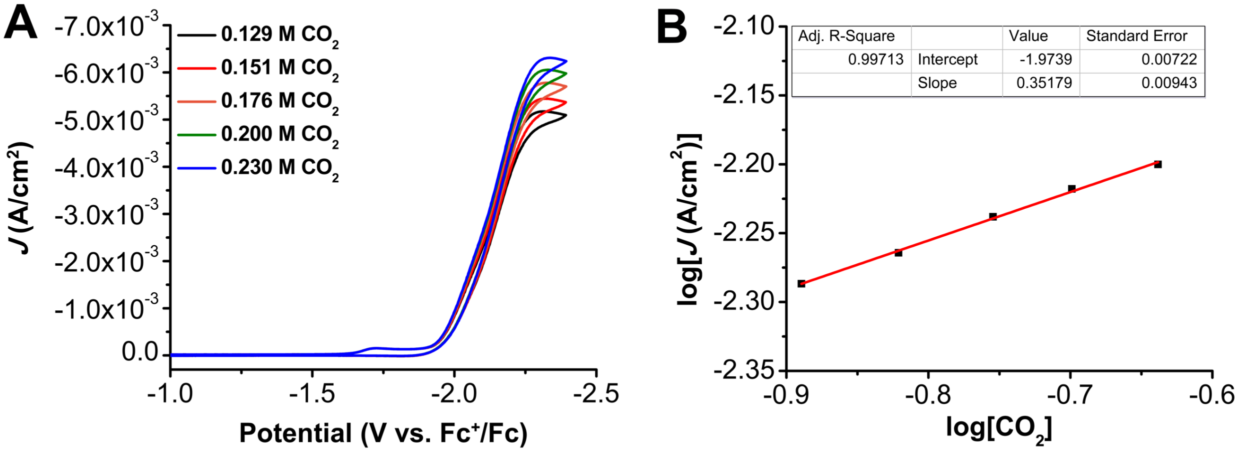

Figure S67. (**A**) CVs of 1.0 mM Cr(^{tbu}dh^{tbu}bpy)Cl(H_2O) **2**, 2.5 mM Ph_2DBTD, 0.325 M PhOH at varied CO_2 concentrations. Conditions: 0.1 M $TBAPF_6$/*N,N*-DMF; glassy carbon working electrode, glassy carbon counter electrode, Ag/AgCl pseudoreference electrode; 100 mV/s scan rate; referenced to internal ferrocene standard. (**B**) Log-log plot from data obtained from CVs in **A** at −2.33 V vs. Fc^+/Fc.

Controlled Potential Electrolysis Experiments (Protic Conditons)

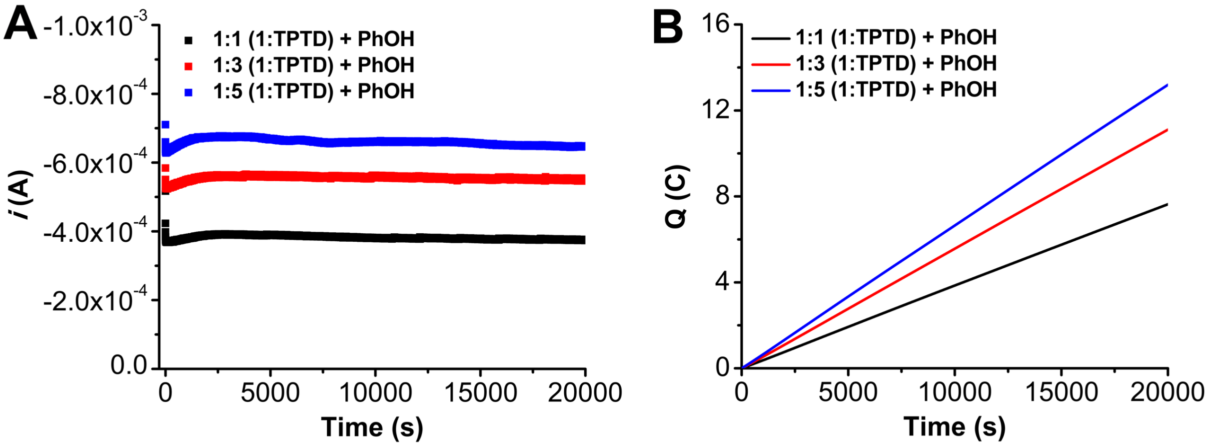

Figure S68. (**A**) Current versus time trace from CPE experiments of **1**+TPTD+PhOH. (**B**) Charge passed versus time for the CPE experiments shown in **A**. Conditions were 0.1 mM Cr(^{tbu}dhbpy)Cl(H_2O) **1**, 0.12 M PhOH, and either 0.1, 0.3, or 0.5 (blue) mM TPTD under a CO_2 atmosphere at −2.25 V vs Fc^+/Fc in 0.1 M $TBAPF_6$/*N,N*-DMF; working electrode was a glassy carbon rod, counter electrode was a graphite rod, and the reference was a nonaqueous Ag/AgCl pseudoreference electrode; 0.075 M Fc was used as sacrificial oxidant.

Table S7. Results from CPE experiment in Figure S68, 1:1 (**1**:TPTD) + PhOH (black).

Time (s)	Charge (coulombs)	moles (e^-)	Moles of CO	FE_{CO}
10828	4.17	4.32×10^{-5}	2.02×10^{-5}	93.5
12125	4.66	4.83×10^{-5}	2.70×10^{-5}	111.9
20000*	7.63	7.91×10^{-5}	4.50×10^{-5}	113.8
20000*	7.63	7.91×10^{-5}	4.19×10^{-5}	105.9
20000*	7.63	7.91×10^{-5}	4.15×10^{-5}	104.8

* indicates a triplicate series of injections carried out upon completion of electrolysis

Table S8. Results from CPE experiment in Figure S68, 1:3 (**1**:TPTD) + PhOH (black).

Time (s)	Charge (coulombs)	moles (e^-)	Moles of CO	FE_{CO}
20000*	11.1	1.15×10^{-4}	6.00×10^{-5}	104.3
20000*	11.1	1.15×10^{-4}	5.97×10^{-5}	103.7
20000*	11.1	1.15×10^{-4}	5.72×10^{-5}	99.3

* indicates a triplicate series of injections carried out upon completion of electrolysis

Table S9. Results from CPE experiment in Figure S68, 1:5 (**1**:TPTD) + PhOH (blue).

Time (s)	Charge (coulombs)	moles (e^-)	Moles of CO	FE$_{CO}$
15932	10.6	1.09 x 10^{-4}	6.34 x 10^{-5}	115.9
17894	11.8	1.23 x 10^{-4}	7.47 x 10^{-5}	121.9
20000*	13.2	1.37 x 10^{-4}	5.83 x 10^{-5}	85.2
20000*	13.2	1.37 x 10^{-4}	5.84 x 10^{-5}	85.4
20000*	13.2	1.37 x 10^{-4}	5.76 x 10^{-5}	84.3

* indicates a triplicate series of injections carried out upon completion of electrolysis

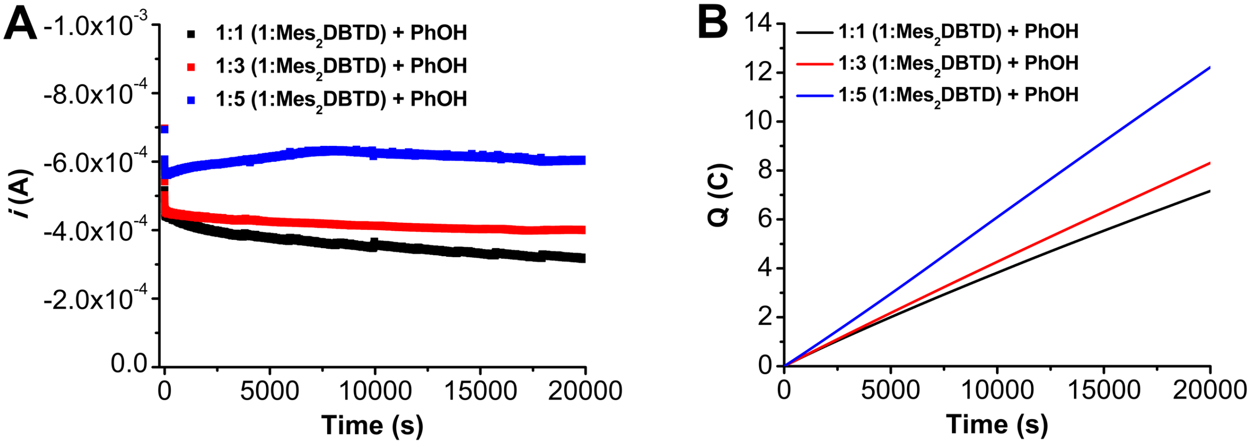

Figure S69. (**A**) Current versus time trace from CPE experiments with **1**+Mes$_2$DBTD+PhOH. (**B**) Charge passed versus time for the CPE experiments shown in **A**. Conditions were 0.1 mM Cr(^{tbu}dhbpy)Cl(H_2O) **1**, 0.12 M PhOH, and either 0.1, 0.3 (red), or 0.5 (blue) mM Mes$_2$DBTD under a CO_2 atmosphere at −2.25 V vs Fc$^+$/Fc in 0.1 M TBAPF$_6$/*N,N*-DMF; working electrode was a glassy carbon rod, counter electrode was a graphite rod, and the reference was a nonaqueous Ag/AgCl pseudoreference electrode; 0.075 M Fc was used as sacrificial oxidant.

Table S10. Results from CPE experiment in Figure S69, 1:1 (**1**:Mes$_2$DBTD) + PhOH (red).

Time (s)	Charge (coulombs)	moles (e^{-})	Moles of CO	FE$_{CO}$
5895	2.33	2.42 x 10^{-5}	1.10 x 10^{-5}	90.7
8147	3.16	3.28 x 10^{-5}	1.59 x 10^{-5}	97.2
9925	3.80	3.93 x 10^{-5}	2.11 x 10^{-5}	107.3
12005	4.52	4.69 x 10^{-5}	2.37 x 10^{-5}	101.1
13897	5.17	5.36 x 10^{-5}	2.53 x 10^{-5}	94.3
15696	5.77	5.98 x 10^{-5}	2.91 x 10^{-5}	97.2
20001*	7.16	7.42 x 10^{-5}	3.33 x 10^{-5}	89.7
20001*	7.16	7.42 x 10^{-5}	3.45 x 10^{-5}	92.8
20001*	7.16	7.42 x 10^{-5}	3.47 x 10^{-5}	93.4

* indicates a triplicate series of injections carried out upon completion of electrolysis

Table S11. Results from CPE experiment in Figure S69, 1:3 (1:Mes$_2$DBTD) + PhOH (red).

Time (s)	Charge (coulombs)	moles (e^{-})	Moles of CO	FE$_{CO}$
16050	6.73	6.73 x 10^{-5}	3.42 x 10^{-5}	98.1
18000	7.51	7.78 x 10^{-5}	4.31 x 10^{-5}	110.8
20000*	8.31	8.61 x 10^{-5}	4.35 x 10^{-5}	101.1
20000*	8.31	8.61 x 10^{-5}	4.76 x 10^{-5}	110.5
20000*	8.31	8.61 x 10^{-5}	4.41 x 10^{-5}	102.4

* indicates a triplicate series of injections carried out upon completion of electrolysis

Table S12. Results from CPE experiment in Figure S69, 1:5 (**1**:Mes$_2$DBTD) + PhOH (blue).

Time (s)	Charge (coulombs)	moles (e^{-})	Moles of CO	FE$_{CO}$
20000*	12.2	1.27 x 10^{-4}	6.78 x 10^{-5}	107.1
20000*	12.2	1.27 x 10^{-4}	5.85 x 10^{-5}	92.3
20000*	12.2	1.27 x 10^{-4}	6.05 x 10^{-5}	95.5

* indicates a triplicate series of injections carried out upon completion of electrolysis

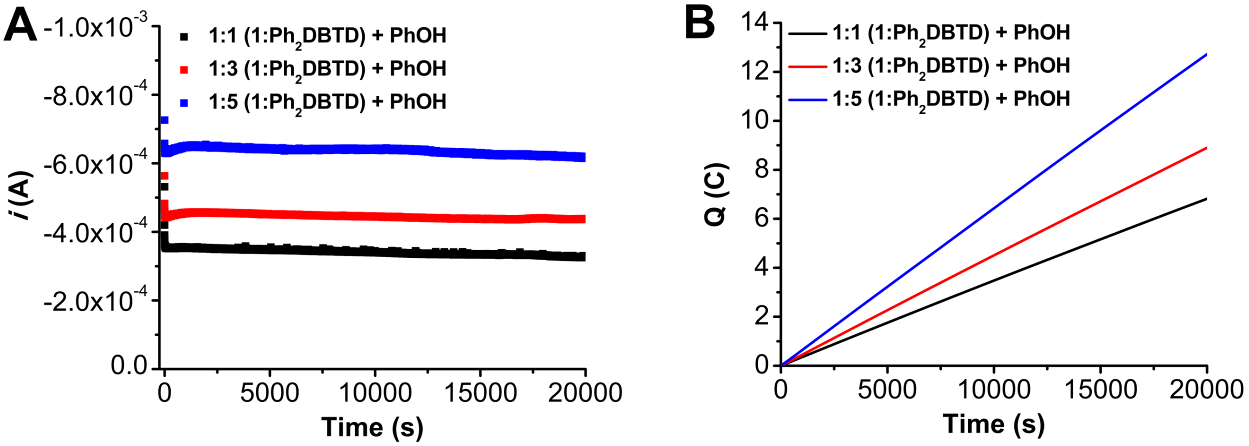

Figure S70. (**A**) Current versus time trace from CPE experiments with **1**+Ph$_2$DBTD+PhOH. (**B**) Charge passed versus time for the CPE experiments shown in **A**. Conditions were 0.1 mM Cr(^{tbu}dhbpy)Cl(H_2O) **1**, 0.12 M PhOH, and either 0.1 (black), 0.3 (red), or 0.5 (blue) mM Ph$_2$DBTD under a CO_2 atmosphere at −2.20 V vs Fc$^+$/Fc in 0.1 M TBAPF$_6$/*N,N*-DMF; working electrode was a glassy carbon rod, counter electrode was a graphite rod, and the reference was a nonaqueous Ag/AgCl pseudoreference electrode; 0.075 M Fc was used as sacrificial oxidant.

Table S13. Results from CPE experiment in Figure S70, 1:1 (**1**:Ph$_2$DBTD) + PhOH (black).

Time (s)	Charge (coulombs)	moles (e$^-$)	Moles of CO	FE$_{CO}$
20000*	6.8	7.07 x 10^{-5}	3.73 x 10^{-5}	105.4
20000*	6.8	7.07 x 10^{-5}	3.62 x 10^{-5}	102.4
20000*	6.8	7.07 x 10^{-5}	3.47 x 10^{-5}	98.3

* indicates a triplicate series of injections carried out upon completion of electrolysis

Table S14. Results from CPE experiment in Figure S70, 1:3 (**1**:Ph$_2$DBTD) + PhOH (red).

Time (s)	Charge (coulombs)	moles (e$^-$)	Moles of CO	FE$_{CO}$
20000*	8.9	9.23 x 10^{-5}	4.48 x 10^{-5}	97.2
20000*	8.9	9.23 x 10^{-5}	4.65 x 10^{-5}	100.8
20000*	8.9	9.23 x 10^{-5}	4.78 x 10^{-5}	103.5

* indicates a triplicate series of injections carried out upon completion of electrolysis

Table S15. Results from CPE experiment in Figure S70, 1:5 (**1**:Ph$_2$DBTD) + PhOH (blue).

Time (s)	**Charge (coulombs)**	**moles (e$^-$)**	**Moles of CO**	**FE$_{CO}$**
20000*	12.7	1.32×10^{-4}	7.28×10^{-5}	110.4
20000*	12.7	1.32×10^{-4}	6.76×10^{-5}	102.6
20000*	12.7	1.32×10^{-4}	6.45×10^{-5}	97.9

* indicates a triplicate series of injections carried out upon completion of electrolysis

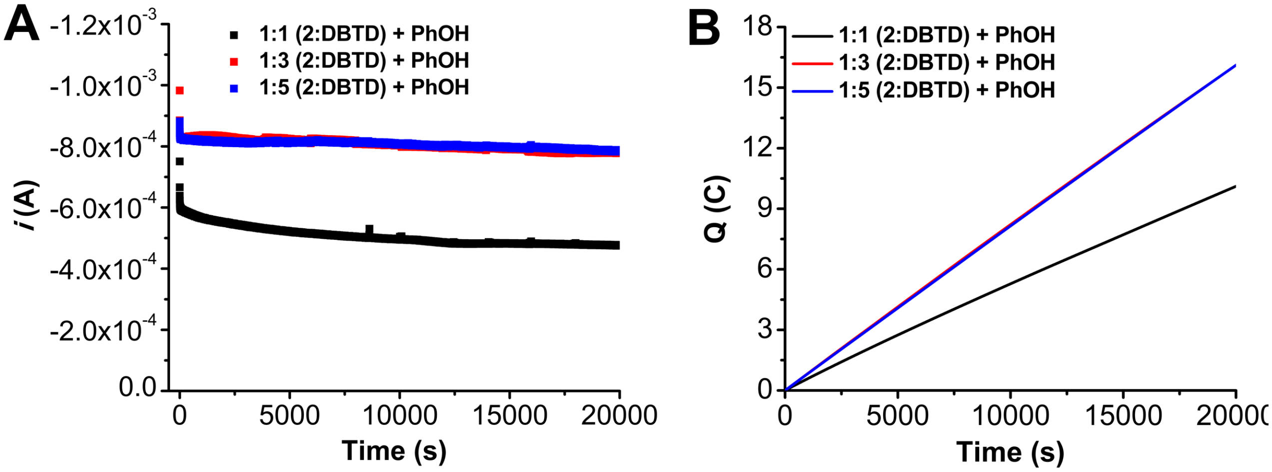

Figure S71. (**A**) Current versus time trace from CPE experiments with **2**+DBTD+PhOH. (**B**) Charge passed versus time for the CPE experiments shown in **A**. Conditions were 0.1 mM Cr(^{tbu}dh^{tbu}bpy)Cl(H$_2$O) **2**, 0.12 M PhOH, and either 0.1 (black), 0.3 (red), or 0.5 (blue) mM DBTD under a CO$_2$ atmosphere at −2.30 V vs Fc$^+$/Fc in 0.1 M TBAPF$_6$/*N,N*-DMF; working electrode was a glassy carbon rod, counter electrode was a graphite rod, and the reference was a nonaqueous Ag/AgCl pseudoreference electrode; 0.075 M Fc was used as sacrificial oxidant.

Table S16. Results from CPE experiment in Figure S71, 1:1 (**2**:DBTD) + PhOH (black).

Time (s)	**Charge (coulombs)**	**moles (e$^-$)**	**Moles of CO**	**FE$_{CO}$**
20000*	10.1	1.05×10^{-4}	5.25×10^{-5}	100.1
20000*	10.1	1.05×10^{-4}	5.64×10^{-5}	107.7
20000*	10.1	1.05×10^{-4}	5.35×10^{-5}	102.1

* indicates a triplicate series of injections carried out upon completion of electrolysis

Table S17. Results from CPE experiment in Figure S71, 1:3 (**2**:DBTD) + PhOH (red).

Time (s)	Charge (coulombs)	moles (e^{-})	Moles of CO	FE_{CO}
20000*	16.2	1.68×10^{-4}	8.22×10^{-5}	98.1
20000*	16.2	1.68×10^{-4}	8.25×10^{-5}	98.4
20000*	16.2	1.68×10^{-4}	8.41×10^{-5}	100.4

* indicates a triplicate series of injections carried out upon completion of electrolysis

Table S18. Results from CPE experiment in Figure S71, 1:5 (**2**:DBTD) + PhOH (blue).

Time (s)	Charge (coulombs)	moles (e^{-})	Moles of CO	FE_{CO}
3758	3.07	3.18×10^{-5}	1.34×10^{-5}	84.4
5893	4.81	4.98×10^{-5}	2.74×10^{-5}	110.0
7873	6.42	6.65×10^{-5}	3.88×10^{-5}	116.9
11924	9.70	1.00×10^{-4}	5.93×10^{-5}	118.1
13648	11.1	1.15×10^{-4}	6.74×10^{-5}	117.4
15918	12.9	1.34×10^{-4}	7.46×10^{-5}	111.6
17982	14.5	1.51×10^{-4}	8.37×10^{-5}	111.2
20000*	16.1	1.67×10^{-4}	9.32×10^{-5}	111.6
20000*	16.1	1.67×10^{-4}	9.20×10^{-5}	110.1
20000*	16.1	1.67×10^{-4}	8.61×10^{-5}	103.1

* indicates a triplicate series of injections carried out upon completion of electrolysis

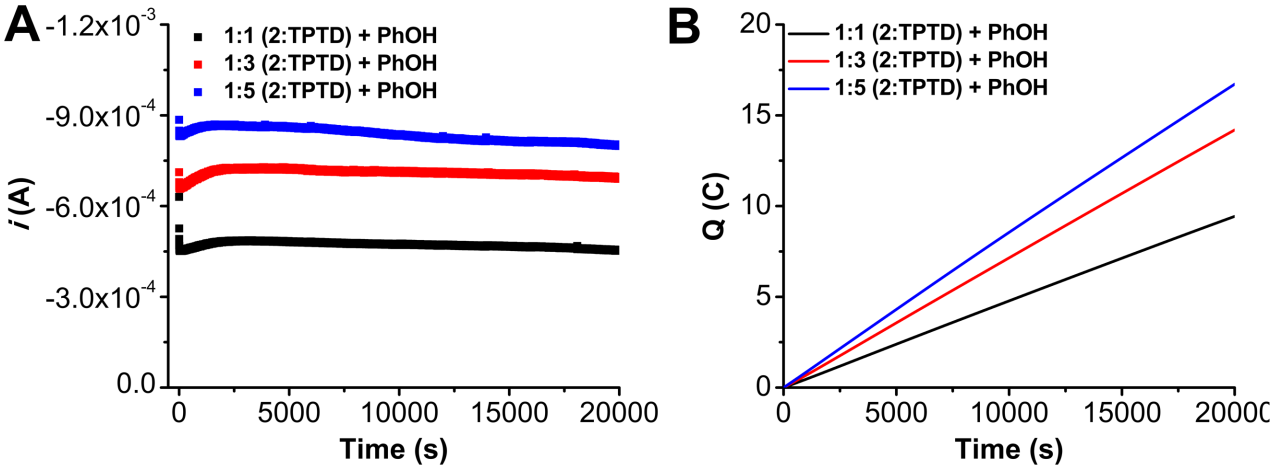

Figure S72. (**A**) Current versus time trace from CPE experiments with **2**+TPTD+PhOH. (**B**) Charge passed versus time for the CPE experiments shown in **A**. Conditions were 0.1 mM Cr(^{tbu}dh^{tbu}bpy)Cl(H_2O) **2**, 0.12 M PhOH, and either 0.1 (black), 0.3 (red), or 0.5 (blue) mM TPTD under a CO_2 atmosphere at −2.25 V vs Fc^+/Fc in 0.1 M $TBAPF_6$/*N,N*-DMF; working electrode was a glassy carbon rod, counter electrode was a graphite rod, and the reference was a nonaqueous Ag/AgCl pseudoreference electrode; 0.075 M Fc was used as sacrificial oxidant.

Table S19. Results from CPE experiment in Figure S72, 1:1 (**2**:TPTD) + PhOH (black).

Time (s)	Charge (coulombs)	moles (e^-)	Moles of CO	FE_{CO}
20000*	9.43	9.78×10^{-5}	4.99×10^{-5}	102.1
20000*	9.43	9.78×10^{-5}	4.99×10^{-5}	102.0
20000*	9.43	9.78×10^{-5}	4.54×10^{-5}	92.8

* indicates a triplicate series of injections carried out upon completion of electrolysis

Table S20. Results from CPE experiment in Figure S72, 1:3 (**2**:TPTD) + PhOH (red).

Time (s)	Charge (coulombs)	moles (e^-)	Moles of CO	FE_{CO}
5783	4.13	4.28×10^{-5}	2.11×10^{-5}	98.5
7901	5.65	5.85×10^{-5}	2.99×10^{-5}	102.2
20000*	14.2	1.47×10^{-4}	8.01×10^{-5}	108.9
20000*	14.2	1.47×10^{-4}	7.96×10^{-5}	108.2
20000*	14.2	1.47×10^{-4}	7.65×10^{-5}	104.0

* indicates a triplicate series of injections carried out upon completion of electrolysis

Table S21. Results from CPE experiment in Figure S72, 1:5 (**2**:TPTD) + PhOH (blue).

Time (s)	**Charge (coulombs)**	**moles (e^-)**	**Moles of CO**	**FE_{CO}**
5976	5.14	5.33×10^{-5}	2.39×10^{-5}	89.6
7970	6.85	7.09×10^{-5}	3.29×10^{-5}	92.6
9975	8.53	8.84×10^{-5}	4.39×10^{-5}	99.3
11992	10.2	1.06×10^{-4}	5.84×10^{-5}	110.4
13938	11.8	1.22×10^{-4}	6.04×10^{-5}	98.8
15938	13.4	1.39×10^{-4}	7.35×10^{-5}	105.6
17858	15.0	1.55×10^{-4}	7.59×10^{-5}	97.7
20000*	16.7	1.73×10^{-4}	7.96×10^{-5}	91.9
20000*	16.7	1.73×10^{-4}	8.40×10^{-5}	97.0
20000*	16.7	1.73×10^{-4}	7.86×10^{-5}	90.7

* indicates a triplicate series of injections carried out upon completion of electrolysis

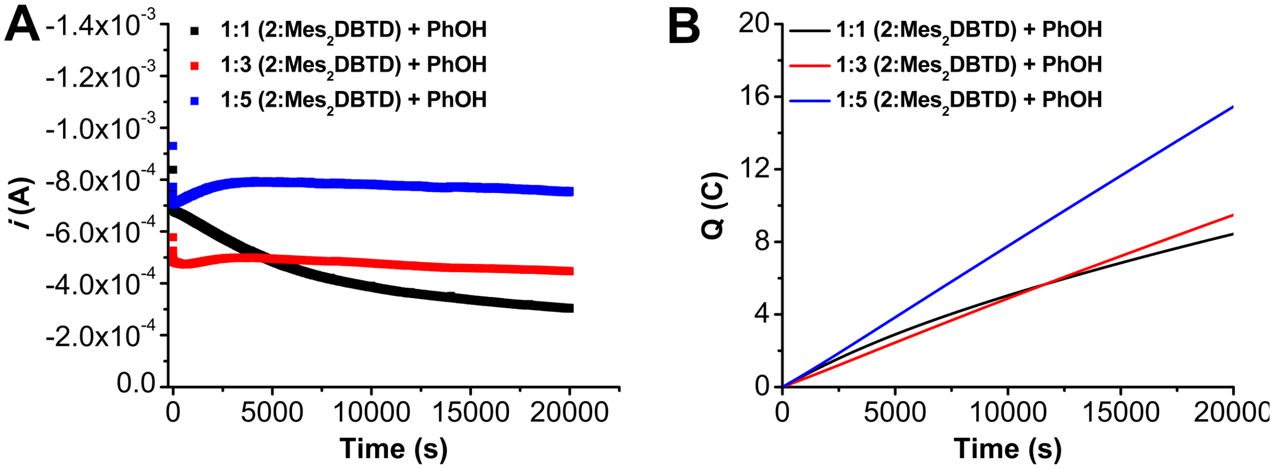

Figure S73. (**A**) Current versus time trace from CPE experiments with **2**+Mes_2DBTD+PhOH. (**B**) Charge passed versus time for the CPE experiments shown in **A**. Conditions were 0.1 mM $Cr(^{tbu}dh^{tbu}bpy)Cl(H_2O)$ **2**, 0.12 M PhOH, and either 0.1 (black), 0.3 (red), or 0.5 (blue) mM Mes_2DBTD under a CO_2 atmosphere at −2.30 V vs Fc^+/Fc in 0.1 M $TBAPF_6$/*N,N*-DMF; working electrode was a glassy carbon rod, counter electrode was a graphite rod, and the reference was a nonaqueous Ag/AgCl pseudoreference electrode; 0.075 M Fc was used as sacrificial oxidant.

Table S22. Results from CPE experiment in Figure S73, 1:1 (**2**:Mes_2DBTD) + PhOH (black).

Time (s)	Charge (coulombs)	moles (e^-)	Moles of CO	FE_{CO}
11926	5.76	5.97×10^{-5}	2.82×10^{-5}	94.6
13952	6.48	6.72×10^{-5}	3.54×10^{-5}	105.5
15926	7.15	7.41×10^{-5}	3.79×10^{-5}	102.2
17896	7.78	8.07×10^{-5}	4.12×10^{-5}	102.1
20000*	8.44	8.74×10^{-5}	4.56×10^{-5}	104.3
20000*	8.44	8.74×10^{-5}	5.06×10^{-5}	115.7
20000*	8.44	8.74×10^{-5}	4.64×10^{-5}	106.1

* indicates a triplicate series of injections carried out upon completion of electrolysis

Table S23. Results from CPE experiment in Figure S73, 1:3 (**2**:Mes_2DBTD) + PhOH (red).

Time (s)	Charge (coulombs)	moles (e^-)	Moles of CO	FE_{CO}
9923	4.85	5.02×10^{-5}	2.31×10^{-5}	91.8
11855	5.76	5.97×10^{-5}	3.07×10^{-5}	102.7
14146	6.82	7.07×10^{-5}	3.94×10^{-5}	111.4
15810	7.59	7.86×10^{-5}	4.17×10^{-5}	105.9
17805	8.50	8.80×10^{-5}	4.39×10^{-5}	99.6
20000*	9.48	9.83×10^{-5}	5.20×10^{-5}	105.8
20000*	9.48	9.83×10^{-5}	5.54×10^{-5}	112.7
20000*	9.48	9.83×10^{-5}	5.44×10^{-5}	110.8

* indicates a triplicate series of injections carried out upon completion of electrolysis

Table S24. Results from CPE experiment in Figure S73, 1:5 (**2**:Mes_2DBTD) + PhOH (blue).

Time (s)	Charge (coulombs)	moles (e^-)	Moles of CO	FE_{CO}
13925	10.8	$1.12 \text{ x } 10^{-4}$	$5.78 \text{ x } 10^{-5}$	103.2
15940	12.4	$1.28 \text{ x } 10^{-4}$	$6.01 \text{ x } 10^{-5}$	93.9
18120	14.0	$1.45 \text{ x } 10^{-4}$	$6.98 \text{ x } 10^{-5}$	96.1
20000*	15.5	$1.60 \text{ x } 10^{-4}$	$7.69 \text{ x } 10^{-5}$	96.0
20000*	15.5	$1.60 \text{ x } 10^{-4}$	$7.92 \text{ x } 10^{-5}$	99.0
20000*	15.5	$1.60 \text{ x } 10^{-4}$	$7.54 \text{ x } 10^{-5}$	94.1

* indicates a triplicate series of injections carried out upon completion of electrolysis

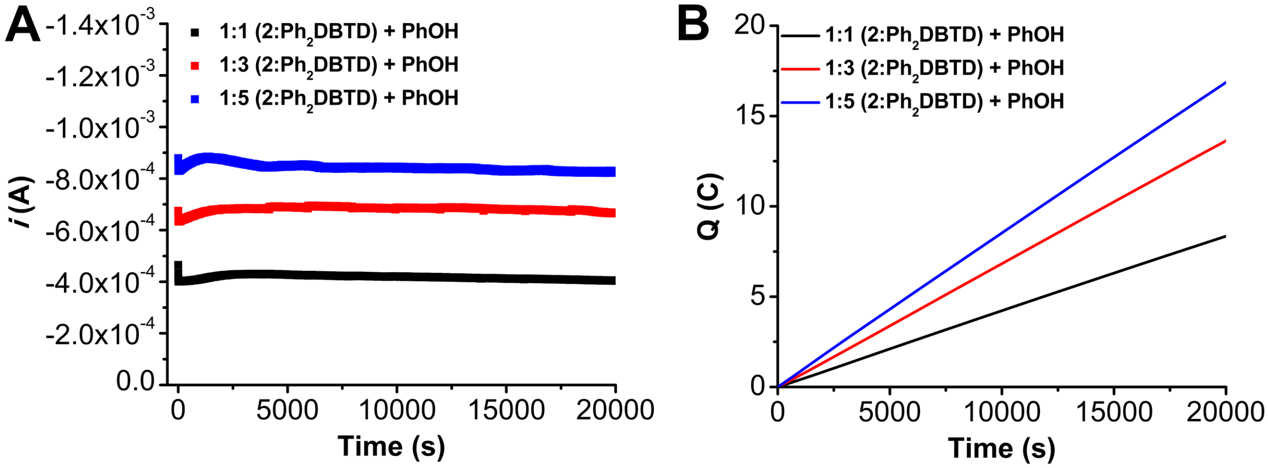

Figure S74. (**A**) Current versus time trace from CPE experiments with **2**+Ph_2DBTD+PhOH. (**B**) Charge passed versus time for the CPE experiments shown in **A**. Conditions were 0.1 mM Cr(^{tbu}dh^{tbu}bpy)Cl(H_2O) **2**, 0.12 M PhOH, and either 0.1 (black), 0.3 (red), or 0.5 (blue) mM Ph_2DBTD under a CO_2 atmosphere at −2.20 V vs Fc^+/Fc in 0.1 M $TBAPF_6$/*N,N*-DMF; working electrode was a glassy carbon rod, counter electrode was a graphite rod, and the reference was a nonaqueous Ag/AgCl pseudoreference electrode; 0.075 M Fc was used as sacrificial oxidant.

Table S25. Results from CPE experiment in Figure S74, 1:1 (**2**:Ph_2DBTD) + PhOH (black).

Time (s)	**Charge (coulombs)**	**moles (e^-)**	**Moles of CO**	**FE_{CO}**
7888	3.33	3.64×10^{-5}	1.71×10^{-5}	99.0
9711	4.10	4.25×10^{-5}	2.26×10^{-5}	106.4
20000*	8.35	8.65×10^{-5}	4.94×10^{-5}	114.3
20000*	8.35	8.65×10^{-5}	5.11×10^{-5}	118.1
20000*	8.35	8.65×10^{-5}	4.88×10^{-5}	112.8

* indicates a triplicate series of injections carried out upon completion of electrolysis

Table S26. Results from CPE experiment in Figure S74, 1:3 (**2**:Ph_2DBTD) + PhOH (red).

Time (s)	**Charge (coulombs)**	**moles (e^-)**	**Moles of CO**	**FE_{CO}**
20000*	13.6	1.41×10^{-4}	6.83×10^{-5}	96.7
20000*	13.6	1.41×10^{-4}	6.76×10^{-5}	95.7
20000*	13.6	1.41×10^{-4}	7.14×10^{-5}	101.0

* indicates a triplicate series of injections carried out upon completion of electrolysis

Table S27. Results from CPE experiment in Figure S74, 1:5 (**2**:Ph_2DBTD) + PhOH (blue).

Time (s)	**Charge (coulombs)**	**moles (e^-)**	**Moles of CO**	**FE_{CO}**
20000*	16.8	1.75×10^{-4}	8.30×10^{-5}	95.0
20000*	16.8	1.75×10^{-4}	8.09×10^{-5}	92.6
20000*	16.8	1.75×10^{-4}	9.10×10^{-5}	104.1

* indicates a triplicate series of injections carried out upon completion of electrolysis

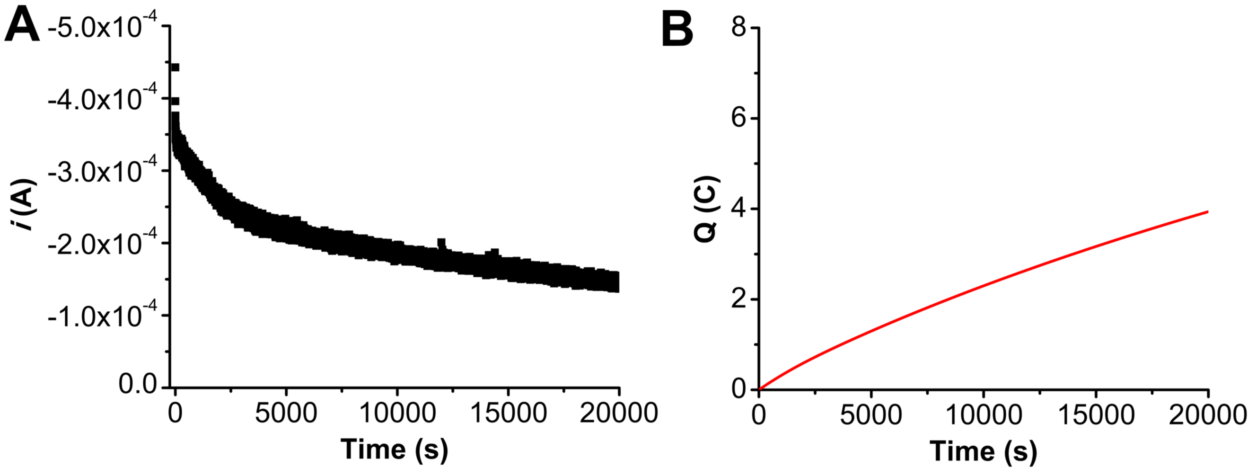

Figure S75. (**A**) Current versus time trace from CPE experiment with TPTD+PhOH. (**B**) Charge passed versus time for the CPE experiment shown in **A**. Conditions were 0.5 mM TPTD and 0.12 M PhOH under a CO_2 atmosphere at −2.25 V vs Fc^+/Fc in 0.1 M $TBAPF_6$/*N,N*-DMF; working electrode was a glassy carbon rod, counter electrode was a graphite rod, and the reference was a nonaqueous Ag/AgCl pseudoreference electrode; 0.075 M Fc was used as sacrificial oxidant.

Table S28. Results from CPE experiment in Figure S75, Ph_2DBTD + PhOH.

Time (s)	Charge (coulombs)	moles (e^-)	Moles of CO
20000*	3.94	4.08×10^{-5}	< LOQ
20000*	3.94	4.08×10^{-5}	< LOQ
20000*	3.94	4.08×10^{-5}	< LOQ

* indicates a triplicate series of injections carried out upon completion of electrolysis

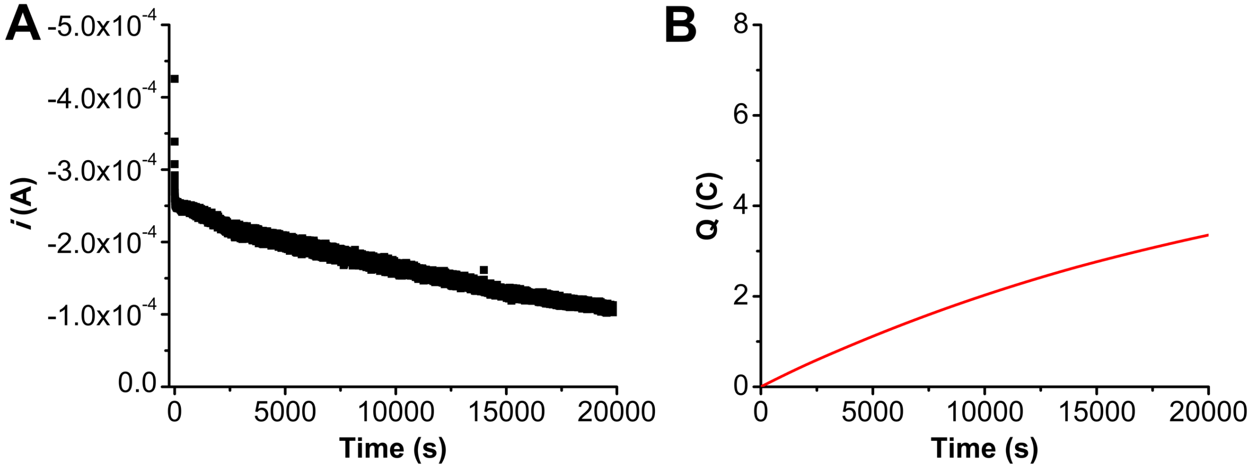

Figure S76. (**A**) Current versus time trace from CPE experiment with Mes_2DBTD+PhOH. (**B**) Charge passed versus time for the CPE experiment shown in **A**. Conditions were 0.5 mM Mes_2DBTD and 0.12 M PhOH under a CO_2 atmosphere at −2.30 V vs Fc^+/Fc in 0.1 M $TBAPF_6$/*N,N*-DMF; working electrode was a glassy carbon rod, counter electrode was a graphite rod, and the reference was a nonaqueous Ag/AgCl pseudoreference electrode; 0.075 M Fc was used as sacrificial oxidant.

Table S29. Results from CPE experiment in Figure S76, Mes_2DBTD + PhOH.

Time (s)	**Charge (coulombs)**	**moles (e$^-$)**	**Moles of CO**
20000*	3.35	3.48 x 10^{-5}	< LOQ
20000*	3.35	3.48 x 10^{-5}	< LOQ
20000*	3.35	3.48 x 10^{-5}	< LOQ

* indicates a triplicate series of injections carried out upon completion of electrolysis

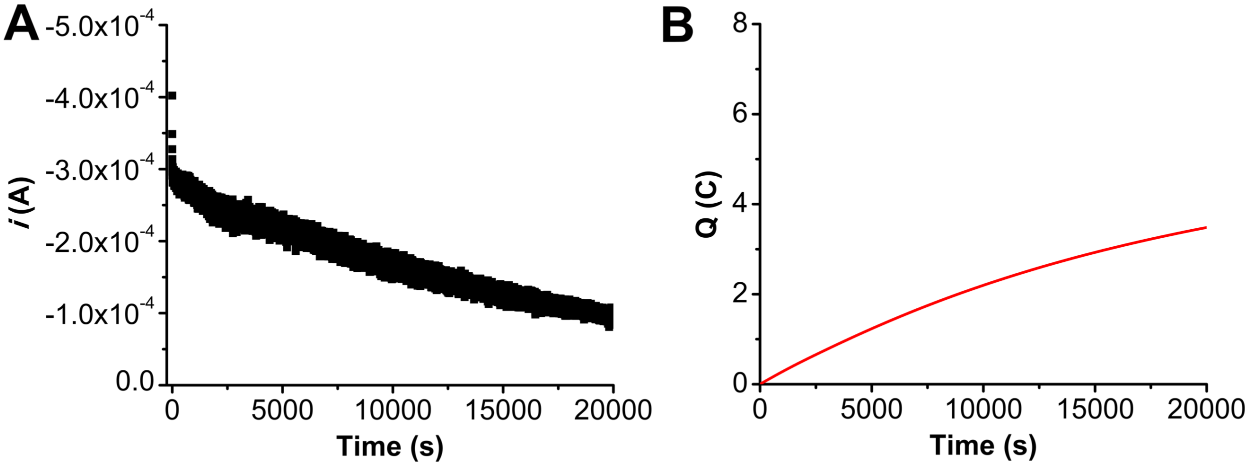

Figure S77. (**A**) Current versus time trace from CPE experiment with Ph_2DBTD+PhOH. (**B**) Charge passed versus time for the CPE experiment shown in **A**. Conditions were 0.5 mM Ph_2DBTD and 0.12 M PhOH under a CO_2 atmosphere at −2.20 V vs Fc^+/Fc in 0.1 M $TBAPF_6$/*N,N*-DMF; working electrode was a glassy carbon rod, counter electrode was a graphite rod, and the reference was a nonaqueous Ag/AgCl pseudoreference electrode; 0.075 M Fc was used as sacrificial oxidant.

Table S30. Results from CPE experiment in Figure S77, Mes_2DBTD + PhOH.

Time (s)	**Charge (coulombs)**	**moles (e^-)**	**Moles of CO**
20000*	3.48	3.61×10^{-5}	< LOQ
20000*	3.48	3.61×10^{-5}	< LOQ
20000*	3.48	3.61×10^{-5}	< LOQ

* indicates a triplicate series of injections carried out upon completion of electrolysis

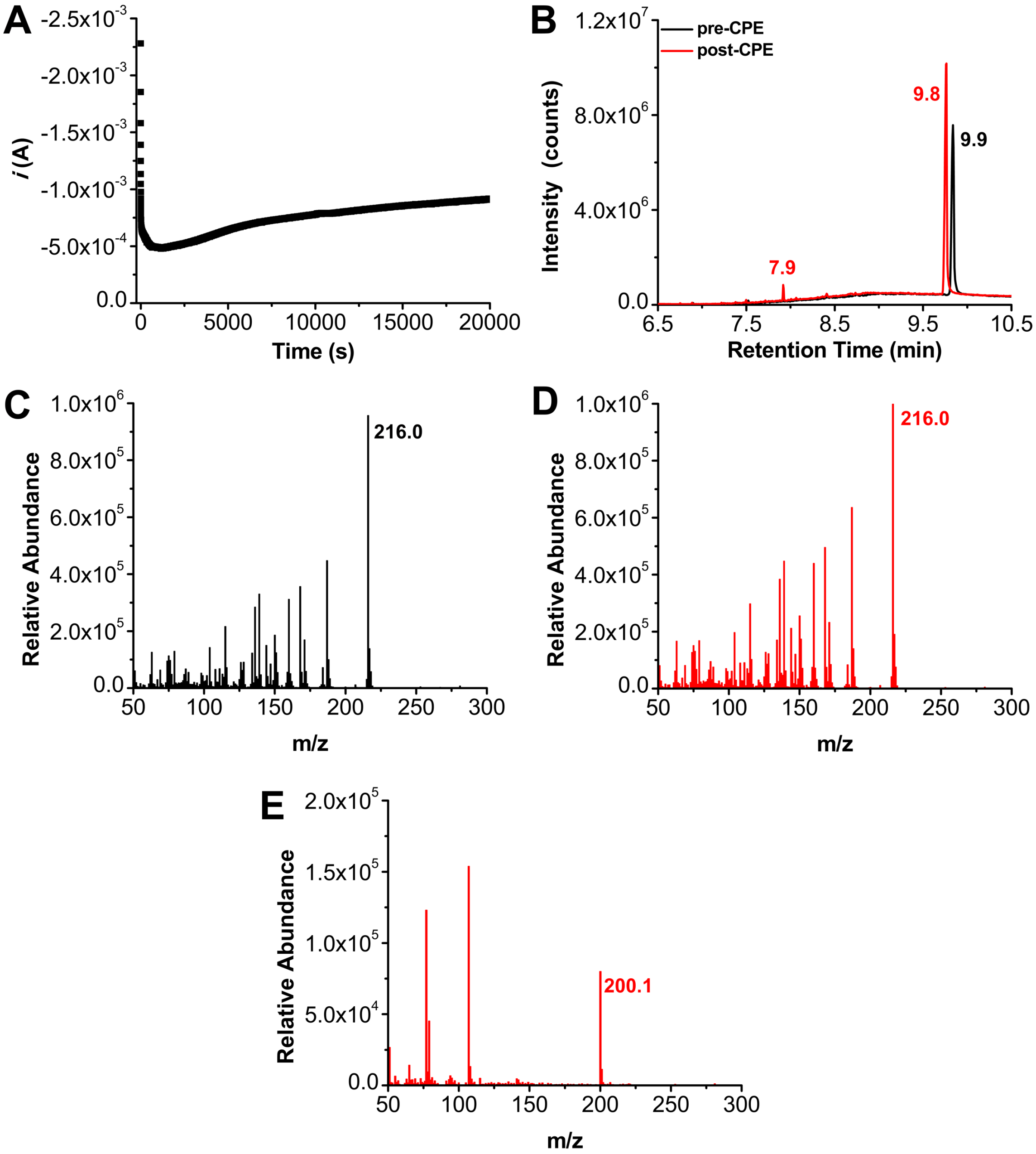

Figure S78. (**A**) Current versus time trace of control CPE experiment with DBTD and PhOH under N_2. (**B**) Gas chromatograph of the pre- and post-CPE solution. The mass spectrum for the peak at 9.9 min in the pre-CPE sample (**C**) and 9.8 min for the post-CPE sample (**D**) corresponds to DBTD. The MS spectrum of the peak at 7.9 min in the post-CPE sample corresponds to dibenzothiophene 5-oxide (**E**). Conditions for (**A**) were 5 mM DBTD and 0.1 M PhOH under a N_2 atmosphere at −2.30 V vs Fc^+/Fc in 0.1 M $TBAPF_6$/*N,N*-DMF; working and counter electrodes were carbon cloth and the reference was a nonaqueous Ag/AgCl pseudoreference electrode; 0.075 M Fc was used as sacrificial oxidant.

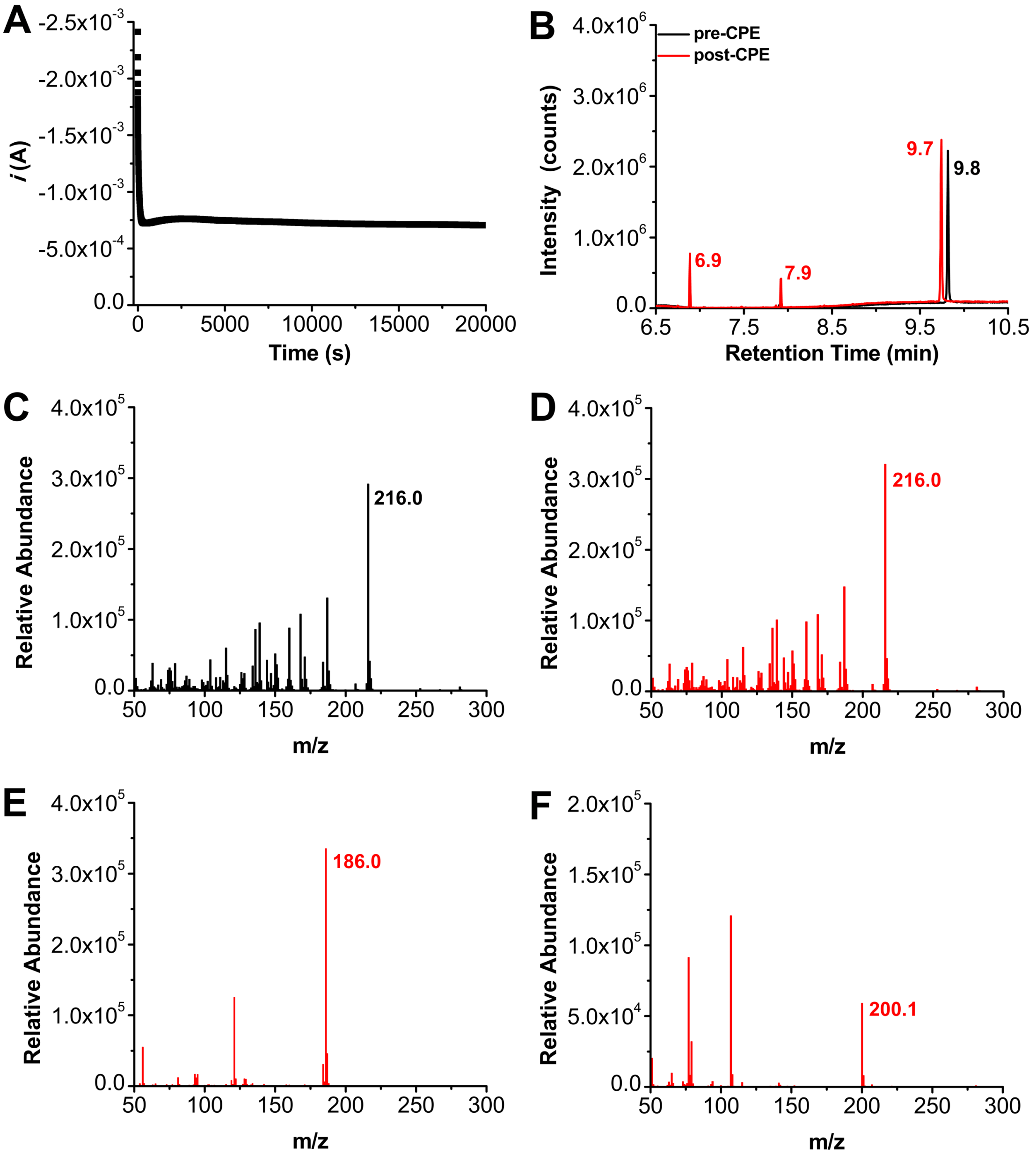

Figure S79. (**A**) Current versus time trace of control CPE experiment with **1**, DBTD, and PhOH under CO_2. (**B**) Gas chromatograph of the pre- and post-CPE solution. The mass spectrum for the peak at 9.8 min in the pre-CPE sample (**C**) and 9.7 min for the post-CPE sample (**D**) corresponds to DBTD. The MS spectrum of the peak at 6.9 min in the post-CPE sample likely corresponds to [1,1′-biphenyl]-2-thiol (**E**). The MS spectrum of the peak at 7.9 min in the post-CPE sample corresponds to dibenzothiophene 5-oxide (**F**). Conditions for (**A**) were 0.5 mM Cr(^{tbu}dhbpy)Cl(H_2O) **1**, 2.5 mM DBTD and 0.6 M PhOH under a N_2 atmosphere at −2.30 V vs Fc^+/Fc in 0.1 M $TBAPF_6$/*N,N*-DMF; working and counter electrodes were graphite rods, and the reference was a nonaqueous Ag/AgCl pseudoreference electrode; 0.075 M Fc was used as sacrificial oxidant.

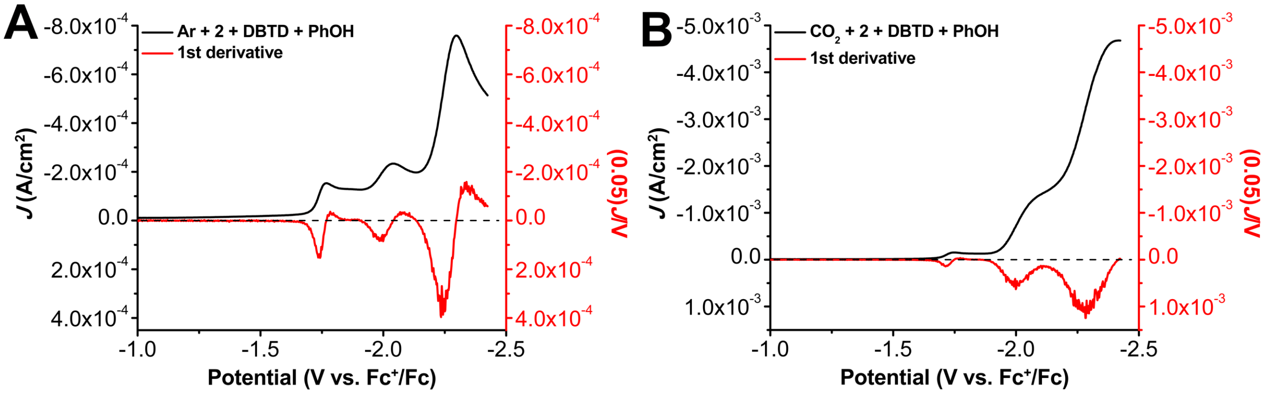

Figure S80. Example forward CV trace and first derivative plot used in $i_{\mathrm{cat}}/i_{\mathrm{p}}$ calculations for 1.0 mM Cr($^{\mathrm{tbu}}$dh$^{\mathrm{tbu}}$bpy)Cl(H_2O) **2** with 2.5 mM DBTD and 0.1 M PhOH under Ar (**A**) and CO_2 (**B**).

Computational Studies

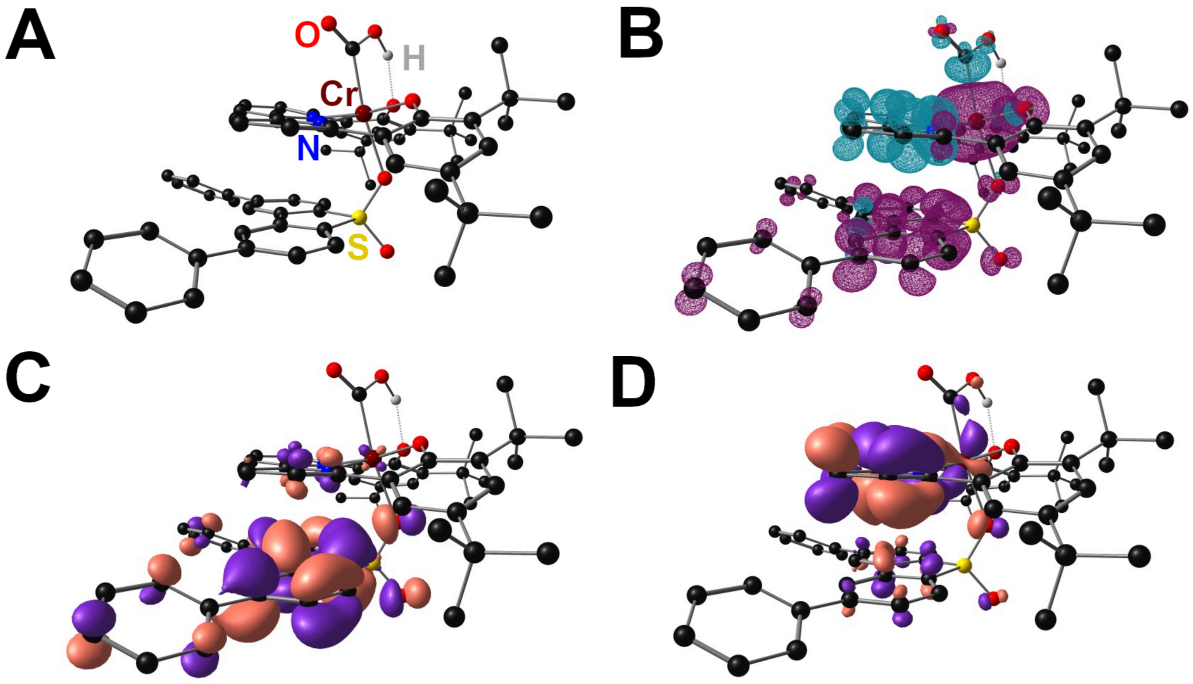

Figure S81. Molecular geometry of the ${}^{4}_{0}\mathbf{Cr(CO_2H)(Ph_2DBTD)}^{-2}$ adduct (**A**) DFT calculated spin density (**B**) Kohn-Sham orbital projection of SOMO (**C**) and SOMO^{-1} (**D**). Where Cr = Cr($^{\mathrm{tbu}}$dhbpy).

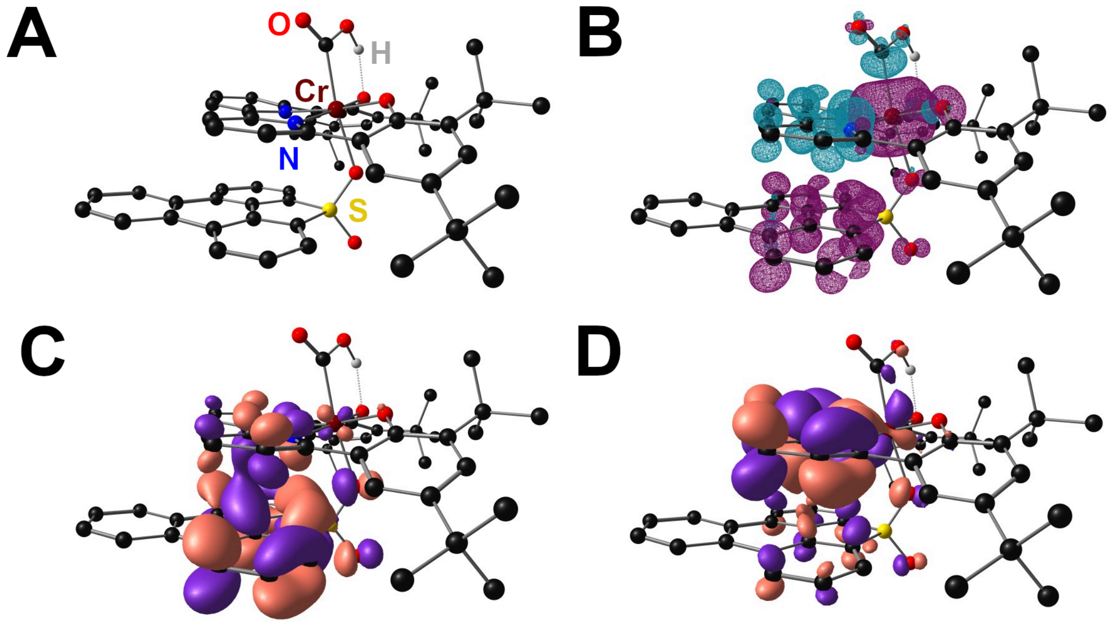

Figure S82. Molecular geometry of the ${}^{4}_{0}\mathbf{Cr(CO_2H)(TPTD)}^{-2}$ adduct (**A**) DFT calculated spin density (**B**) Kohn-Sham orbital projection of SOMO (**C**) and SOMO^{-1} (**D**). Where Cr = Cr($^{\mathrm{tbu}}$dhbpy).

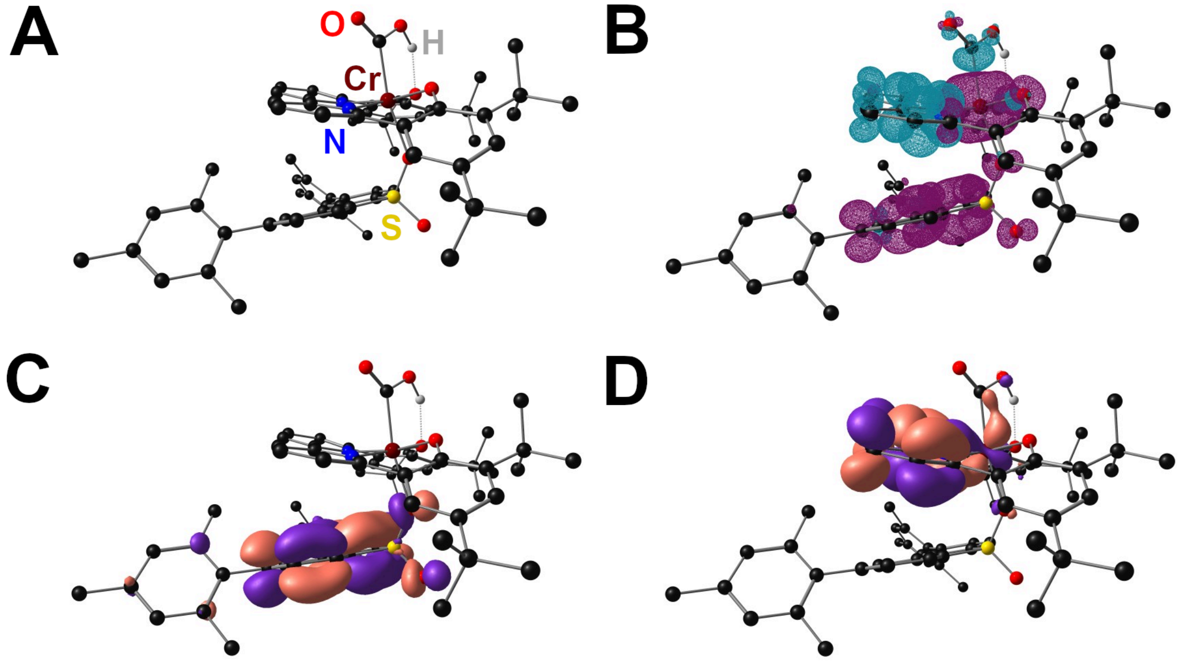

Figure S83. Molecular geometry of the ${}^{4}_{0}\mathbf{Cr(CO_2H)(Mes_2DBTD)}^{-2}$ adduct (**A**) DFT calculated spin density (**B**) Kohn-Sham orbital projection of SOMO (**C**) and SOMO^{-1} (**D**). Where Cr = Cr($^{\mathrm{tbu}}$dhbpy).

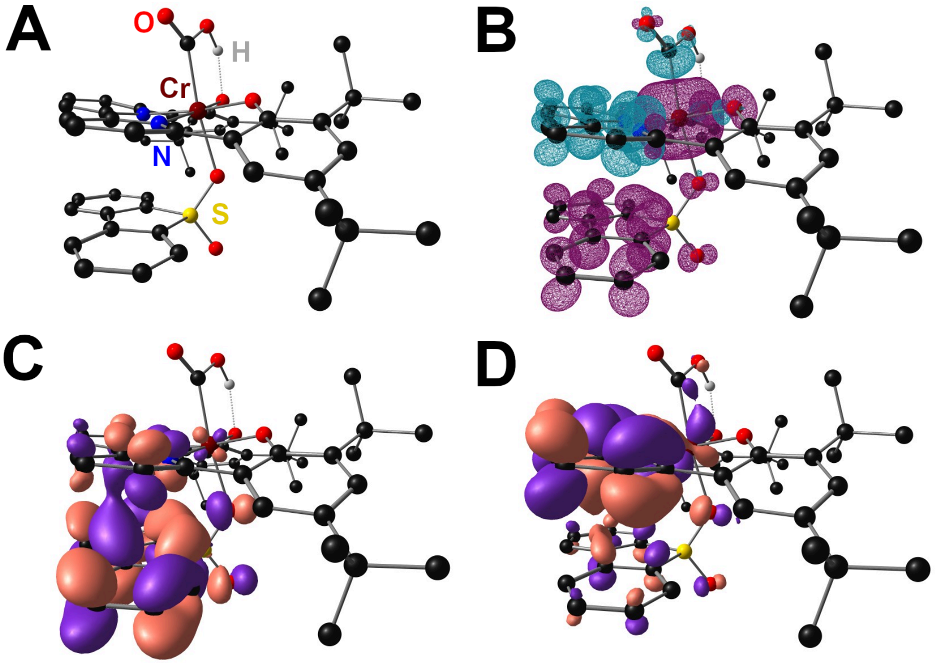

Figure S84. Molecular geometry of the $^{4}_{0}\mathbf{Cr(CO_2H)(DBTD)}^{-2}$ adduct (**A**) DFT calculated spin density (**B**) Kohn-Sham orbital projection of SOMO (**C**) and SOMO^{-1} (**D**). Where Cr = Cr($^{\text{tbu}}$dhbpy).

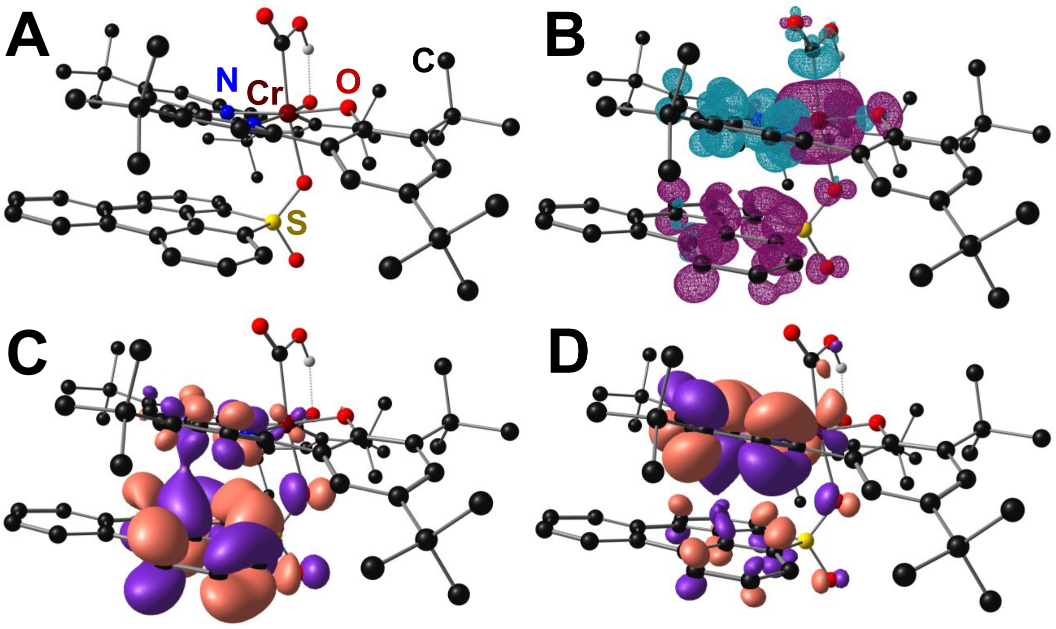

Figure S85. Molecular geometry of the $^{4}_{0}\mathbf{Cr(CO_2H)(TPTD)}^{-2}$ adduct (**A**) DFT calculated spin density (**B**) Kohn-Sham orbital projection of SOMO (**C**) and SOMO^{-1} (**D**). Where Cr = Cr($^{\text{tbu}}$dh$^{\text{tbu}}$bpy).

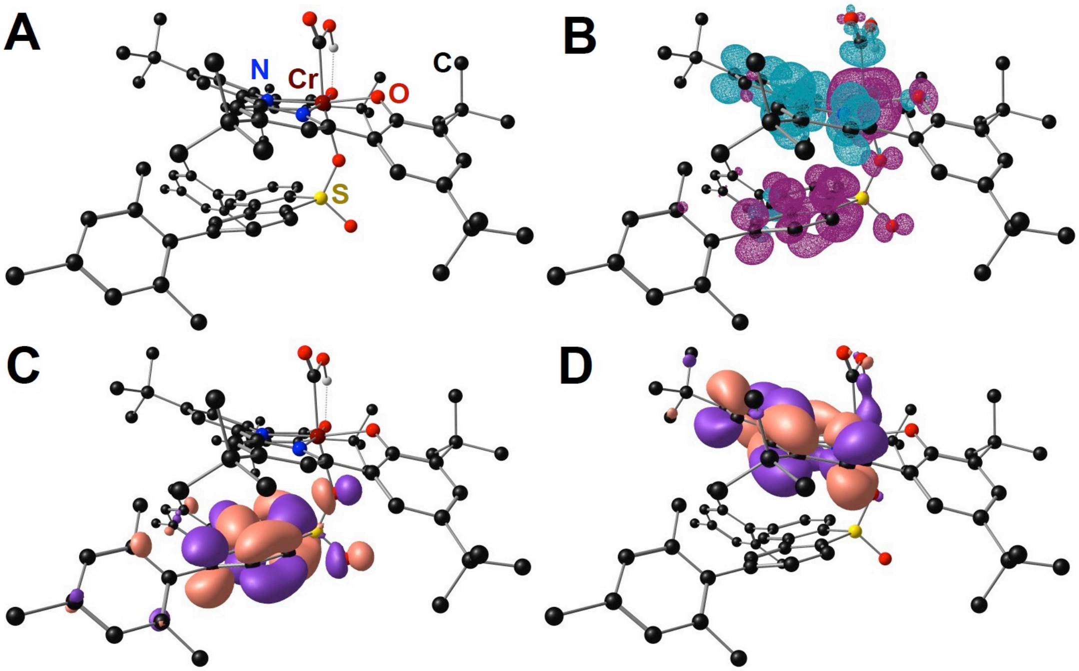

Figure S86. Molecular geometry of the ${}^{4}_{0}\mathbf{Cr(CO_2H)(Mes_2DBTD)}^{-2}$ adduct (**A**) DFT calculated spin density (**B**) Kohn-Sham orbital projection of SOMO (**C**) and SOMO^{-1} (**D**). Where Cr = Cr($^{\text{tbu}}$dh$^{\text{tbu}}$bpy).

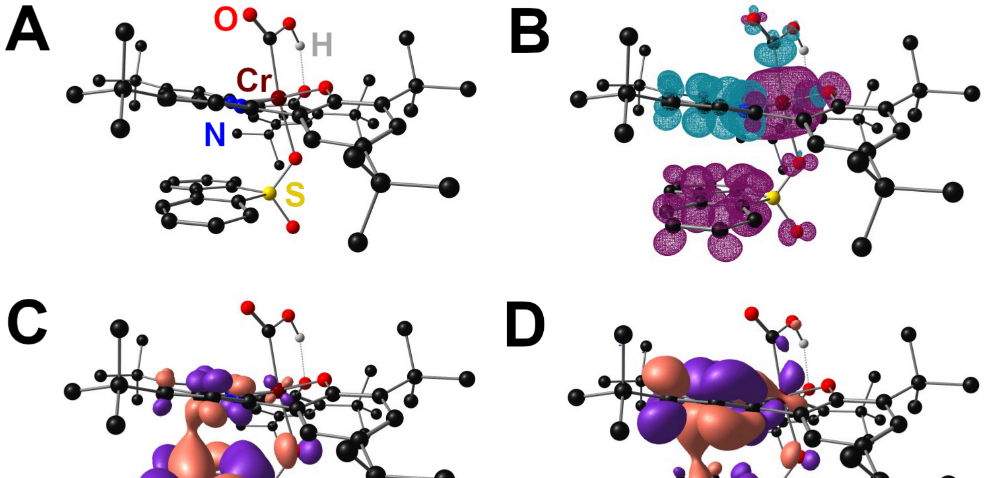

Figure S87. Molecular geometry of the ${}^{4}_{0}\mathbf{Cr(CO_2H)(DBTD)}^{-2}$ adduct (**A**) DFT calculated spin density (**B**) Kohn-Sham orbital projection of SOMO (**C**) and SOMO^{-1} (**D**). Where Cr = Cr($^{\text{tbu}}$dh$^{\text{tbu}}$bpy).

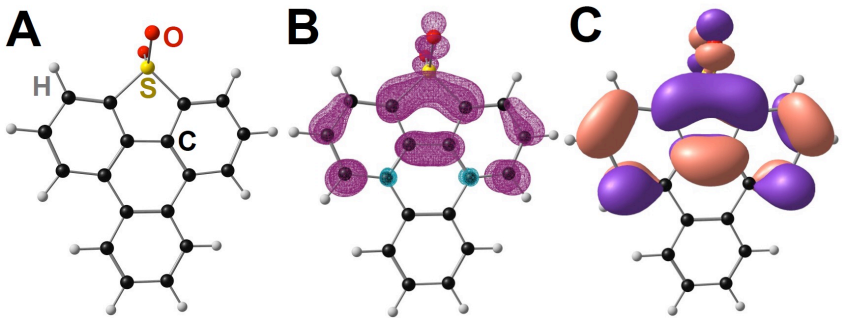

Figure S88. Molecular geometry of the $^{2}\mathbf{TPTD}^{-1}$ RM (**A**) DFT calculated spin density (**B**) Kohn-Sham orbital projection of SOMO (**C**).

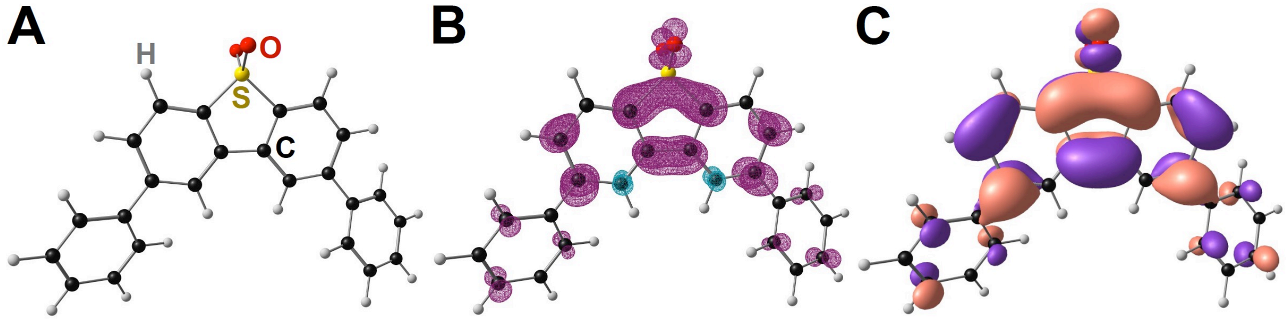

Figure S89. Molecular geometry of the $^{2}\mathbf{Ph_2DBTD}^{-1}$ RM (**A**) DFT calculated spin density (**B**) Kohn-Sham orbital projection of SOMO (**C**).

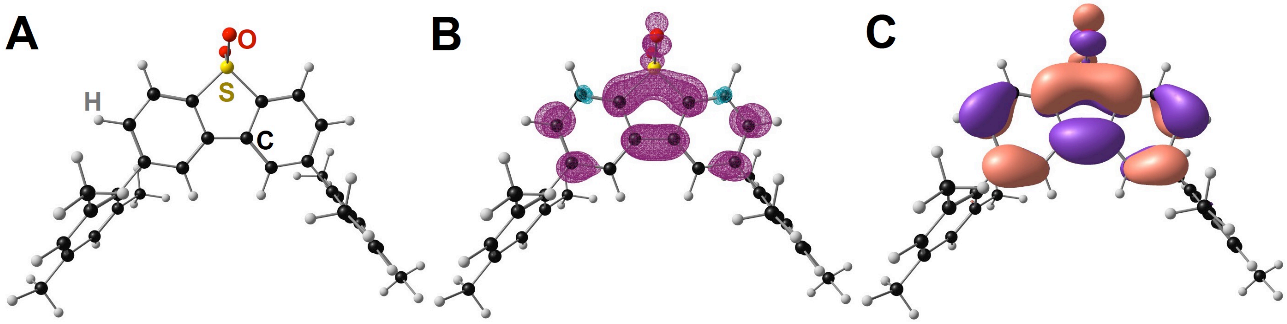

Figure S90. Molecular geometry of the $^{2}\mathbf{Mes_2DBTD}^{-1}$ RM (**A**) DFT calculated spin density (**B**) Kohn-Sham orbital projection of SOMO (**C**).

Table S31. Calculated NICS(0) values for DBTD.

Ring	**[RM]^0 NICS(0)**	**[RM]$^–$ NICS(0)**	**ΔNICS(0)**
A	+2.913	–6.703	–9.616
B	–6.916	–1.709	+5.207

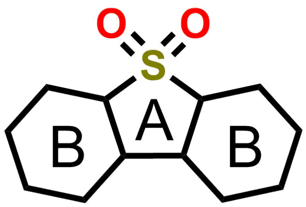

Table S32. Calculated NICS(0) values for TPTD.

Ring	**$[RM]^0$ NICS(0)**	**$[RM]^-$ NICS(0)**	**ΔNICS(0)**
A	+4.084	–9.162	–13.246
B	–7.820	–1.190	+6.630
C	–1.836	–1.339	+0.497
D	–7.554	–9.010	+1.456

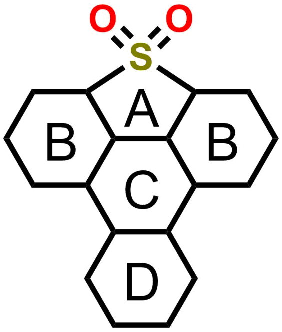

Table S33. Calculated NICS(0) values for Ph_2DBTD.

Ring	**$[RM]^0$ NICS(0)**	**$[RM]^-$ NICS(0)**	**ΔNICS(0)**
A	+2.798	–5.583	–8.381
B	–6.181	–2.214	+3.967
C	–7.177	–5.980	+1.197

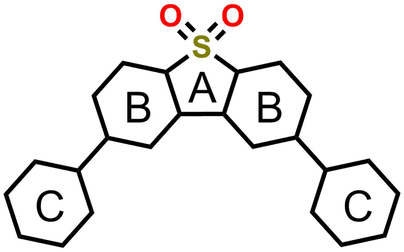

Table S34. Calculated NICS(0) values for Mes_2DBTD.

Ring	**$[RM]^0$ NICS(0)**	**$[RM]^-$ NICS(0)**	**ΔNICS(0)**
A	+3.041	–6.074	–9.115
B	–6.462	–1.403	+5.059
C	–7.299	–7.283	+0.016

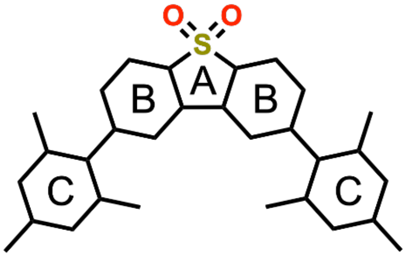

Table S35. Calculated centroid–centroid distances (benzene rings of the dibenzothiophene core to the bpy ligand of the Cr complex) and Cr–sulfone bond distances for all $[Cr(L)(CO_2H)(RM)]^{2-}$ adducts. Where L is $[^{tbu}dhbpy]^{2-}$ or $[^{tbu}dh^{tbu}bpy]^{2-}$ and S=3/2.

Cr Complex	Centroid–Centroid Distances (Å)	Cr–Sulfone Distance (Å)
$[Cr(^{tbu}dhbpy)(CO_2H)(DBTD)]^{2-}$	3.329 3.287	2.189
$[Cr(^{tbu}dhbpy)(CO_2H)(Mes_2DBTD)]^{2-}$	4.678 3.889	2.164
$[Cr(^{tbu}dhbpy)(CO_2H)(TPTD)]^{2-}$	3.252 3.229	2.195
$[Cr(^{tbu}dhbpy)(CO_2H)(Ph_2DBTD)]^{2-}$	3.326 3.278	2.187
$[Cr(^{tbu}dh^{tbu}bpy)(CO_2H)(DBTD)]^{2-}$	3.361 3.316	2.185
$[Cr(^{tbu}dh^{tbu}bpy)(CO_2H)(Mes_2DBTD)]^{2-}$	4.852 3.862	2.165
$[Cr(^{tbu}dh^{tbu}bpy)(CO_2H)(TPTD)]^{2-}$	3.314 3.285	2.188
$[Cr(^{tbu}dh^{tbu}bpy)(CO_2H)(Ph_2DBTD)]^{2-}$	3.465 3.649	2.184

Analysis of Electrochemical CO_2 Reduction Under Aprotic Conditions

Previously we observed that the addition of DBTD to a solution of **1** under CO_2 saturation conditions lead to the appearance of an aprotic catalytic feature that is not intrinsic to either component.[45] The addition of TPTD (**Figure S91**) to a solution of **1** and CO_2 leads to the appearance of an irreversible redox feature at the $E_{1/2}$ of TPTD (−2.19 V vs. Fc^+/Fc), although the increase is less than that observed for DBTD. Despite a 120 mV difference in standard potential, Mes_2DBTD and Ph_2DBTD RMs demonstrate roughly the same increase in the observed current density and some retention of the return oxidation feature of the RM. This suggests an excess of the RM radical anion is being generated with respect to its rate of interaction with complex **1**, and as a result, on the return CV sweep the radical anion is still present for re-oxidation, leading to the observed quasi-reversibility. When we compare these data with the aprotic CV data for all four RMs with **2**, we see a deviation from the trend described for **1** above: the addition of all RMs lead to a completely irreversible wave (**Figure S91**). Notably, TPTD shows a significant increase in current density over DBTD when added to a solution of **2** under CO_2 saturation conditions (**Figure S91B**, red). Variable concentration studies were completed for all systems that produce an electrochemically irreversible system under aprotic conditions: the observed current density is proportional to the concentration of all reaction components (**Figures S92-S108**).

CPE experiments were then performed to assess reaction efficiency under aprotic conditions. Unlike the results for **1**+DBTD, all new systems reported here (**1** with the new RMs and **2** with all RMs) demonstrated insignificant catalytic properties under tested electrolysis conditions. The CPE experiments for **1** with Mes_2DBTD and TPTD as the RM and **2** with all four RMs led to a rapid loss of activity: following an initial stable period, current quickly diminishes

(**Figures S109-S114**), with no amount of CO detected above limit of quantification (LOQ, see **SI**). Initial stability followed by rapid loss of activity suggests molecular adsorption to the electrode, resulting in a passivation of the electrode surface.[46] Comparing these results with control CPE experiments of **1**,[45] **2**, DBTD,[45] TPTD, Mes_2DBTD, and Ph_2DBTD individually under aprotic conditions (**Figures S115-S118**) also showed either no CO or the presence of non-quantifiable amounts of CO (**Table S42-S44**). A similar phenomenon is observed when Ph_2DBTD is used as the RM with **1** (**Figure S119**), but in this case the system has a FE_{CO} = 26±2% (**Table S45**) and ^{1}H NMR of the post-bulk solution shows the appearance of carbonate (CO_3^{2-}), but no other carbon-containing products (**Figure S120**). Although CV data indicates that some of these combinations should result in aprotic catalytic activity, these combinations are not stable under the tested electrolysis conditions.

Cyclic Voltammetry Under Aprotic Conditions

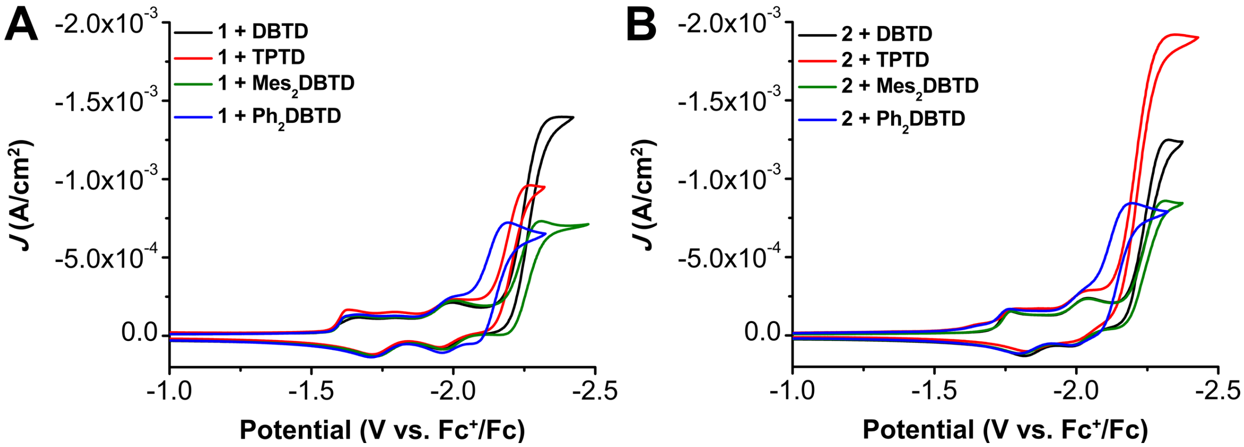

Figure S91. CVs of 1.0 mM Cr(^{tbu}dhbpy)Cl(H_2O) **1** (**A**) or Cr(^{tbu}dh^{tbu}bpy)Cl(H_2O) **2** (**B**) with 2.5 mM DBTD (black), TPTD (red), Mes_2DBTD (green), and Ph_2DBTD (blue) as the RM under CO_2 saturation conditions. Conditions: 0.1 M $TBAPF_6$/DMF; glassy carbon working electrode, glassy carbon rod counter electrode, Ag/AgCl pseudoreference electrode; referenced to Fc^+/Fc internal standard; 100 mV/s scan rate.

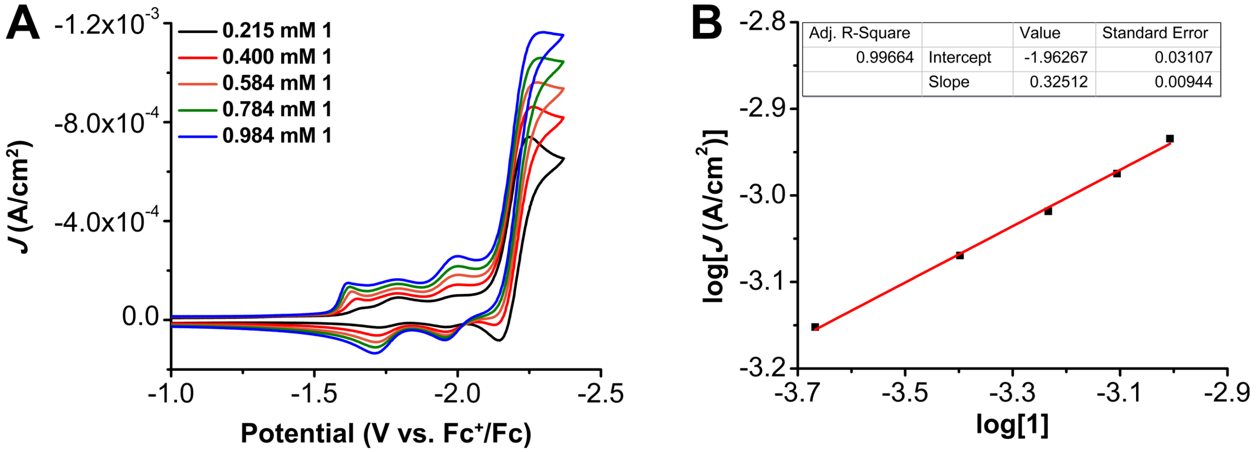

Figure S92. (**A**) CVs of Cr(^{tbu}dhbpy)Cl(H_2O) **1** at variable concentrations, obtained under CO_2 saturation with 2.5 mM TPTD. Conditions: 0.1 M $TBAPF_6$/*N,N*-DMF; glassy carbon working electrode, glassy carbon counter electrode, Ag/AgCl pseudoreference electrode; 100 mV/s scan rate; referenced to internal ferrocene standard. (**B**) Log-log plot from data obtained from CVs in **A** at −2.29 V vs. Fc^+/Fc.

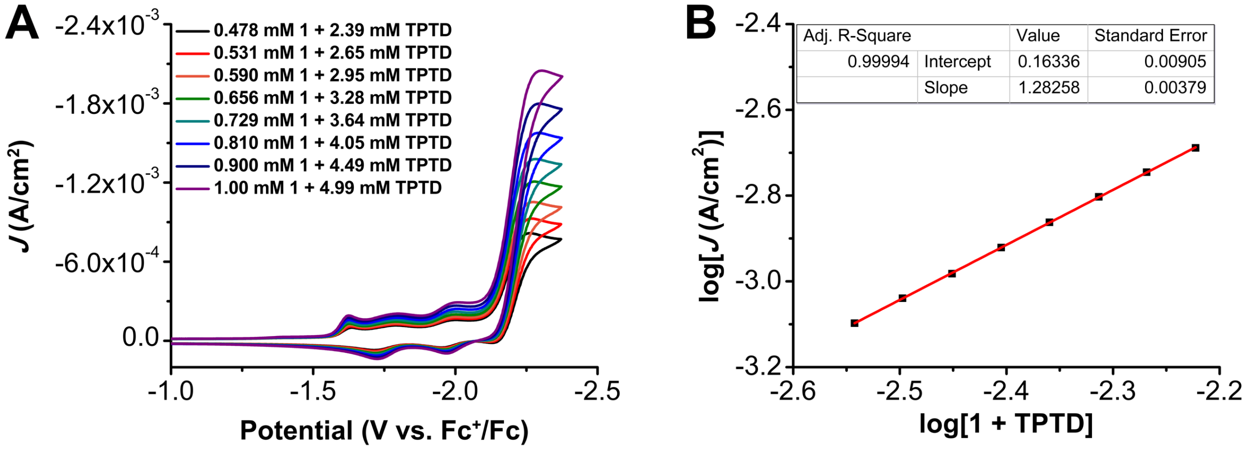

Figure S93. (**A**) CVs where the concentrations of Cr(^{tbu}dhbpy)Cl(H_2O) **1** and TPTD were varied at a fixed 1:5 ratio of **1**:TPTD under CO_2 saturation conditions. Conditions: 0.1 M $TBAPF_6$/*N,N*-DMF; glassy carbon working electrode, glassy carbon counter electrode, Ag/AgCl pseudoreference electrode; 100 mV/s scan rate; referenced to internal ferrocene standard. (B) Log-log plot from data obtained from CVs in A at −2.30 V vs. Fc^+/Fc.

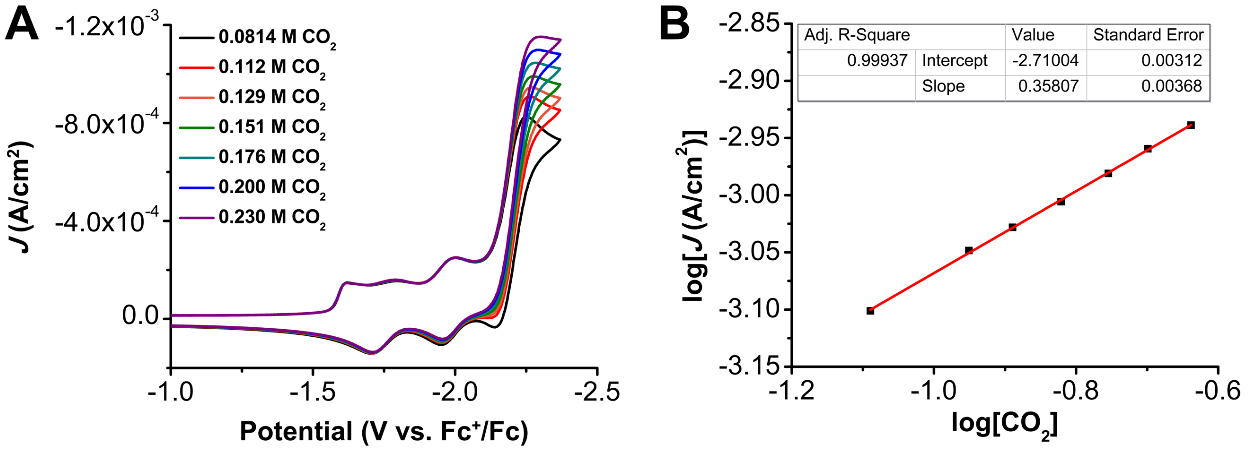

Figure S94. (**A**) CVs of 1.0 mM Cr(^{tbu}dhbpy)Cl(H_2O) **1** and 2.5 mM TPTD at varied CO_2 concentrations. Conditions: 0.1 M $TBAPF_6$/*N,N*-DMF; glassy carbon working electrode, glassy carbon counter electrode, Ag/AgCl pseudoreference electrode; 100 mV/s scan rate; referenced to internal ferrocene standard. (**B**) Log-log plot from data obtained from CVs in **A** at −2.29 V vs. Fc^+/Fc.

The variable concentration experiment for TPTD with fixed concentrations of **1** and CO_2 could not be completed. The co-catalytic effect quickly reached saturation and the irreversible redox feature became obscured by unbound TPTD in solution.

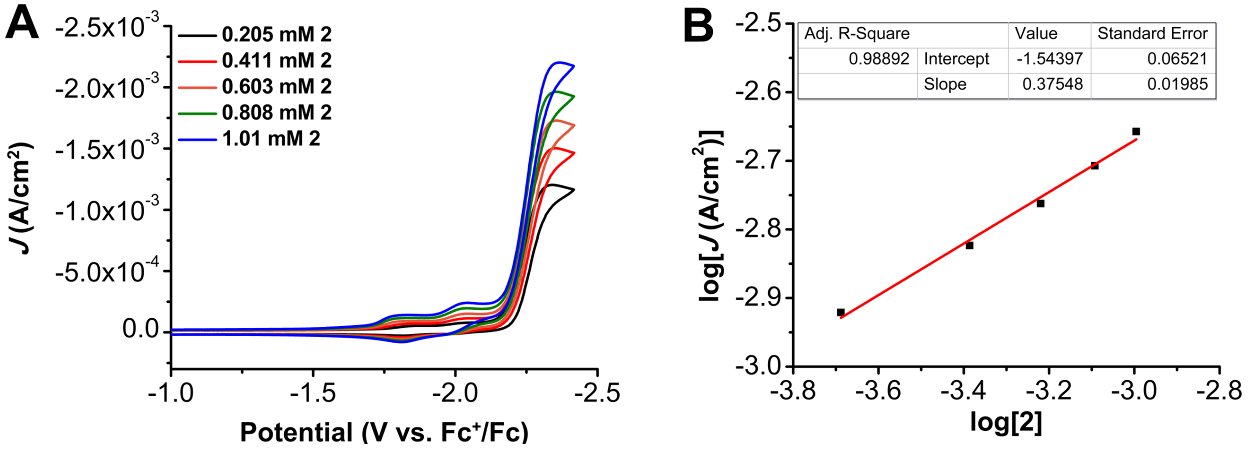

Figure S95. (**A**) CVs of Cr(^{tbu}dh^{tbu}bpy)Cl(H_2O) **2** at variable concentrations, obtained under CO_2 saturation with 2.5 mM DBTD. Conditions: 0.1 M $TBAPF_6$/*N,N*-DMF; glassy carbon working electrode, glassy carbon counter electrode, Ag/AgCl pseudoreference electrode; 100 mV/s scan rate; referenced to internal ferrocene standard. (**B**) Log-log plot from data obtained from CVs in **A** at −2.36 V vs. Fc^+/Fc.

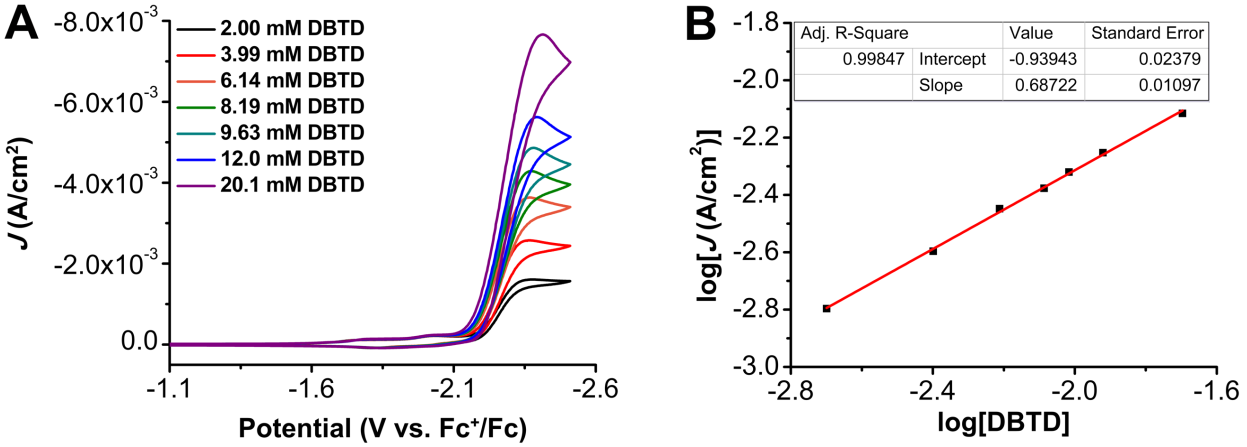

Figure S96. (**A**) CVs of 1.0 mM Cr(^{tbu}dh^{tbu}bpy)Cl(H_2O) **2** at variable DBTD concentrations, obtained under CO_2 saturation. Conditions: 0.1 M $TBAPF_6$/*N,N*-DMF; glassy carbon working electrode, glassy carbon counter electrode, Ag/AgCl pseudoreference electrode; 100 mV/s scan rate; referenced to internal ferrocene standard. (**B**) Log-log plot from data obtained from CVs in **A** at −2.41 V vs. Fc^+/Fc.

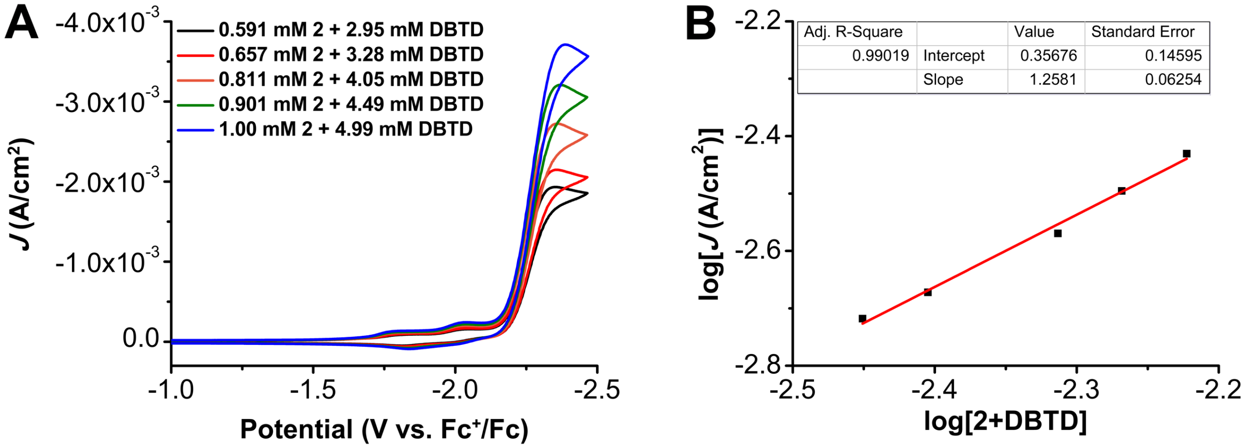

Figure S97. (**A**) CVs where the concentrations of Cr(^{tbu}dh^{tbu}bpy)Cl(H_2O) **2** and DBTD were varied at a fixed 1:5 ratio of **1**:DBTD under CO_2 saturation conditions. Conditions: 0.1 M $TBAPF_6$/*N,N*-DMF; glassy carbon working electrode, glassy carbon counter electrode, Ag/AgCl pseudoreference electrode; 100 mV/s scan rate; referenced to internal ferrocene standard. (**B**) Log-log plot from data obtained from CVs in **A** at −2.38 V vs. Fc^+/Fc.

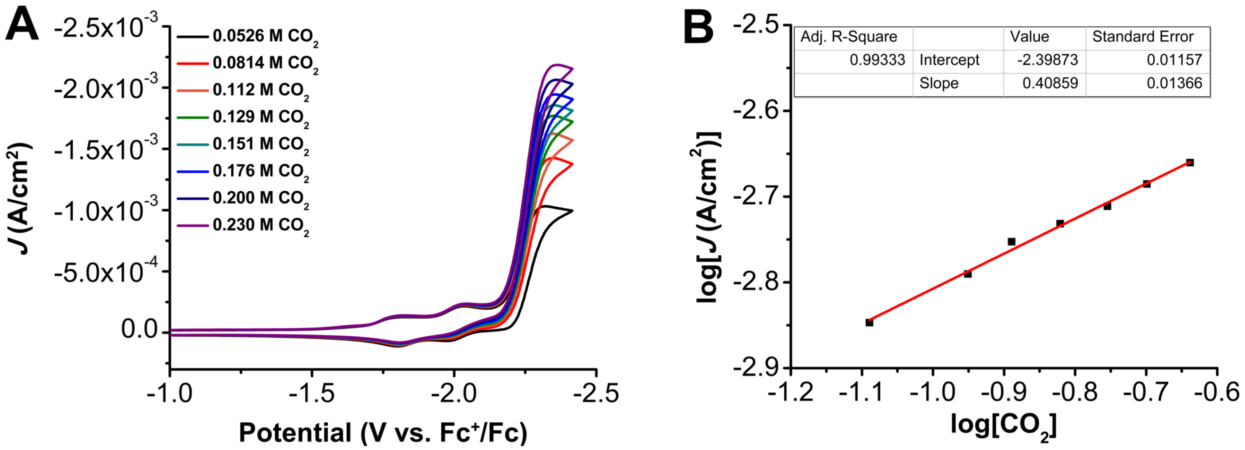

Adj. R-Square		Value	Standard Error
0.99333	Intercept	-2.39873	0.01157
	Slope	0.40859	0.01366

Figure S98. (**A**) CVs of 1.0 mM Cr(^{tbu}dh^{tbu}bpy)Cl(H_2O) **2** and 2.5 mM DBTD at varied CO_2 concentrations. Conditions: 0.1 M $TBAPF_6$/*N,N*-DMF; glassy carbon working electrode, glassy carbon counter electrode, Ag/AgCl pseudoreference electrode; 100 mV/s scan rate; referenced to internal ferrocene standard. (**B**) Log-log plot from data obtained from CVs in **A** at −2.36 V vs. Fc$^+$/Fc.

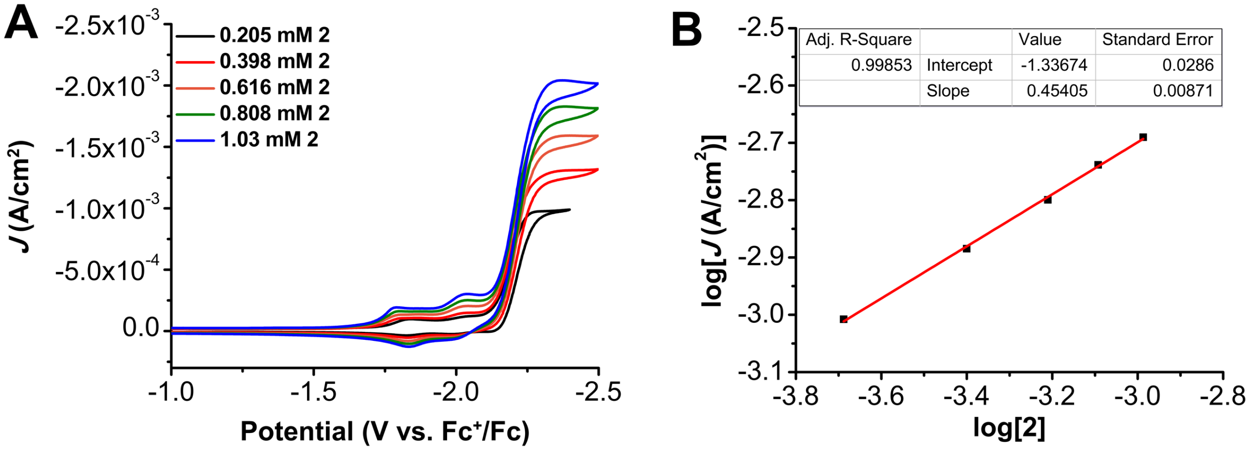

Adj. R-Square		Value	Standard Error
0.99853	Intercept	-1.33674	0.0286
	Slope	0.45405	0.00871

Figure S99. (**A**) CVs of Cr(^{tbu}dh^{tbu}bpy)Cl(H_2O) **2** at variable concentrations, obtained under CO_2 saturation with 2.5 mM TPTD. Conditions: 0.1 M $TBAPF_6$/*N,N*-DMF; glassy carbon working electrode, glassy carbon counter electrode, Ag/AgCl pseudoreference electrode; 100 mV/s scan rate; referenced to internal ferrocene standard. (**B**) Log-log plot from data obtained from CVs in **A** at −2.36 V vs. Fc$^+$/Fc.

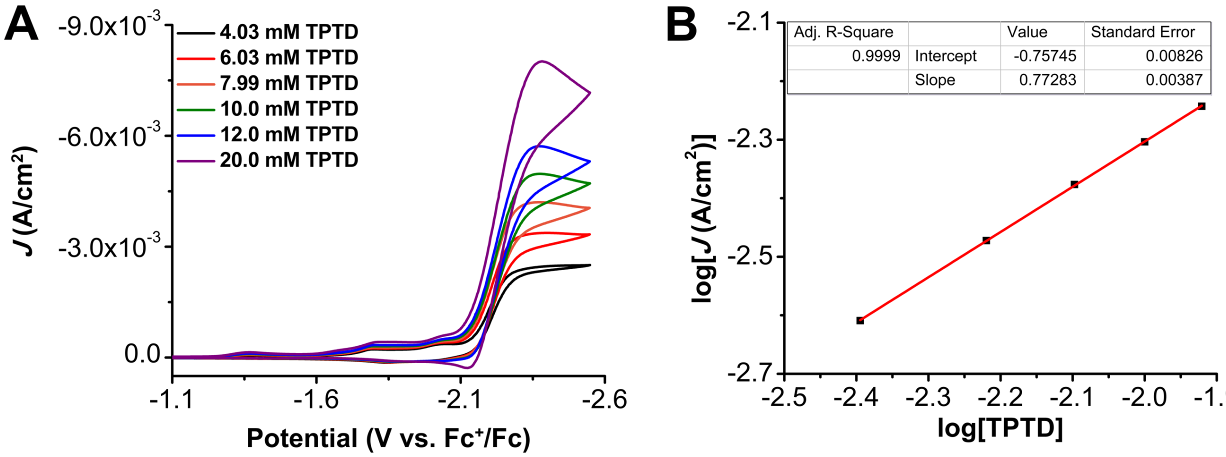

Adj. R-Square		Value	Standard Error
0.9999	Intercept	-0.75745	0.00826
	Slope	0.77283	0.00387

Figure S100. (**A**) CVs of 1.0 mM Cr(^{tbu}dh^{tbu}bpy)Cl(H_2O) **2** at variable TPTD concentrations, obtained under CO_2 saturation. Conditions: 0.1 M TBAPF$_6$/*N,N*-DMF; glassy carbon working electrode, glassy carbon counter electrode, Ag/AgCl pseudoreference electrode; 100 mV/s scan rate; referenced to internal ferrocene standard. (**B**) Log-log plot from data obtained from CVs in **A** at −2.38 V vs. Fc$^+$/Fc.

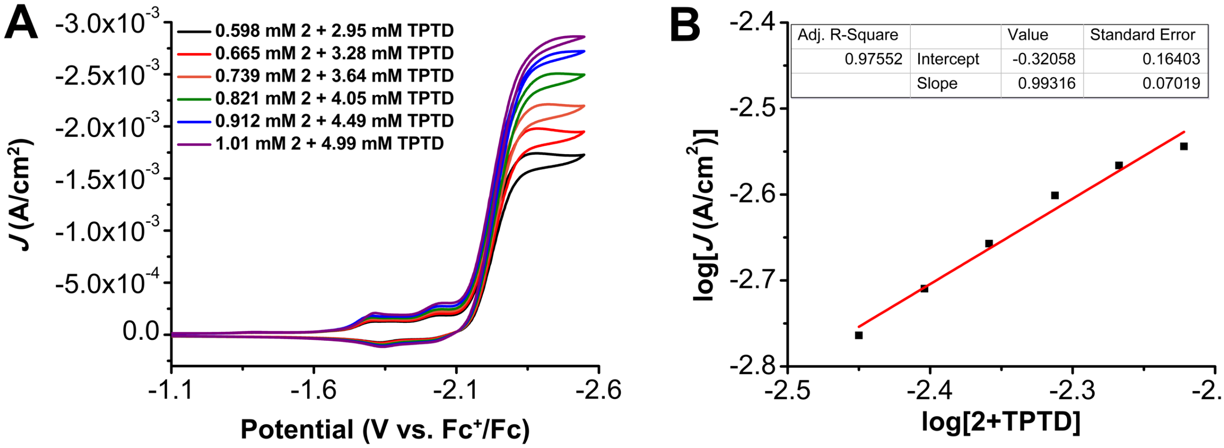

Adj. R-Square		Value	Standard Error
0.97552	Intercept	-0.32058	0.16403
	Slope	0.99316	0.07019

Figure S101. (**A**) CVs where the concentrations of Cr(^{tbu}dh^{tbu}bpy)Cl(H_2O) **2** and TPTD were varied at a fixed 1:5 ratio of **1**:TPTD under CO_2 saturation conditions. Conditions: 0.1 M TBAPF$_6$/*N,N*-DMF; glassy carbon working electrode, glassy carbon counter electrode, Ag/AgCl pseudoreference electrode; 100 mV/s scan rate; referenced to internal ferrocene standard. (**B**) Log-log plot from data obtained from CVs in **A** at −2.48 V vs. Fc$^+$/Fc.

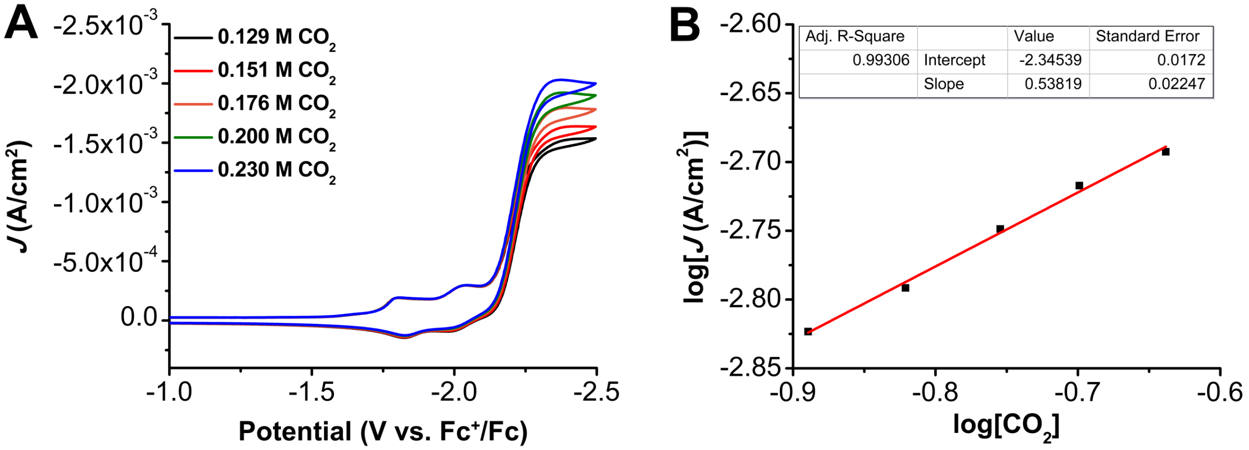

Figure S102. (**A**) CVs of 1.0 mM Cr(^{tbu}dh^{tbu}bpy)Cl(H_2O) **2** and 2.5 mM TPTD at varied CO_2 concentrations. Conditions: 0.1 M $TBAPF_6$/*N,N*-DMF; glassy carbon working electrode, glassy carbon counter electrode, Ag/AgCl pseudoreference electrode; 100 mV/s scan rate; referenced to internal ferrocene standard. (**B**) Log-log plot from data obtained from CVs in **A** at −2.37 V vs. Fc^+/Fc.

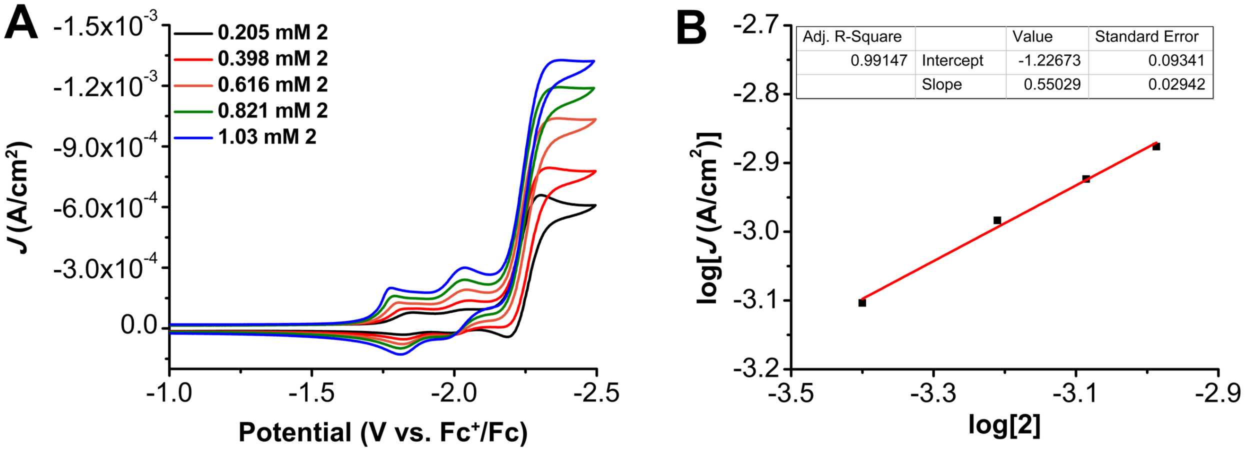

Figure S103. (**A**) CVs of Cr(^{tbu}dh^{tbu}bpy)Cl(H_2O) **2** at variable concentrations, obtained under CO_2 saturation with 2.5 mM Mes_2DBTD. Conditions: 0.1 M $TBAPF_6$/*N,N*-DMF; glassy carbon working electrode, glassy carbon counter electrode, Ag/AgCl pseudoreference electrode; 100 mV/s scan rate; referenced to internal ferrocene standard. (**B**) Log-log plot from data obtained from CVs in **A** at −2.37 V vs. Fc^+/Fc.

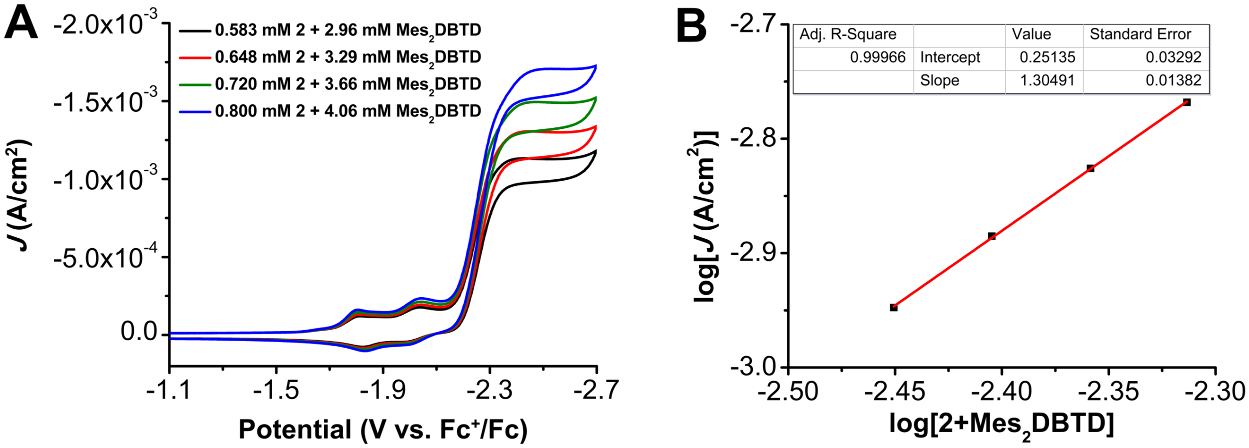

Adj. R-Square		Value	Standard Error
0.99966	Intercept	0.25135	0.03292
	Slope	1.30491	0.01382

Figure S104. (**A**) CVs where the concentrations of Cr(^{tbu}dh^{tbu}bpy)Cl(H_2O) **2** and Mes$_2$DBTD were varied at a fixed 1:5 ratio of **1**:Mes$_2$DBTD under CO_2 saturation conditions. Conditions: 0.1 M TBAPF$_6$/*N,N*-DMF; glassy carbon working electrode, glassy carbon counter electrode, Ag/AgCl pseudoreference electrode; 100 mV/s scan rate; referenced to internal ferrocene standard. (**B**) Log-log plot from data obtained from CVs in **A** at −2.50 V vs. Fc$^+$/Fc.

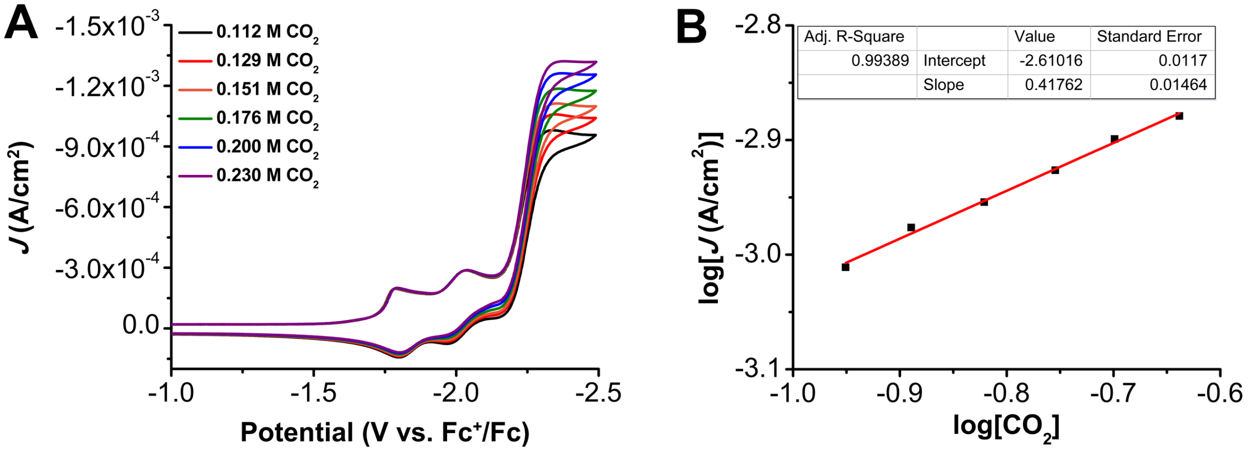

Adj. R-Square		Value	Standard Error
0.99389	Intercept	-2.61016	0.0117
	Slope	0.41762	0.01464

Figure S105. (**A**) CVs of 1.0 mM Cr(^{tbu}dh^{tbu}bpy)Cl(H_2O) **2** and 2.5 mM Mes$_2$DBTD at varied CO_2 concentrations. Conditions: 0.1 M TBAPF$_6$/*N,N*-DMF; glassy carbon working electrode, glassy carbon counter electrode, Ag/AgCl pseudoreference electrode; 100 mV/s scan rate; referenced to internal ferrocene standard. (**B**) Log-log plot from data obtained from CVs in **A** at −2.37 V vs. Fc$^+$/Fc.

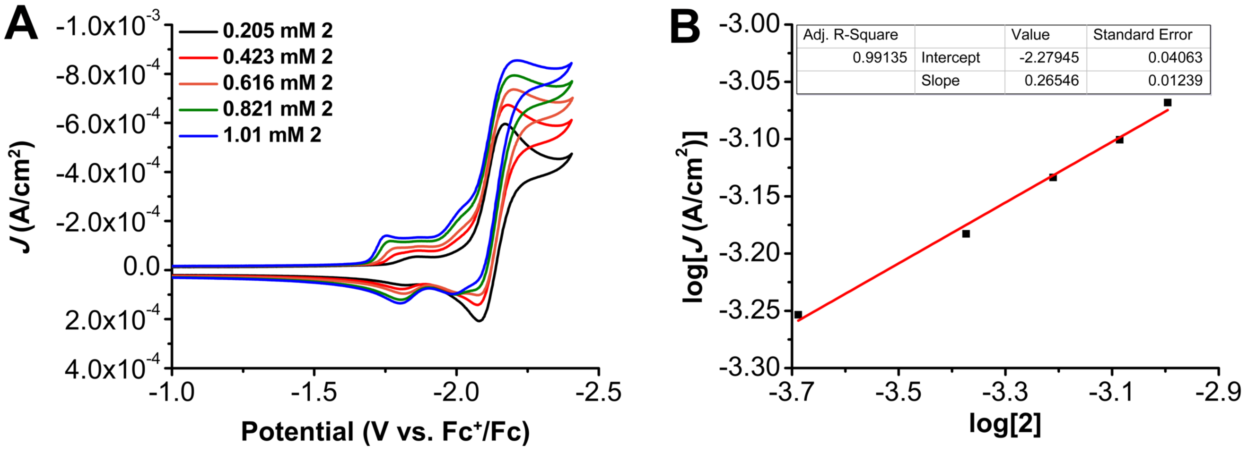

Figure S106. (**A**) CVs of Cr(^{tbu}dh^{tbu}bpy)Cl(H$_2$O) **2** at variable concentrations, obtained under CO$_2$ saturation with 2.5 mM Ph$_2$DBTD. Conditions: 0.1 M TBAPF$_6$/*N,N*-DMF; glassy carbon working electrode, glassy carbon counter electrode, Ag/AgCl pseudoreference electrode; 100 mV/s scan rate; referenced to internal ferrocene standard. (**B**) Log-log plot from data obtained from CVs in **A** at −2.21 V vs. Fc$^+$/Fc.

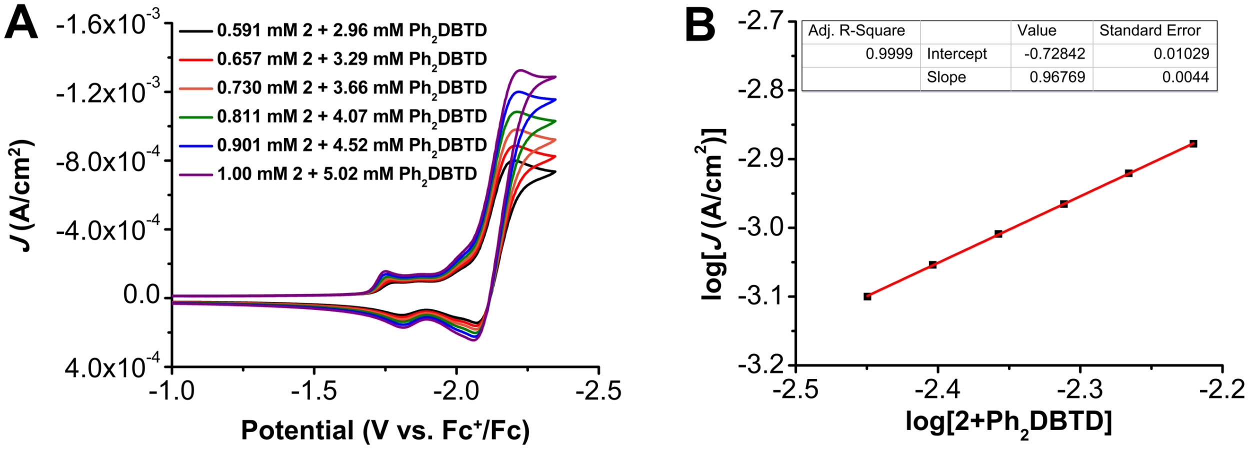

Figure S107. (**A**) CVs where the concentrations of Cr(^{tbu}dh^{tbu}bpy)Cl(H$_2$O) **2** and Ph$_2$DBTD were varied at a fixed 1:5 ratio of **1**:Ph$_2$DBTD under CO$_2$ saturation conditions. Conditions: 0.1 M TBAPF$_6$/*N,N*-DMF; glassy carbon working electrode, glassy carbon counter electrode, Ag/AgCl pseudoreference electrode; 100 mV/s scan rate; referenced to internal ferrocene standard. (**B**) Log-log plot from data obtained from CVs in **A** at −2.22 V vs. Fc$^+$/Fc.

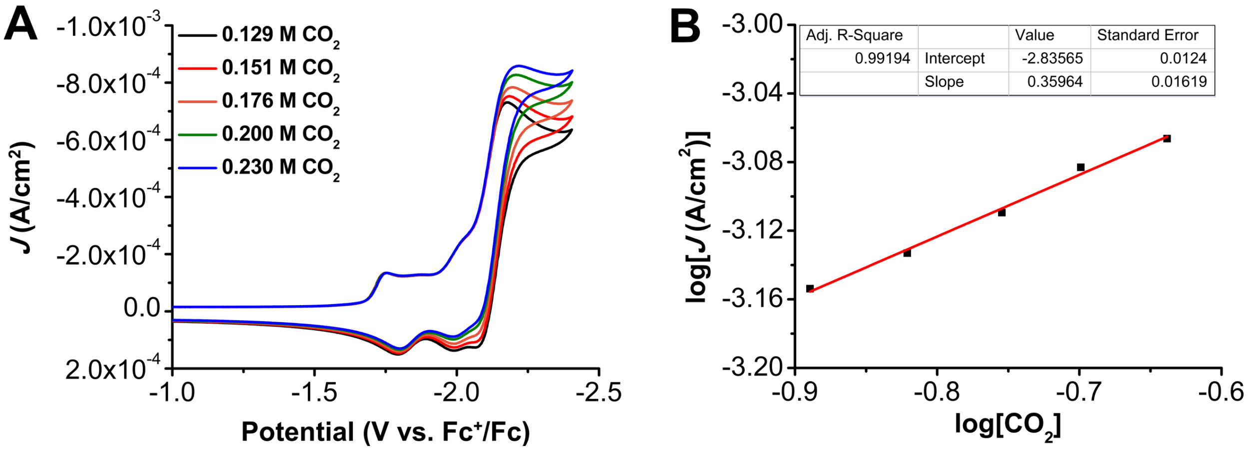

Figure S108. (**A**) CVs of 1.0 mM Cr(^{tbu}dh^{tbu}bpy)Cl(H_2O) **2** and 2.5 mM Ph_2DBTD at varied CO_2 concentrations. Conditions: 0.1 M $TBAPF_6$/*N,N*-DMF; glassy carbon working electrode, glassy carbon counter electrode, Ag/AgCl pseudoreference electrode; 100 mV/s scan rate; referenced to internal ferrocene standard. (**B**) Log-log plot from data obtained from CVs in **A** at −2. 22V vs. Fc^+/Fc.

As was the case for **1** with TPTD, the variable RM experiment for Mes_2DBTD and Ph_2DBTD was not able to be performed. The co-catalytic effect quickly reached saturation and the irreversible redox feature became obscured by unbound RM in solution.

Controlled Potential Electrolysis Experiments (Aprotic Conditions)

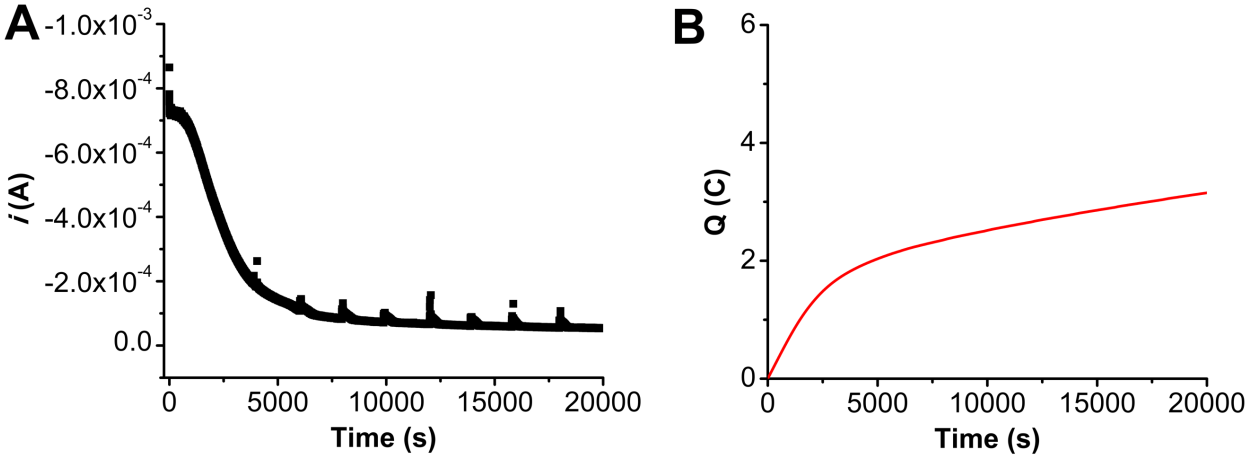

Figure S109. (**A**) Current versus time trace from CPE experiment with **1**+Mes_2DBTD. (**B**) Charge passed versus time for the CPE experiment shown in **A**. Conditions were 0.5 mM Cr(^{tbu}dhbpy)Cl(H_2O) **1** and 2.5 mM Mes_2DBTD under a CO_2 atmosphere at −2.30 V vs Fc^+/Fc in 0.1 M $TBAPF_6$/*N,N*-DMF; working electrode was a glassy carbon rod, counter electrode was a graphite rod, and the reference was a nonaqueous Ag/AgCl pseudoreference electrode; 0.075 M Fc was used as sacrificial oxidant.

Table S36. Results from CPE experiment in Figure S104, 1:5 (**1**:Mes_2DBTD).

Time (s)	Charge (coulombs)	moles (e⁻)	Moles of CO
20000*	3.15	3.27×10^{-5}	< LOQ
20000*	3.15	3.27×10^{-5}	< LOQ
20000*	3.15	3.27×10^{-5}	< LOQ

* indicates a triplicate series of injections carried out upon completion of electrolysis

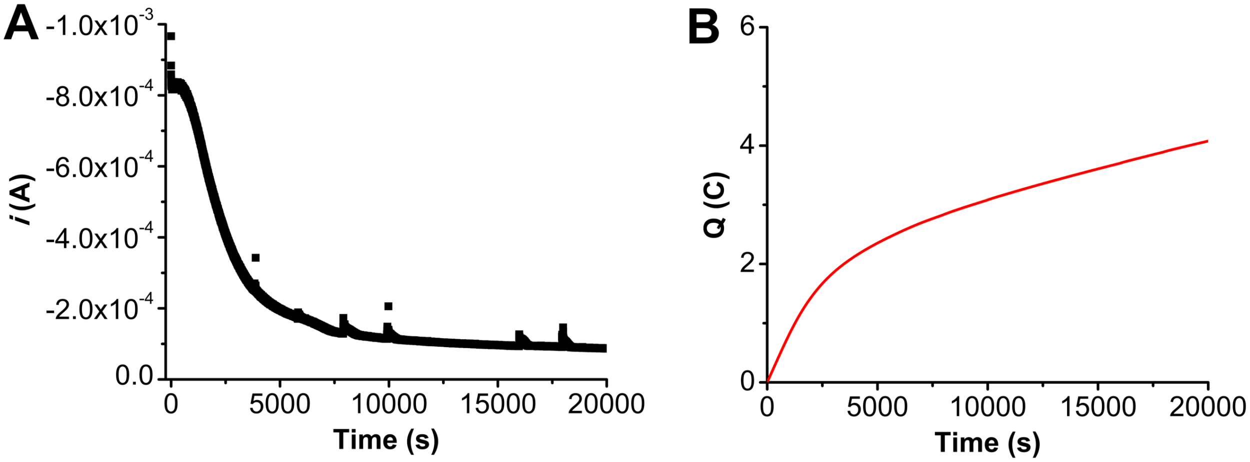

Figure S110. (**A**) Current versus time trace from CPE experiment with **1**+TPTD. (**B**) Charge passed versus time for the CPE experiment shown in **A**. Conditions were 0.5 mM Cr(^{tbu}dhbpy)Cl(H_2O) 1 and 2.5 mM TPTD under a CO_2 atmosphere at −2.25 V vs Fc^+/Fc in 0.1 M $TBAPF_6$/*N,N*-DMF; working electrode was a glassy carbon rod, counter electrode was a graphite rod, and the reference was a nonaqueous Ag/AgCl pseudoreference electrode; 0.075 M Fc was used as sacrificial oxidant.

Table S37. Results from CPE experiment in Figure S105, 1:5 (**1**:TPTD).

Time (s)	Charge (coulombs)	moles (e⁻)	Moles of CO
20000*	4.08	4.23×10^{-5}	< LOQ
20000*	4.08	4.23×10^{-5}	< LOQ
20000*	4.08	4.23×10^{-5}	< LOQ

* indicates a triplicate series of injections carried out upon completion of electrolysis

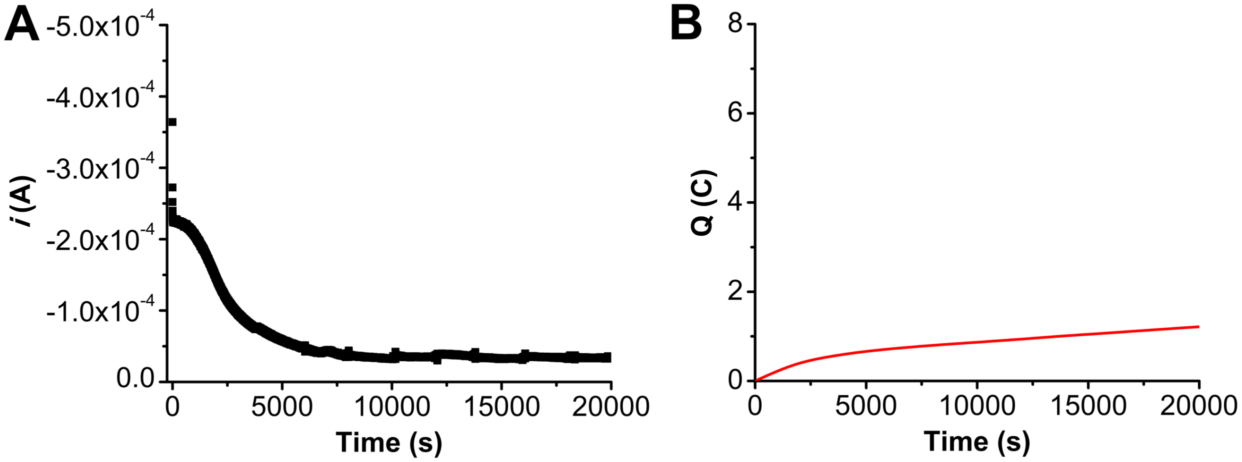

Figure S111. (**A**) Current versus time trace from CPE experiment with **2**+DBTD. (**B**) Charge passed versus time for the CPE experiment shown in **A**. Conditions were 0.1 mM Cr(^{tbu}dh^{tbu}bpy)Cl(H_2O) **2** and 0.5 mM DBTD under a CO_2 atmosphere at −2.30 V vs Fc^+/Fc in 0.1 M $TBAPF_6$/*N,N*-DMF; working electrode was a glassy carbon rod, counter electrode was a graphite rod, and the reference was a nonaqueous Ag/AgCl pseudoreference electrode; 0.075 M Fc was used as sacrificial oxidant.

Table S38. Results from CPE experiment in Figure S106, 1:5 (**2**:DBTD).

Time (s)	**Charge (coulombs)**	**moles (e^-)**	**Moles of CO**
20000*	1.22	1.26 x 10^{-5}	< LOQ
20000*	1.22	1.26 x 10^{-5}	< LOQ
20000*	1.22	1.26 x 10^{-5}	< LOQ

* indicates a triplicate series of injections carried out upon completion of electrolysis

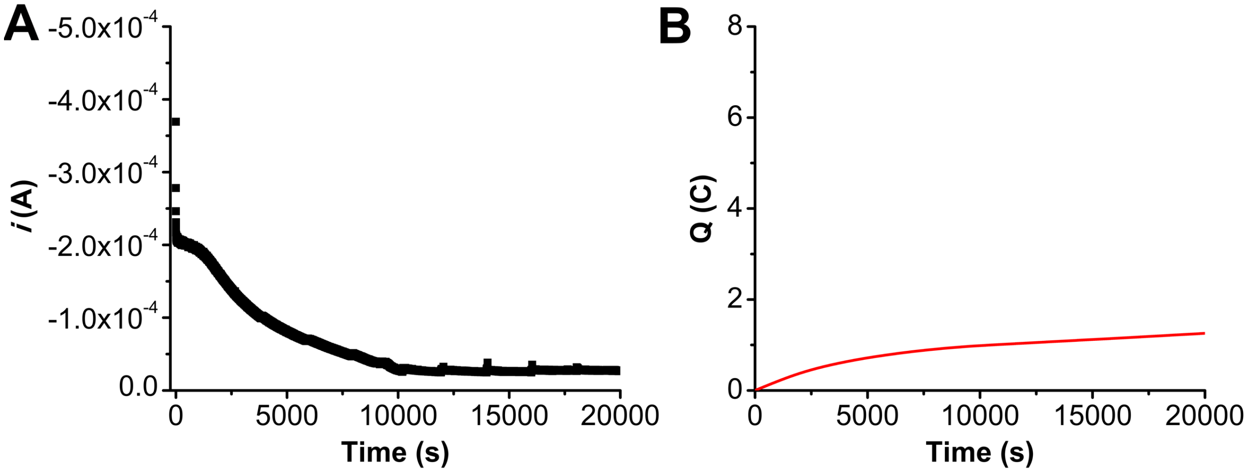

Figure S112. (**A**) Current versus time trace from CPE experiment with **2**+TPTD. (**B**) Charge passed versus time for the CPE experiment shown in **A**. Conditions were 0.1 mM Cr(^{tbu}dh^{tbu}bpy)Cl(H_2O) **2** and 0.5 mM TPTD under a CO_2 atmosphere at −2.25 V vs Fc^+/Fc in 0.1 M $TBAPF_6$/*N,N*-DMF; working electrode was a glassy carbon rod, counter electrode was a graphite rod, and the reference was a nonaqueous Ag/AgCl pseudoreference electrode; 0.075 M Fc was used as sacrificial oxidant.

Table S39. Results from CPE experiment in Figure S107, 1:5 (**2**:TPTD).

Time (s)	**Charge (coulombs)**	**moles (e^-)**	**Moles of CO**
20000*	1.26	1.30 x 10^{-5}	< LOQ
20000*	1.26	1.30 x 10^{-5}	< LOQ
20000*	1.26	1.30 x 10^{-5}	< LOQ

* indicates a triplicate series of injections carried out upon completion of electrolysis

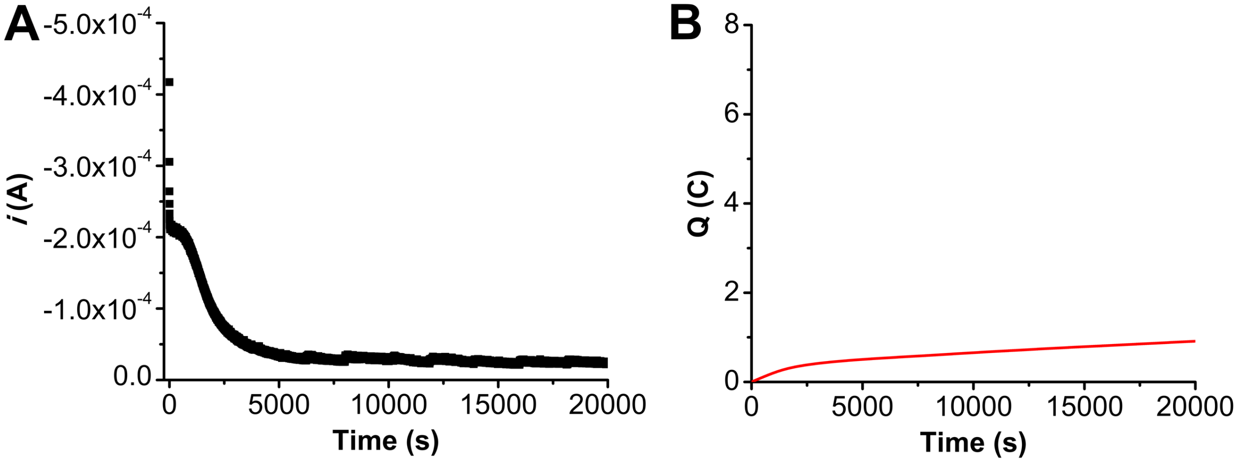

Figure S113. (**A**) Current versus time trace from CPE experiment with **2**+Mes_2DBTD. (**B**) Charge passed versus time for the CPE experiment shown in **A**. Conditions were 0.1 mM Cr(^{tbu}dh^{tbu}bpy)Cl(H_2O) **2** and 0.5 mM Mes_2DBTD under a CO_2 atmosphere at −2.30 V vs Fc^+/Fc in 0.1 M $TBAPF_6$/*N,N*-DMF; working electrode was a glassy carbon rod, counter electrode was a graphite rod, and the reference was a nonaqueous Ag/AgCl pseudoreference electrode; 0.075 M Fc was used as sacrificial oxidant.

Table S40. Results from CPE experiment in Figure S108, 1:5 (**2**:Mes_2DBTD).

Time (s)	**Charge (coulombs)**	**moles (e^-)**	**Moles of CO**
20000*	0.912	9.46×10^{-6}	< LOQ
20000*	0.912	9.46×10^{-6}	< LOQ
20000*	0.912	9.46×10^{-6}	< LOQ

* indicates a triplicate series of injections carried out upon completion of electrolysis

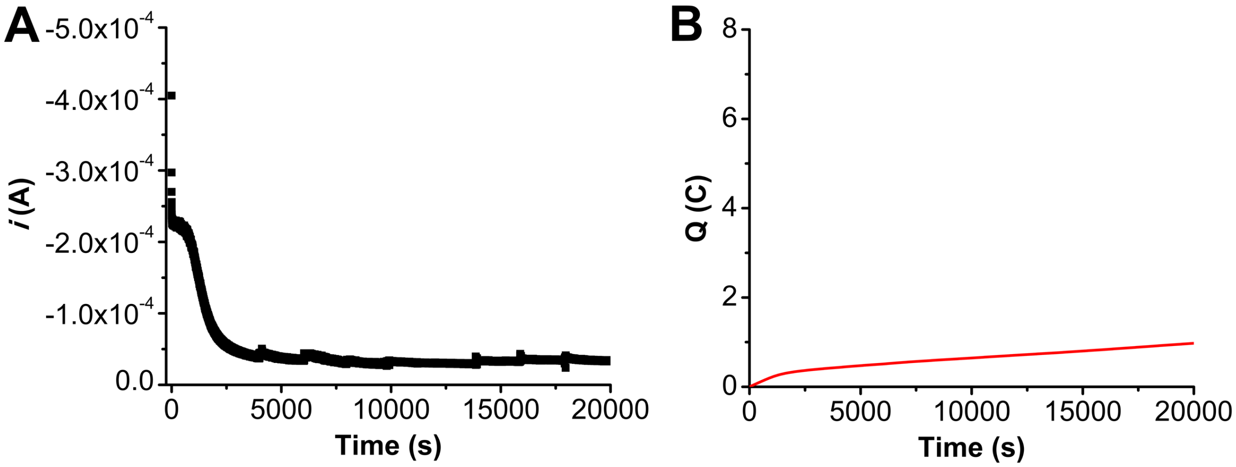

Figure S114. (**A**) Current versus time trace from CPE experiment with **2**+Ph_2DBTD. (**B**) Charge passed versus time for the CPE experiment shown in **A**. Conditions were 0.1 mM Cr(^{tbu}dh^{tbu}bpy)Cl(H_2O) **2** and 0.5 mM Ph_2DBTD under a CO_2 atmosphere at −2.20 V vs Fc^+/Fc in 0.1 M $TBAPF_6$/*N,N*-DMF; working electrode was a glassy carbon rod, counter electrode was a graphite rod, and the reference was a nonaqueous Ag/AgCl pseudoreference electrode; 0.075 M Fc was used as sacrificial oxidant.

Table S41. Results from CPE experiment in Figure S109, 1:5 (**2**:Ph_2DBTD).

Time (s)	Charge (coulombs)	moles (e^-)	Moles of CO
20000*	0.975	1.01×10^{-5}	< LOQ
20000*	0.975	1.01×10^{-5}	< LOQ
20000*	0.975	1.01×10^{-5}	< LOQ

* indicates a triplicate series of injections carried out upon completion of electrolysis

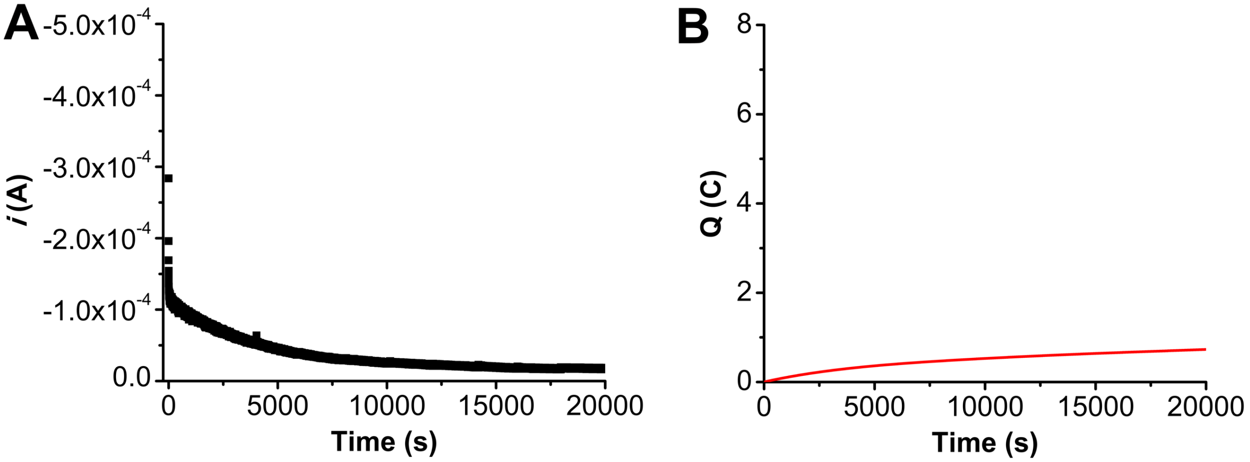

Figure S115. (**A**) Current versus time trace from CPE experiment with **2** under aprotic conditions. (**B**) Charge passed versus time for the CPE experiment shown in **A**. Conditions were 0.1 mM Cr(^{tbu}dh^{tbu}bpy)Cl(H_2O) **2** under a CO_2 atmosphere at −2.30 V vs Fc$^+$/Fc in 0.1 M $TBAPF_6$/*N,N*-DMF; working electrode was a glassy carbon rod, counter electrode was a graphite rod, and the reference was a nonaqueous Ag/AgCl pseudoreference electrode; 0.075 M Fc was used as sacrificial oxidant.

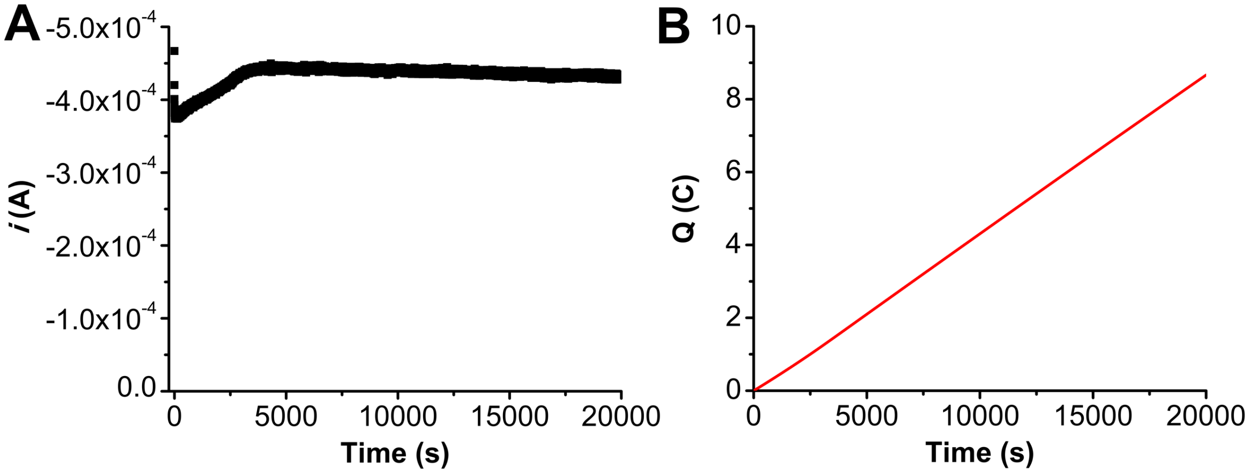

Figure S116. (**A**) Current versus time trace from CPE experiment with TPTD under aprotic conditions. (**B**) Charge passed versus time for the CPE experiment shown in **A**. Conditions were 2.5 mM TPTD under a CO_2 atmosphere at −2.25 V vs Fc$^+$/Fc in 0.1 M $TBAPF_6$/*N,N*-DMF; working electrode was a glassy carbon rod, counter electrode was a graphite rod, and the reference was a nonaqueous Ag/AgCl pseudoreference electrode; 0.075 M Fc was used as sacrificial oxidant.

Table S42. Results from CPE experiment in Figure S111, 2.5 mM TPTD.

Time (s)	**Charge (coulombs)**	**moles (e^-)**	**Moles of CO**
20000*	8.67	8.98×10^{-5}	< LOQ
20000*	8.67	8.98×10^{-5}	< LOQ
20000*	8.67	8.98×10^{-5}	< LOQ

* indicates a triplicate series of injections carried out upon completion of electrolysis

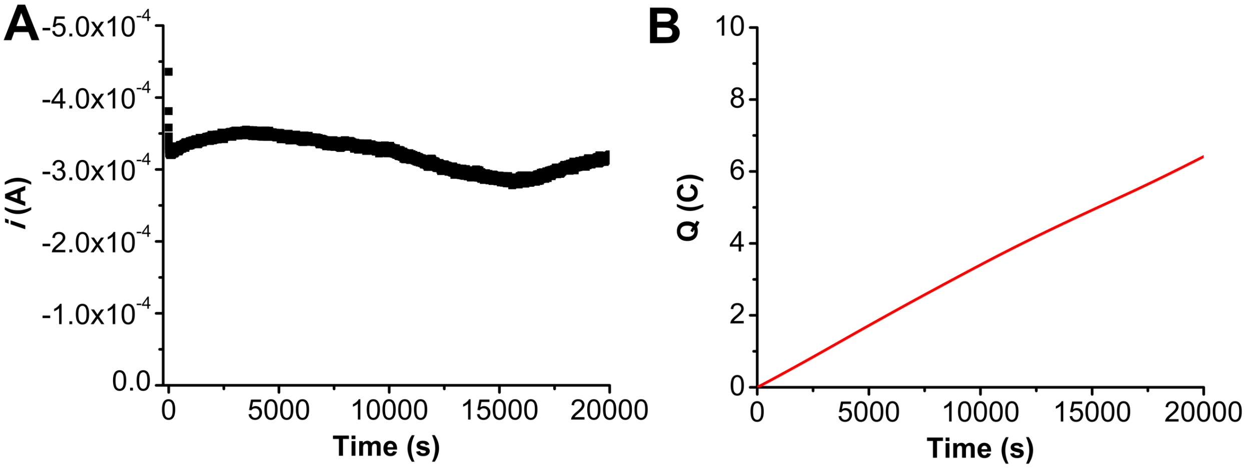

Figure S117. (**A**) Current versus time trace from CPE experiment with Mes_2DBTD under aprotic conditions. (**B**) Charge passed versus time for the CPE experiment shown in **A**. Conditions were 2.5 mM Mes_2DBTD under a CO_2 atmosphere at −2.30 V vs Fc^+/Fc in 0.1 M $TBAPF_6$/*N,N*-DMF; working electrode was a glassy carbon rod, counter electrode was a graphite rod, and the reference was a nonaqueous Ag/AgCl pseudoreference electrode; 0.075 M Fc was used as sacrificial oxidant.

Table S43. Results from CPE experiment in Figure S112, 2.5 mM Mes_2DBTD.

Time (s)	**Charge (coulombs)**	**moles (e^-)**	**Moles of CO**
20000*	6.42	6.65×10^{-5}	< LOQ
20000*	6.42	6.65×10^{-5}	< LOQ
20000*	6.42	6.65×10^{-5}	< LOQ

* indicates a triplicate series of injections carried out upon completion of electrolysis

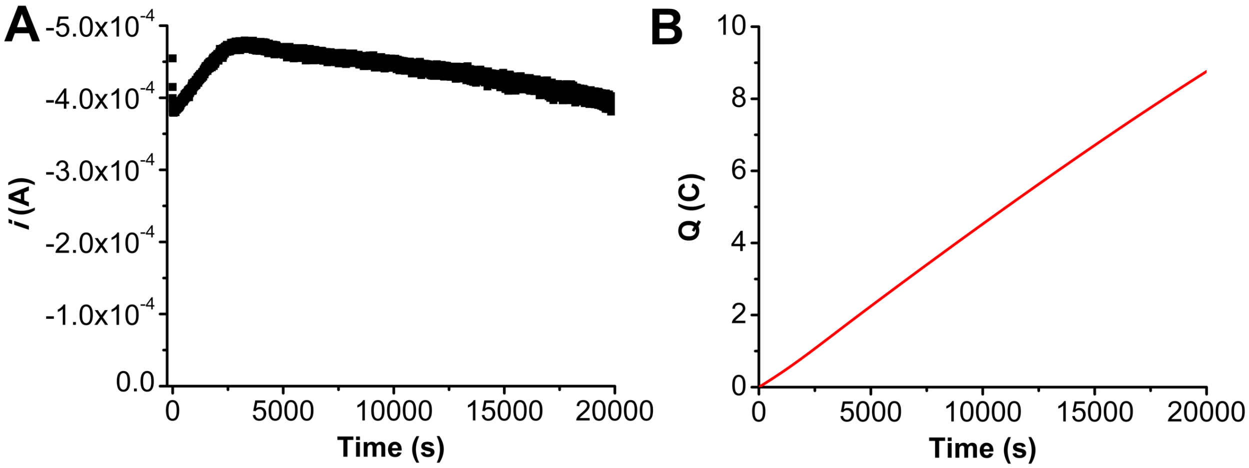

Figure S118. (**A**) Current versus time trace from CPE experiment with Ph_2DBTD under aprotic conditions. (**B**) Charge passed versus time for the CPE experiment shown in **A**. Conditions were 2.5 mM Ph_2DBTD under a CO_2 atmosphere at −2.20 V vs Fc^+/Fc in 0.1 M $TBAPF_6$/*N,N*-DMF; working electrode was a glassy carbon rod, counter electrode was a graphite rod, and the reference was a nonaqueous Ag/AgCl pseudoreference electrode; 0.075 M Fc was used as sacrificial oxidant.

Table S44. Results from CPE experiment in Figure S113, 2.5 mM Ph_2DBTD.

Time (s)	Charge (coulombs)	moles (e^-)	Moles of CO
20000*	8.76	9.08 x 10^{-5}	< LOQ
20000*	8.76	9.08 x 10^{-5}	< LOQ
20000*	8.76	9.08 x 10^{-5}	< LOQ

* indicates a triplicate series of injections carried out upon completion of electrolysis

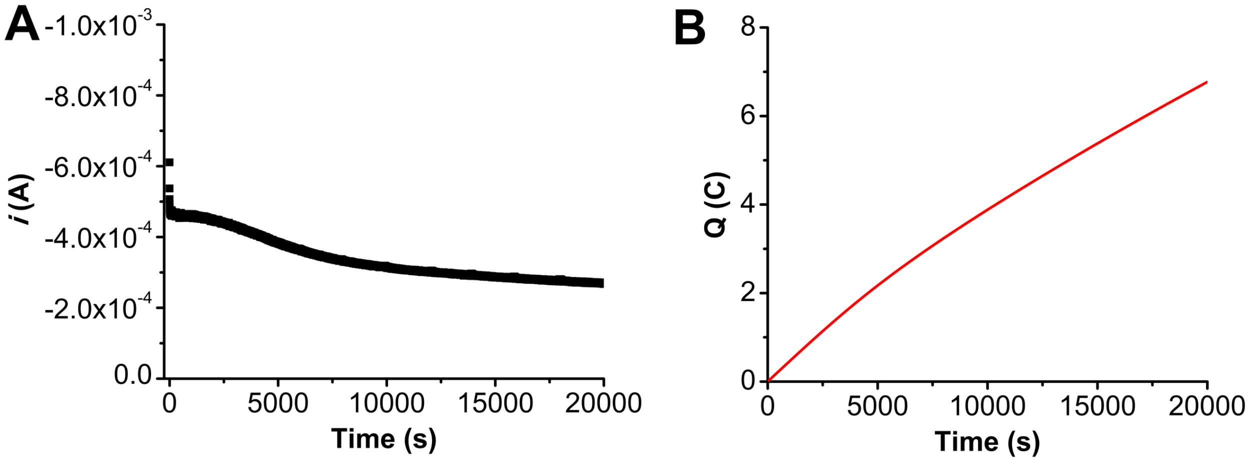

Figure S119. (**A**) Current versus time trace from CPE experiment with **1**+Ph_2DBTD. (**B**) Charge passed versus time for the CPE experiment shown in **A**. Conditions were 0.5 mM Cr(^{tbu}dhbpy)Cl(H_2O) **1** and 2.5 mM Ph_2DBTD under a CO_2 atmosphere at −2.20 V vs Fc^+/Fc in 0.1 M $TBAPF_6$/*N,N*-DMF; working electrode was a glassy carbon rod, counter electrode was a graphite rod, and the reference was a nonaqueous Ag/AgCl pseudoreference electrode; 0.075 M Fc was used as sacrificial oxidant.

Table S45. Results from CPE experiment in Figure S114, 1:5 (1:Ph_2DBTD).

Time (s)	Charge (coulombs)	moles (e^-)	Moles of CO	FE_{CO}
20000*	6.77	7.02×10^{-5}	8.46×10^{-6}	24.1
20000*	6.77	7.02×10^{-5}	8.99×10^{-6}	25.6
20000*	6.77	7.02×10^{-5}	1.02×10^{-5}	29.2

* indicates a triplicate series of injections carried out upon completion of electrolysis

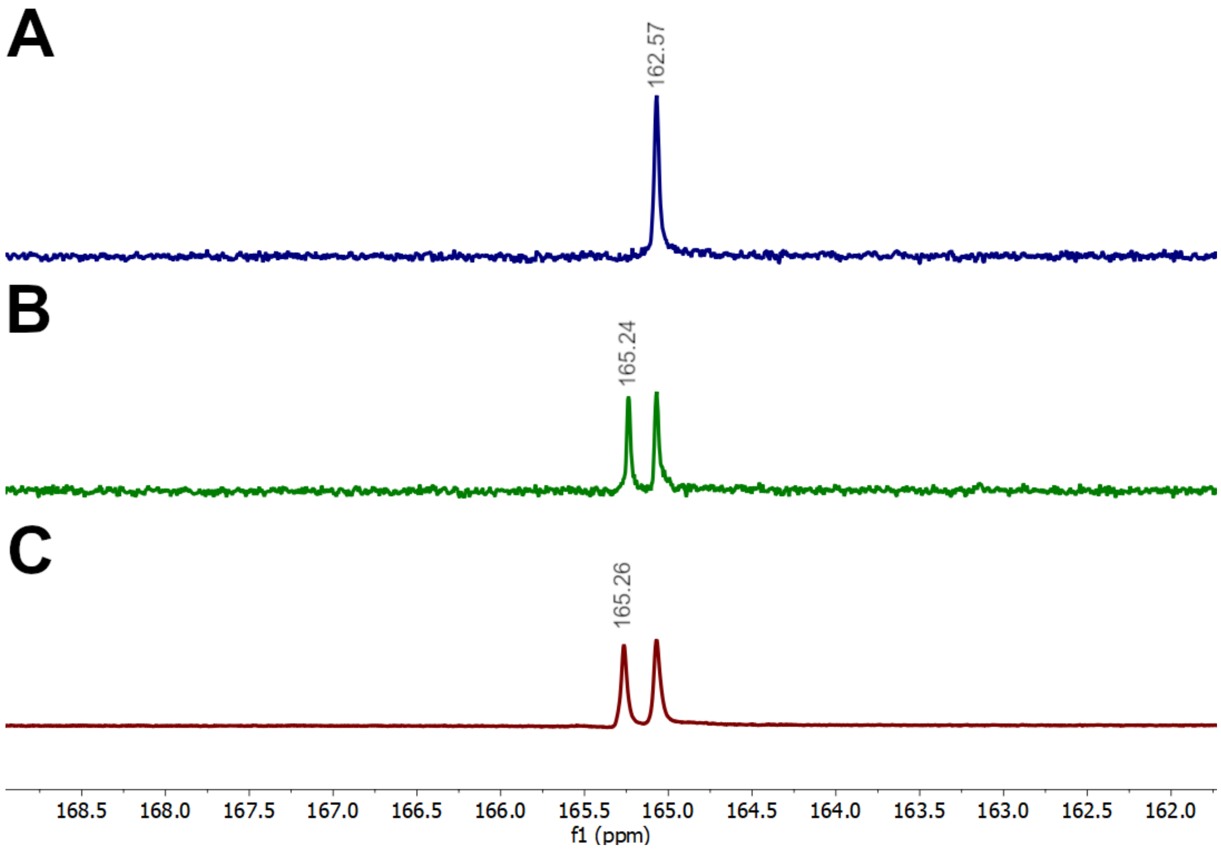

Figure S120. $^{13}C\{^1H\}$ NMRs in CD_2Cl_2 for product analysis of CPE solution with **1**+Ph_2DBTD. (**A**) ^{13}C $\{^1H\}$ NMR in CD_2Cl_2 of *N,N*-DMF. (**B**) ^{13}C $\{^1H\}$ NMR in CD_2Cl_2 and *N,N*-DMF from prepared sample of $TBA^+[HCO_3]^-$ that was synthesized according to reported procedures.[47] (**C**) $^{13}C\{^1H\}$ NMR in CD_2Cl_2 from the post electrolysis solution of Cr(^{tbu}dhbpy)Cl(H_2O) **1** and Ph_2DBTD in *N,N*-DMF under a CO_2 atmosphere at −2.20 V vs. Fc^+/Fc (Figure S114).

Table S46. Summary of Results from CPE experiments under aprotic conditions (Figures S104-S110, S114 and Tables S35-S40, S44).

Conditions	Potential (V vs Fc^+/Fc)	FE_{CO} (%)	TOF_{CPE} s^{-1}	η (V)	Turnovers of CO w.r.t [**1** or **2**]	Turnovers of CO w.r.t [RM]
1[45,a]	−2.30	0	–	0.11	–	–
1 + DBTD[45,a]	−2.30	91±10	36.8	0.69	16	3.1
1 + TPTD[a]	−2.25	0	–	0.63	–	–
1 + Mes_2DBTD[a]	−2.30	0	–	0.68	–	–
1 + Ph_2DBTD[a]	−2.20	26±2	0.1	0.58	0.68	0.14
2[b]	−2.30	0	–	0.16	–	–
2 + DBTD[b]	−2.30	0	–	0.69	–	–
2 + TPTD[b]	−2.25	0	–	0.63	–	–
2 + Mes_2DBTD[b]	−2.30	0	–	0.68	–	–
2 + Ph_2DBTD[b]	−2.20	0	–	0.58	–	–

[a] – 0.5 mM $Cr(^{tbu}dhbpy)Cl(H_2O)$ **1** and 2.5 mM RM

[b] – 0.1 mM $Cr(^{tbu}dh^{tbu}bpy)Cl(H_2O)$ **2** and 0.5 mM RM

Table S47. Comparison of experimental and calculated reduction potentials for RMs.[48]

Redox Mediator	Calculated Potential (V vs Fc^+/Fc)	Experimental Potential (V vs Fc^+/Fc)
$DBTD^{0/–}$	–2.26	–2.25
$TPTD^{0/–}$	–2.24	–2.19
$Mes_2DBTD^{0/–}$	–2.29	–2.24
$Ph_2DBTD^{0/–}$	–2.14	–2.12

References:

1. Hooe, S. L.; Dressel, J. M.; Dickie, D. A.; Machan, C. W., Highly Efficient Electrocatalytic Reduction of CO_2 to CO by a Molecular Chromium Complex. *ACS Catal.* **2020,** *10* (2), 1146-1151.
2. Pegis, M. L.; Wise, C. F.; Martin, D. J.; Mayer, J. M., Oxygen Reduction by Homogeneous Molecular Catalysts and Electrocatalysts. *Chem. Rev.* **2018,** *118* (5), 2340-2391.
3. Pegis, M. L.; Roberts, J. A. S.; Wasylenko, D. J.; Mader, E. A.; Appel, A. M.; Mayer, J. M., Standard Reduction Potentials for Oxygen and Carbon Dioxide Couples in Acetonitrile and *N,N*-Dimethylformamide. *Inorg. Chem.* **2015,** *54* (24), 11883-11888.
4. Nielsen, M. F.; Hammerich, O.; Rise, F.; Gogoll, A.; Undheim, K.; Wang, D. N.; Christensen, S. B., The Effect of Hydrogen Bonding between Methyl-Substituted Phenols and Dipolar Aprotic Solvents on the Rate Constants for. *Acta. Chem. Scan.* **1992,** *46*, 883-896.
5. Roy, S.; Sharma, B.; Pécaut, J.; Simon, P.; Fontecave, M.; Tran, P. D.; Derat, E.; Artero, V., Molecular Cobalt Complexes with Pendant Amines for Selective Electrocatalytic Reduction of Carbon Dioxide to Formic Acid. *J. Am. Chem. Soc.* **2017,** *139* (10), 3685-3696.
6. Matsubara, Y., Unified Benchmarking of Electrocatalysts in Noninnocent Second Coordination Spheres for CO_2 Reduction. *ACS Energy Lett.* **2019,** *4* (8), 1999-2004.
7. Franco, F.; Pinto, M. F.; Royo, B.; Lloret-Fillol, J., A Highly Active N-Heterocyclic Carbene Manganese(I) Complex for Selective Electrocatalytic CO_2 Reduction to CO. *Angew. Chem. Int. Ed.* **2018,** *57* (17), 4603-4606.
8. Costentin, C.; Drouet, S.; Robert, M.; Savéant, J.-M., Turnover Numbers, Turnover Frequencies, and Overpotential in Molecular Catalysis of Electrochemical Reactions. Cyclic Voltammetry and Preparative-Scale Electrolysis. *J. Am. Chem. Soc.* **2012,** *134* (27), 11235-11242.
9. Costentin, C.; Drouet, S.; Robert, M.; Savéant, J.-M., Correction to Turnover Numbers, Turnover Frequencies, and Overpotential in Molecular Catalysis of Electrochemical Reactions. Cyclic Voltammetry and Preparative-Scale Electrolysis. *J. Am. Chem. Soc.* **2012,** *134* (48), 19949-19950.
10. Cometto, C.; Chen, L.; Lo, P.-K.; Guo, Z.; Lau, K.-C.; Anxolabéhère-Mallart, E.; Fave, C.; Lau, T.-C.; Robert, M., Highly Selective Molecular Catalysts for the CO_2-to-CO Electrochemical Conversion at Very Low Overpotential. Contrasting Fe vs Co Quaterpyridine Complexes upon Mechanistic Studies. *ACS Catal.* **2018,** *8* (4), 3411-3417.
11. Baur, J. E., Chapter 19 Diffusion Coefficients. In *Handbook of Electrochemistry*, Zoski, C. G., Ed. Elsevier: 2007; pp 829-848.
12. Elgrishi, N.; McCarthy, B. D.; Rountree, E. S.; Dempsey, J. L., Reaction Pathways of Hydrogen-Evolving Electrocatalysts: Electrochemical and Spectroscopic Studies of Proton-Coupled Electron Transfer Processes. *ACS Catal.* **2016,** *6* (6), 3644-3659.
13. Frisch, M. J.; Trucks, G. W.; Schlegel, H. B.; Scuseria, G. E.; Robb, M. A.; Cheeseman, J. R.; Scalmani, G.; Barone, V.; Petersson, G. A.; Nakatsuji, H.; Li, X.; Caricato, M.; Marenich, A. V.; Bloino, J.; Janesko, B. G.; Gomperts, R.; Mennucci, B.; Hratchian, H. P.; Ortiz, J. V.; Izmaylov, A. F.; Sonnenberg, J. L.; Williams; Ding, F.; Lipparini, F.; Egidi, F.; Goings, J.; Peng, B.; Petrone, A.; Henderson, T.; Ranasinghe, D.; Zakrzewski, V. G.; Gao, J.; Rega, N.; Zheng, G.; Liang, W.; Hada, M.; Ehara, M.; Toyota, K.; Fukuda, R.; Hasegawa, J.; Ishida, M.; Nakajima, T.; Honda, Y.; Kitao, O.; Nakai, H.; Vreven, T.; Throssell, K.; Montgomery Jr., J. A.; Peralta, J. E.; Ogliaro, F.; Bearpark, M.

J.; Heyd, J. J.; Brothers, E. N.; Kudin, K. N.; Staroverov, V. N.; Keith, T. A.; Kobayashi, R.; Normand, J.; Raghavachari, K.; Rendell, A. P.; Burant, J. C.; Iyengar, S. S.; Tomasi, J.; Cossi, M.; Millam, J. M.; Klene, M.; Adamo, C.; Cammi, R.; Ochterski, J. W.; Martin, R. L.; Morokuma, K.; Farkas, O.; Foresman, J. B.; Fox, D. J. *Gaussian 16 Rev. B.01*, Wallingford, CT, 2016.

14. Becke, A. D., Density-functional thermochemistry. III. The role of exact exchange. *J. Chem. Phys.* **1993,** *98* (7), 5648-5652.
15. Lee, C.; Yang, W.; Parr, R. G., Development of the Colle-Salvetti correlation-energy formula into a functional of the electron density. *Phys. Rev. B* **1988,** *37* (2), 785-789.
16. Vosko, S. H.; Wilk, L.; Nusair, M., Accurate spin-dependent electron liquid correlation energies for local spin density calculations: a critical analysis. *Can. J. Phys.* **1980,** *58* (8), 1200-1211.
17. Stephens, P. J.; Devlin, F. J.; Chabalowski, C. F.; Frisch, M. J., Ab Initio Calculation of Vibrational Absorption and Circular Dichroism Spectra Using Density Functional Force Fields. *J. Phys. Chem.* **1994,** *98* (45), 11623-11627.
18. Weigend, F.; Ahlrichs, R., Balanced basis sets of split valence, triple zeta valence and quadruple zeta valence quality for H to Rn: Design and assessment of accuracy. *Phys. Chem. Chem. Phys.* **2005,** *7* (18), 3297-3305.
19. Weigend, F., Accurate Coulomb-fitting basis sets for H to Rn. *Phys. Chem. Chem. Phys.* **2006,** *8* (9), 1057-1065.
20. Grimme, S.; Antony, J.; Ehrlich, S.; Krieg, H., A consistent and accurate ab initio parametrization of density functional dispersion correction (DFT-D) for the 94 elements H-Pu. *J. Chem. Phys.* **2010,** *132* (15), 154104.
21. Grimme, S.; Ehrlich, S.; Goerigk, L., Effect of the damping function in dispersion corrected density functional theory. *J. Comput. Chem.* **2011,** *32* (7), 1456-1465.
22. Barone, V.; Cossi, M., Quantum Calculation of Molecular Energies and Energy Gradients in Solution by a Conductor Solvent Model. *J. Phys. Chem. A* **1998,** *102* (11), 1995-2001.
23. Ribeiro, R. F.; Marenich, A. V.; Cramer, C. J.; Truhlar, D. G., Use of Solution-Phase Vibrational Frequencies in Continuum Models for the Free Energy of Solvation. *J. Phys. Chem. B* **2011,** *115* (49), 14556-14562.
24. Luchini, G.; Alegre-Requena, J.; Funes-Ardoiz, I.; Rodríguez-Guerra, J.; Chen, J. T.; Paton, R. *Goodvibes v3.0.1*, 2019.
25. Schleyer, P. v. R.; Maerker, C.; Dransfeld, A.; Jiao, H.; van Eikema Hommes, N. J. R., Nucleus-Independent Chemical Shifts: A Simple and Efficient Aromaticity Probe. *J. Am. Chem. Soc.* **1996,** *118* (26), 6317-6318.
26. McWeeny, R., Perturbation Theory for the Fock-Dirac Density Matrix. *Physical Review* **1962,** *126* (3), 1028-1034.
27. Cheeseman, J. R.; Trucks, G. W.; Keith, T. A.; Frisch, M. J., A comparison of models for calculating nuclear magnetic resonance shielding tensors. *The Journal of Chemical Physics* **1996,** *104* (14), 5497-5509.
28. Ditchfield, R., Self-consistent perturbation theory of diamagnetism. *Molecular Physics* **1974,** *27* (4), 789-807.
29. Wolinski, K.; Hinton, J. F.; Pulay, P., Efficient implementation of the gauge-independent atomic orbital method for NMR chemical shift calculations. *J. Am. Chem. Soc.* **1990,** *112* (23), 8251-8260.

30. Neese, F., Software update: The ORCA program system—Version 5.0. *WIREs Computational Molecular Science* **2022,** *n/a* (n/a), e1606.
31. Bruker *Saint; SADABS;TWINABS; APEX3*, Bruker AXS Inc.: Madison, Wisconsin, USA, 2012.
32. Sheldrick, G., SHELXT - Integrated space-group and crystal-structure determination. *Acta Cryst.* **2015,** *71* (1), 3-8.
33. Dolomanov, O. V.; Bourhis, L. J.; Gildea, R. J.; Howard, J. A. K.; Puschmann, H., OLEX2: a complete structure solution, refinement and analysis program. *J. Appl. Cryst.* **2009,** *42* (2), 339-341.
34. Sheldrick, G. M. *Cell_now*, version 2008/4; Georg-August-Universität Göttingen: Göttingen, Germany, 2008.
35. Spek, A., PLATON SQUEEZE: a tool for the calculation of the disordered solvent contribution to the calculated structure factors. *Acta Crystallogr. Sect C: Struct. Chem.* **2015,** *71* (1), 9-18.
36. Lewis, F. W.; Harwood, L. M.; Hudson, M. J.; Distler, P.; John, J.; Stamberg, K.; Núñez, A.; Galán, H.; Espartero, A. G., Synthesis and Evaluation of Lipophilic BTBP Ligands for An/Ln Separation in Nuclear Waste Treatment: The Effect of Alkyl Substitution on Extraction Properties and Implications for Ligand Design. *Eur. J. Org. Chem.* **2012,** *2012* (8), 1509-1519.
37. Fujita, K.-i.; Wada, T.; Shiraishi, T., Reversible Interconversion between 2,5-Dimethylpyrazine and 2,5-Dimethylpiperazine by Iridium-Catalyzed Hydrogenation/Dehydrogenation for Efficient Hydrogen Storage. *Angew. Chem. Int. Ed.* **2017,** *56* (36), 10886-10889.
38. Chintala, S. M.; Petroff II, J. T.; Barnes, A.; McCulla, R. D., Photodeoxygenation of phenanthro[4,5-bcd]thiophene S-oxide, triphenyleno[1,12-bcd]thiophene S-oxide and perylo[1,12-bcd]thiophene S-oxide. *J. Sulphur Chem.* **2019,** *40* (5), 503-515.
39. Klemm, L. H.; Lawrence, R. F., The insertion and extrusion of heterosulfur bridges. X. Conversions in the triphenylene-triphenylo[4,5-bcd] thiophene system. *J. Heterocycl. Chem.* **1979,** *16* (3), 599-601.
40. Gilman, H.; Nobis, J. F., Rearrangement with 4-Iododibenzothiophene in Amination by Sodamide. *J. Am. Chem. Soc.* **1945,** *67* (9), 1479-1480.
41. Yang, W.; Hou, Q.; Liu, C.; Niu, Y.; Huang, J.; Yang, R.; Cao, Y., Improvement of color purity in blue-emitting polyfluorene by copolymerization with dibenzothiophene. *J. Mater. Chem.* **2003,** *13* (6), 1351-1355.
42. Grant, D. H., Paramagnetic Susceptibility by NMR: The "Solvent Correction" Reexamined. *J. Chem. Educ.* **1995,** *72* (1), 39.
43. Bain, G. A.; Berry, J. F., Diamagnetic corrections and Pascal's constants. *J. Chem. Educ.* **2008,** *85* (4), 532-536.
44. Sathrum, A. J.; Kubiak, C. P., Kinetics and Limiting Current Densities of Homogeneous and Heterogeneous Electrocatalysts. *J. Phys. Chem. Lett.* **2011,** *2* (18), 2372-2379.
45. (a) Hooe, S. L.; Moreno, J. J.; Reid, A. G.; Cook, E. N.; Machan, C. W., Mediated Inner-Sphere Electron Transfer Induces Homogeneous Reduction of CO_2 via Through-Space Electronic Conjugation**. *Angew. Chem. Int. Ed.* **2022,** *61* (1), e202109645; (b) *Corrigendum* **2022**, *61*, e202205139.

46. Lee, K. J.; McCarthy, B. D.; Dempsey, J. L., On decomposition, degradation, and voltammetric deviation: the electrochemist's field guide to identifying precatalyst transformation. *Chem. Soc. Rev.* **2019,** *48* (11), 2927-2945.
47. Cheng, S. C.; Blaine, C. A.; Hill, M. G.; Mann, K. R., Electrochemical and IR Spectroelectrochemical Studies of the Electrocatalytic Reduction of Carbon Dioxide by $[Ir_2(dimen)_4]^{2+}$ (dimen = 1,8-Diisocyanomenthane). *Inorg. Chem.* **1996,** *35* (26), 7704-7708.
48. Moreno, J. J.; Hooe, S. L.; Machan, C. W., DFT Study on the Electrocatalytic Reduction of CO_2 to CO by a Molecular Chromium Complex. *Inorg. Chem.* **2021,** *60* (6), 3635-3650.